SEMMELWEIS EGYETEM DOKTORI ISKOLA

Ph.D. értekezések

3358.

ERDEI ESZTER

A gyógyszerészeti tudományok korszerű kutatási irányai című program

Programvezető: Dr. Antal István, egyetemi tanár

Témavezető: Dr. Mándity István, egyetemi docens

INTEGRATING NANOTECHNOLOGY AND LIGHT: GOLD NANOCLUSTERS AND PHOTOSWITCHABLE SYSTEMS WITH BIOMEDICAL APPLICATION

PhD thesis

Eszter Erdei, PharmD

Semmelweis University Doctoral School Pharmaceutical Sciences and Health Technologies Division



Supervisor: István Mándity, PharmD, habil. Ph.D.

Official reviewers: András Wacha, Ph.D

Szilvia Erika Bősze, Ph.D

Head of the Complex Examination Committee: Zoltán Benyó, MD, habil. DS.c

Members of the Complex Examination Committee: László Őrfi, Ph.D

Tamás Gáti, Ph.D

Budapest 2025

Table of contents

List	of abbrev	iations	3
1.	Introduct	tion	5
1.	1. Lite	rature survey on gold nanoclusters	6
	1.1.1.	Synthesis and characterization techniques of AuNCs	7
	1.1.2.	Properties of AuNCs	8
	1.1.3.	Biomedical application	9
	1.1.3.1	Imaging techniques	9
	1.1.3.2	2. Therapeutics and drug delivery	9
	1.1.3.3	3. Biosensing applications	11
	1.1.3.4	4. Recent innovations and concerns	12
1.	.2. Lite	rature survey on photoswitchable peptides and foldamers	13
	1.2.1.	Photopharmacology	13
	1.2.2.	Overview of photoswitchable peptides	14
	1.2.3.	Mechanisms of photoswitching	15
	1.2.4.	Design and synthesis of photoswitchable peptides	16
	1.2.5.	Applications in biological systems	17
	1.2.6.	Advancements in foldamers	18
	1.2.7.	Biomedical application of photoswitchable foldamers	19
2.	Objective	es	21
3.	Methods		23
3.	.1. Dat	a collection and processing	23
3.	.2. Dat	abase design and implementation	23
4.	Results		24
4.	.1. Ana	alysis of the manually added columns data in BioGoldNCDB	24
	4.1.1.	Application	24
	4.1.2.	Cell line	26
	4.1.3.	Particle size	27
	4.1.4.	Excitation/ emission wavelength	28
	4.1.5.	Nanobioconjugates	30
4.	.2. Pho	toswitchable peptides and foldamers	32
5.	Discussion	on	38

5	.1. Dat	tabase overview	38
	5.1.1.	BioGoldNCDB's help desk	38
	5.1.2.	Examples	40
5	.2. Pho	otoswitchable peptides and foldamers	43
6.	Conclusi	ions	45
7.	Summar	y	48
8.	. References		49
9.	Bibliogra	aphy of the candidate's publications	63
10.	Acknow	ledgements	64

List of abbreviations

1D one-dimensional2D two dimensional

A549 adenocarcinomic human alveolar basal epithelial cells

ATP adenosine triphosphate

AuNCs gold nanoclusters

AuNPs gold nanoparticles

BiGC@PNA bi-valent gold nanocluster with peptide nucleic acid

BODIPY 4,4-difluoro-4-bora-3a,4a-diaza-s-indacene

CAS Chemical Abstracts Service
CAN Chemical Abstracts Number

CD circular dichroism

DCT decitabine

DMNB 2,3-dimethyl-2,3-dinitrobutane

DOI digital object identifier

E. coli Escherichia coli

ECD electronic circular dichroism

ESI electrospray ionization

FT-IR Fourier transform infrared spectroscopy

GPC gel permeation chromatography

GSDME gasdermin EHeLa human cervical cancer cell line

HepG2 hepatocellular carcinoma cell line

HMGB1 high mobility group box 1

HPLC high-performance liquid chromatography

HPLC-MS high-performance liquid chromatography- mass spectrometry

HSQC heteronuclear single quantum coherence

ICD immunogenic cell death

IL1β interleukin-1β

IR infrared spectroscopy

MALDI-MS matrix-assisted laser desorption/ionization mass

spectrometry

MCF-7 human breast cancer cell line

MDA-MB-231 human breast cancer cell line

MLL1 mixed lineage leukemia 1 protein

MS mass spectrometry

MW microwave
NIR near-infrared

NMR nuclear magnetic resonance

NOESY nuclear overhauser effect spectroscopy

PC propylene carbonate

PD-1 programmed cell death protein 1

PD-L1 programmed death-ligand 1

PNA peptide nucleic acid

PSS photostationary state ratio

RF radiofrequency

SPPS solid-phase peptide synthesis

S. aureus Staphylococcus aureus

TOC table of contents

TOF-MS time of flight mass spectrometry

U87 human glioblastoma cell line

UV ultraviolet spectroscopy

UV/VIS ultraviolet-visible spectroscopy

1. Introduction

The intersection of nanotechnology (1) and biomedical science (2) has given rise to an array of novel functional materials, among which gold nanoclusters (AuNCs) have emerged as a particularly promising class. Characterized by their ultrasmall core size—typically less than 2 nm—AuNCs exhibit distinct optical, electronic, and catalytic properties (3) that set them apart from larger nanoparticles (AuNPs) (4) and bulk gold. Their high surface-to-volume ratio, quantum confinement effects, and excellent biocompatibility make them ideal candidates for numerous applications, including biomedical imaging, diagnostics, drug delivery and biosensing (5).

The rapid advancement in the synthesis and functionalization of AuNCs has led to an exponential increase in research publications in recent years. However, the dispersion of data across various journals and the lack of centralized, curated resources have presented significant challenges to researchers attempting to navigate this growing body of knowledge.

Despite their promise, several challenges remain. Precise control over size, composition, and surface chemistry is difficult, as slight variations can dramatically affect optical and catalytic behavior. Stability under physiological or harsh chemical conditions is another limitation, and scalable, reproducible synthesis methods are still under development. Furthermore, understanding and controlling their interactions with biological systems or complex chemical environments remains a major research focus. Addressing these issues is crucial for translating the unique properties of AuNCs into reliable applications.

Parallel to the growing interest in nanomaterials, the field of photopharmacology (6) has gained momentum as a cutting-edge approach to achieving spatiotemporal control over biological processes. This emerging discipline integrates photochemistry with pharmacological strategies to enable precise, reversible modulation of biomolecular activity using light. Central to this approach are photoswitchable compounds, including specially designed peptides and foldamers, which undergo conformational changes in response to specific wavelengths of light. These structural transitions allow the compounds to toggle between biologically active and inactive states, offering exceptional control over their function in both *in vitro* and *in vivo* settings (7).

Photoswitchable systems have opened new avenues in targeted drug delivery, real-time molecular sensing, and the engineering of dynamic biomaterials. Their ability to respond to external stimuli with high specificity and minimal invasiveness makes them ideally suited for the development of "smart" therapeutics-agents that can be activated or deactivated by light, thereby minimizing systemic side effects and enhancing therapeutic precision. Moreover, light-responsive biomaterials have shown potential in tissue engineering and regenerative medicine, as well as in the design of optical devices and biosensors (8).

Despite their promise, several challenges remain before these systems can be fully translated into clinical practice. Issues such as photostability, biocompatibility, and efficiency of light penetration in biological tissues must be addressed. Recent advances in nanotechnology, including the integration of AuNCs with photosensitive moieties, offer promising solutions to some of these challenges by combining the favourable characteristics of both platforms.

Taken together, the convergence of AuNC-based nanotechnology and light-controlled pharmacological systems holds transformative potential for modern biomedicine. This dissertation aims to explore this multidisciplinary frontier. Streamlined access to nanocluster data, along with the investigation of the synergy between AuNCs and photopharmacological agents, is essential for next-generation biomedical applications. Through this integrated approach, we seek to advance the rational design of photoresponsive nanomaterials and contribute to the growing field of precision medicine.

1.1. Literature survey on gold nanoclusters

AuNCs are molecular-sized assemblies of gold atoms that typically less than 2 nm (9). These nanoclusters exhibit remarkable properties that differ significantly from bulk gold due to quantum effects (3) (Figure 1). Their high surface-to-volume ratio allows for significant modification with various ligands, enhancing their stability and functionality for specific applications, particularly in the biomedical field (10,11).

Research has demonstrated that the interaction of AuNCs with biological molecules can enhance their stability and functionality, making them promising candidates for therapeutic and diagnostic applications (12–15). Over the past few years, numerous reports have been published showcasing the use of AuNCs in various oncological

applications, including imaging, diagnostics (16), targeted therapy (17), radiotherapy (18), and immunotherapy (19).

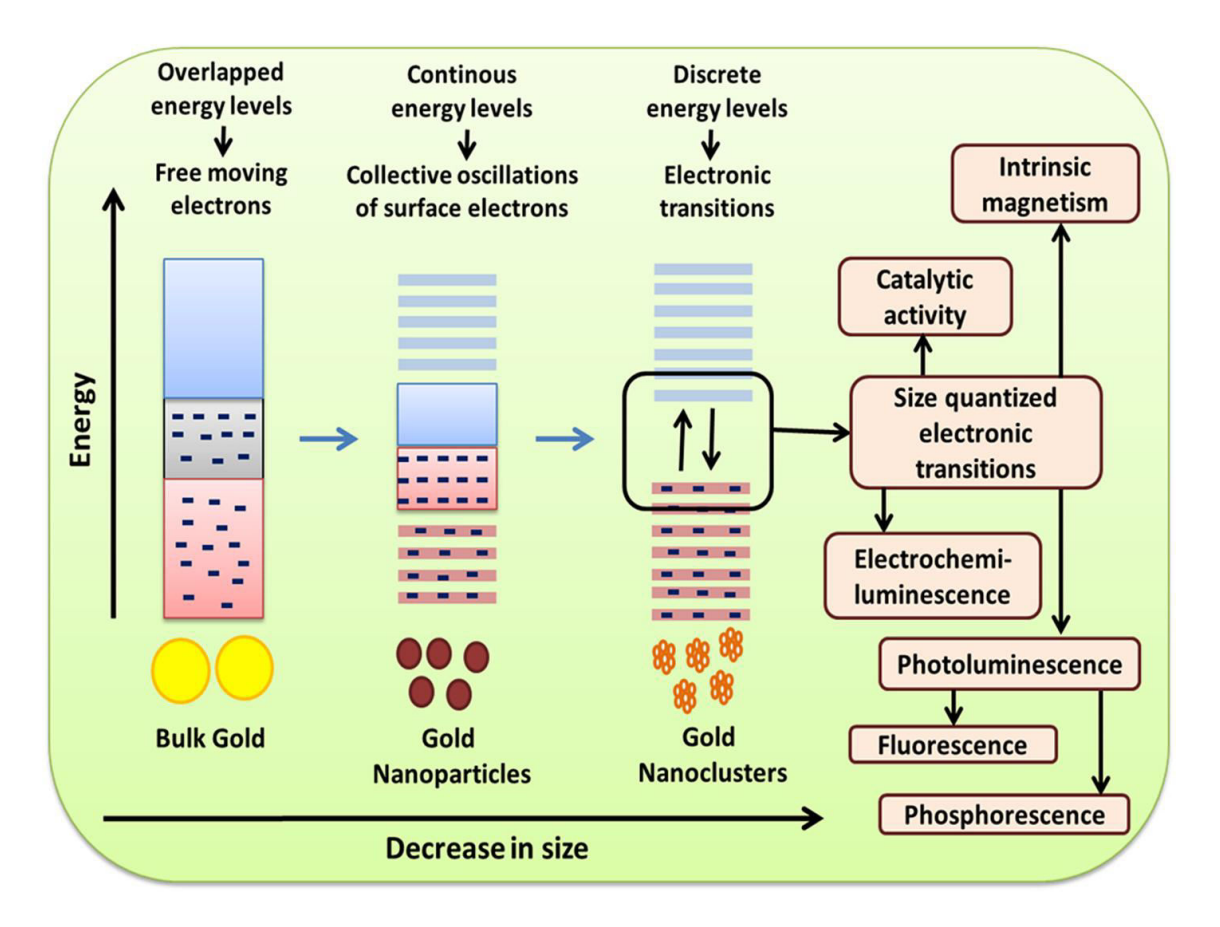


Figure 1. Schematic representation of the origins of distinct properties of bulk gold, AuNPs and AuNCs (3).

1.1.1. Synthesis and characterization techniques of AuNCs

Recent advancements in the synthesis of AuNCs have focused on producing well-defined structures with high yields and biocompatibility. Solid-phase (20,21) techniques have gained popularity owing to their simplicity and scalability. Common methods include chemical reduction techniques, where precursors are reduced under controlled conditions, and biosynthesis methods utilizing biological materials as reducing agents (22,23).

The synthesis of AuNCs commonly involves specific ligands that serve as stabilizing agents by strongly interacting with metal atoms. One significant approach is the use of proteins as stabilizers and reducing agents. For instance, bovine serum albumin (BSA)

has been successfully employed to encapsulate gold atoms and improve the luminescent properties of AuNCs produced (24,25). Furthermore, micellar methods and one-pot syntheses have gained traction for producing isomerically pure AuNCs (25).

The ligand engineering approach is critical in synthesizing AuNCs with desired properties. Modification of ligands effect the clustering process, helping to control aspects such as solubility and quantum yield (26,27). Quantum yield refers to the percentage of the irradiated light that the gold nanocluster is able to emit. The higher the value, the more detectable the given cluster becomes, thereby reducing the amount of material required. This is of particular importance in the fields of imaging and diagnostics. Among these, thiolated ligands (28) are especially notable for forming weak coordination bonds with the gold core, thereby improving the nanoclusters' sensing and catalytic capabilities. Novel ligand systems, such as polymers and polypeptides, are being explored for their efficiency in stabilizing and functionalizing AuNCs (29,30).

Characterizing AuNCs necessitates advanced analytical techniques to understand their structure and properties. High-resolution transmission electron microscopy (HRTEM) helps elucidate the morphology and structure of AuNCs at the atomic level (31), while spectroscopic methods like UV-VIS and fluorescence spectroscopy provide insight into their optical properties (32).

Other useful techniques include X-ray diffraction for crystalline phase determination (33), and mass spectrometry for analysing the size distribution of nanoclusters (34). Recent studies have focused on employing time-resolved spectroscopy to investigate excited-state dynamics in protein-encapsulated AuNCs, revealing insights into their luminescent properties and potential applications in bioimaging (35,36).

1.1.2. Properties of AuNCs

AuNCs exhibit unique optical properties, attributed to their small size and quantum effects. They demonstrate strong photoluminescence and possess surface plasmon resonance characteristics, which can be tuned by altering their size and environmental conditions (37–39).

Because of their ultrasmall dimensions, AuNCs show molecule-like behaviour rather than the typical properties associated with nanoparticles. This arises from their size being comparable to the Fermi wavelength (40) of electrons, which leads to the loss of

conventional metallic characteristics. Instead, strong quantum confinement effects cause the continuous energy bands to break into discrete electronic states, giving AuNCs unique optical properties distinct from those of larger nanoparticles.

The catalytic capabilities of AuNCs are being exploited in various chemical reactions, including oxidation and reduction processes. Their unique electronic environment facilitates reactions that are unfavourable for larger gold nanoparticles (41,42).

Due to their unique properties, AuNCs hold great potential for a wide range of biomedical applications, such as: (i) Fluorescent AuNCs are used as bioimaging and cell imaging agents due to their non-toxic cores (5); (ii) Functionalized AuNCs possess enzyme-mimetic activity (43), allowing their application in protein activity inhibition (44) and the colorimetric detection of analytes (27); (iii) Ultrasmall AuNCs exhibit broadspectrum antimicrobial effects, effectively targeting both Gram-positive and Gramnegative bacteria by disrupting metabolic processes and inducing intracellular reactive oxygen species (ROS) accumulation, ultimately causing bacterial cell death (45,46).

1.1.3. Biomedical application

1.1.3.1. Imaging techniques

AuNCs have emerged as excellent candidates for various imaging modalities, particularly fluorescence imaging, due to their tuneable emission spectra and high quantum yields (47,48). Studies have demonstrated their effectiveness in cellular and tissue imaging, including real-time tracking of cellular processes and disease markers (49,50). Their application in photoacoustic imaging has been highlighted for tumor detection, leveraging their strong light absorption in the near-infrared (NIR) region for enhanced imaging depth (51–53).

1.1.3.2. Therapeutics and drug delivery

In therapy, AuNCs are promising agents for photothermal treatment where they convert absorbed light into heat to ablate tumor cells selectively (54). Strategically functionalizing AuNCs with targeting ligands allows for improved specificity, minimizing side effects on healthy tissue (55,56) (Figure 2). The efficacy of AuNCs has been thoroughly evaluated across a range of cancer cell lines, including HeLa (29), HepG2 (57), A549

(58), MCF-7 (59), U87 (60), and MDA-MB-231 cells (61), as well as in mouse models (62).

Furthermore, they can be used as delivery vehicles for various therapeutic agents, enhancing their solubility and bioavailability (31,63). Notably, a wide range of biomolecules—such as peptides, proteins, and polymers—can be used as capping agents for AuNCs, offering potential to enhance biocompatibility, reduce toxicity, and improve targeting. These qualities make AuNCs a promising and adaptable platform for biomedical use. The growing number of studies on AuNCs in imaging, sensing, and therapy over the past 15 years highlights the rising interest in the field and suggests that clinical application may be approaching (64).

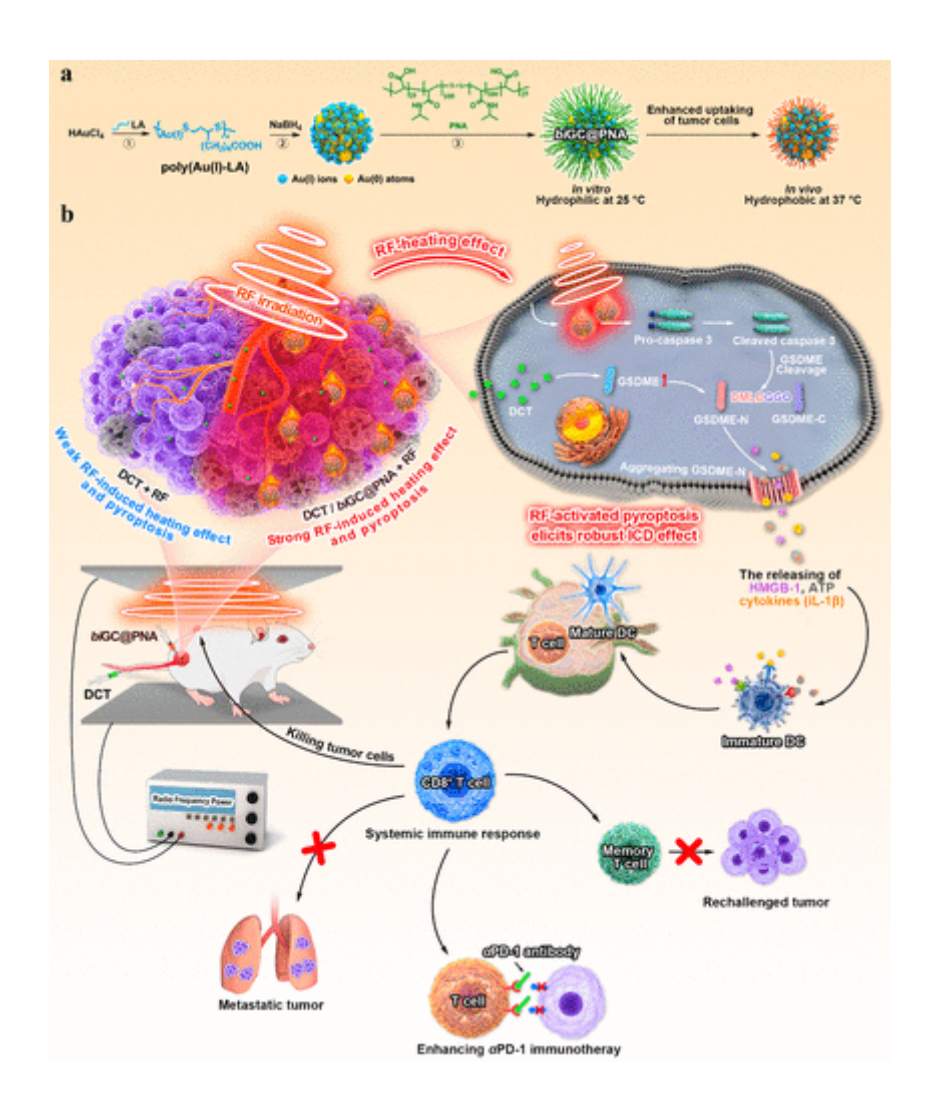


Figure 2. Schematic illustration of radiofrequency (RF)-induced pyroptosis mediated by biGC@PNA for cancer immunotherapy. (a) Preparation, mechanism, and hydrophilic–hydrophobic transition of biGC@PNA. (b) Schematic representation of the immunological effects of RF-responsive biGC@PNA, demonstrating caspase-3/GSDME-N-mediated tumor cell pyroptosis triggered by its RF-heating effect. This process induces pyroptosis of tumor cells, initiates immunogenic cell death (ICD), enhances anti-PD-1 cancer immunotherapy, and promotes immune activation, thereby suppressing distant tumors, lung metastases, and rechallenged tumors (19).

1.1.3.3. Biosensing applications

AuNCs are being utilized in biosensing applications due to their sensitivity to environmental changes and interactions with biomolecules. Their fluorescence quenching capabilities can facilitate the detection of specific analytes, making them suitable for clinical diagnostics (65,66). Recent advances in AuNCs-based sensors have shown effectiveness in detecting heavy metals, pathogens, and other vital biomolecules, highlighting their versatility (67,68).

1.1.3.4. Recent innovations and concerns

Research continues to unveil exciting developments in AuNCs technology. Innovations in the synthesis and functionalization techniques are yielding multifunctional platforms that integrate imaging and therapeutic properties (69,70). Future perspectives include further exploration of chiral AuNCs for applications in asymmetric synthesis and catalysis, as well as the investigation of their behaviour in biological environments for enhanced therapeutic efficacy (19,71).

Achieving precise control over the size, composition, and surface chemistry of AuNCs remains a significant challenge. The synthesis methods often result in polydisperse mixtures, complicating the reproducibility and scalability of production. Additionally, the stability of AuNCs is influenced by factors such as ligand type, solvent, and environmental conditions. For instance, studies have shown that the stability of AuNCs can be modulated by different ligands and doped metal atoms, which is crucial for their applications in, therapy, imagning and in sensing (72).

While AuNCs exhibit promising properties for biomedical applications, their interactions within biological systems are complex and not fully understood. Factors such as cellular uptake, biodistribution, and clearance rates are influenced by the size, surface charge, and ligand composition of AuNCs. Recent reviews have discussed the biological interactions and imaging capabilities of ultrasmall AuNPs, highlighting challenges in predicting their behavior *in vivo* and the need for more comprehensive studies to ensure safety and efficacy (73).

The lack of standardized protocols for the synthesis and characterization of AuNCs leads to variability in results across different laboratories. This variability hinders the comparison of data and the development of reliable applications. Efforts are being made to establish guidelines and best practices to improve reproducibility and facilitate the translation of AuNCs into practical applications.

Traditional synthesis methods for AuNCs often involve toxic reagents and harsh conditions, raising concerns about environmental impact and scalability. There is a

growing interest in developing green synthesis routes that utilize environmentally friendly materials and processes. For example, the use of natural extracts for the synthesis of AuNPs has been explored as a sustainable alternative (74).

1.2. Literature survey on photoswitchable peptides and foldamers

Photoswitchable peptides and foldamers are revolutionary in the realm of materials science and biomedicine due to their ability to undergo reversible conformational changes when exposed to light stimuli. These properties open up pathways for novel applications in targeted drug delivery, biological sensing, and advanced therapeutic interventions (75). The phenomenon wherein these structures exhibit changes in their physical or chemical properties when irradiated with light is largely based on the integration of chromophores such as azobenzene, spiropyrans, or other photo-responsive moieties. This literature survey aims to explore recent advancements in the design, synthesis, and application of photoswitchable peptides and foldamers, underlining their potential utility in various scientific fields, particularly in enhancing drug efficacy and developing novel therapeutic strategies.

1.2.1. Photopharmacology

A significant portion of current photopharmacology research is dedicated to developing molecules capable of altering cellular behaviour. Photopharmacology is a field that employs molecular photoswitches to precisely control the activity of bioactive compounds (76).

There are two broad approaches: photoswitch and photocages. Photopharmacology with irreversible photocages uses light-activated protecting groups to "uncage" drugs in a one-way, permanent manner. This gives excellent spatial and temporal control for applications like neuroscience, cancer therapy, and gene regulation — but faces challenges in wavelength, byproducts, and irreversibility. Common photocages: nitrobenzyl derivatives (*o*-nitrobenzyl, DMNB), coumarins, BODIPY, and newer redshifted cages (77–79).

Its goal is to minimize systemic drug toxicity and the development of resistance, while enabling highly targeted therapeutic interventions. By relying on small molecules, photopharmacology offers a practical alternative to optogenetics. Optogenetics is a technique in neuroscience (and increasingly in other fields) that uses light to control the activity of specific cells—typically neurons—after they have been genetically modified to express light-sensitive proteins (80). Light of the appropriate wavelength is delivered through thin optical fibers or LEDs precisely to the desired brain region or tissue. In response to light, the target cells can be switched on or off within milliseconds. Light can thus almost instantly initiate or halt cellular activity. Not only neurons but also muscle cells, pancreatic cells, cardiac muscle tissue, and others can be manipulated. The method is more precise than electrical stimulation (which excites all nearby neurons, not just certain types) and faster and more reversible than chemical-based activation or inhibition (75,81).

Photopharmacology currently focused on identifying molecular targets and assessing efficacy through *in vitro* studies, including receptor binding and enzyme inhibition. Significant progress has been made in areas like cancer treatment (82), neurology (83), diabetes (84), and antimicrobial therapies (85) using light-controlled approaches. Future advancements will depend on *in vivo* testing, comprehensive toxicity evaluations, and the integration of molecular imaging to verify targeted drug activation and support the development of therapostic strategies combining diagnosis and treatment (86,87).

1.2.2. Overview of photoswitchable peptides

Photoswitchable peptides are typically synthesized by embedding photosensitive moieties into their peptide frameworks. These modifications allow for significant and tuneable alterations in conformation upon exposure to specific wavelengths of light. The work by Lawrence *et al.* detailed the development of such azobenzene-flanked maleimide photoswitches, which successfully facilitate conformational shifts in peptide structures. This capability not only modulates the peptides' catalytic properties but also enhances their potential within sensor systems to detect environmental changes or disease-related biomarkers (88). Importantly, the incorporation of photoswitchable units enables multiple cycles of activity without degradation of the materials involved, which suggests opportunities for sustained applications in therapeutic contexts (89).

Moreover, Szymański et al. described the incorporation of a molecular photoswitch within peptides that allows precise control over biological interactions, bringing forth

opportunities to manipulate cellular processes with high specificity (7). This study elucidates the dynamic influence of optical control on peptide behaviour, as seen in muscle physiology where the resultant conformational changes can lead to notable variations in contractile ability (7).

1.2.3. Mechanisms of photoswitching

Photocontrol of peptides, proteins, or drugs offers a non-invasive method to modulate biological networks and study their effects or induce specific outcomes. This is achieved by incorporating a photoresponsive element that alters the molecule's properties upon light exposure, with certain photochromic compounds undergoing bond changes or E/Z isomerization. Molecules that photoswitch between E and Z forms via light-induced isomerization provide predictable structural control, with relaxation dynamics governed by thermal stability and energy barriers. Among various photoswitches, like stilbenes (90), diarylethenes (91) or acylhydrazones (92), azobenzenes are especially favoured due to their broad activation wavelength range and stable photoactivated states, enabling precise and reliable molecular control (87,93).

The underlying mechanisms of photoswitching within peptide structures are complex and engage various forms of structural rearrangements triggered by light activation. For instance, Janković *et al.* demonstrated that photocontrol over protein-peptide interactions could be attained through this method, indicating the significant efficacy of photoswitchable peptide designs for targeted therapeutic applications (94). The conformational changes ensuing from light exposure can enhance or diminish binding affinities, which is critical for drug design strategies that necessitate precision in targeting specific cellular receptors or enzymes.

Studies focused on azobenzene photoswitches, revealed that the coupling of isomerization with peptide conformation could efficiently modulate biological activity (95). Their findings illustrated how variations in peptide structure prompted by light stimulus can dictate functional outcomes in therapeutic settings, such as optimizing the affinity of drug conjugates to biomolecular targets. The light-induced *trans*-to-*cis* isomerization triggered the transformation from capsids to aggregates, allowing precise control over the encapsulation and release of guest molecules, highlighting the potential of photoswitchable peptides as light-responsive nanocarriers (96).

The PSS (photo-stationary state) ratio describes the proportion of molecules in the cis form vs. the trans form at that equilibrium. Precisely, after illumination with light of a given wavelength and once the system has reached equilibrium, what fraction of the molecules are found in each of the isomeric forms. The peptide's structure and function can change depending on whether it is in the *cis* or *trans* form. These properties are particularly important for controlling protein folding and unfolding, regulating binding affinity and triggering biological activity with light.

Incorporating photoswitches into peptides allows light-controlled modulation of their secondary structures, such as α -helices, β -turns, and β -hairpins, enabling precise regulation of biological activity. For example, azobenzene-based photoisomerization has been used to stabilize a β -hairpin in a peptide targeting the PD-1/PD-L1 interaction, achieving nanomolar inhibition in the *cis* form with high selectivity-demonstrating the potential of photoswitchable peptides in cancer immunotherapy (97).

1.2.4. Design and synthesis of photoswitchable peptides

The synthesis of photoswitchable peptides often employs SPPS techniques that facilitate the integration of functional photoswitches into the peptide backbone. Recent works have showcased diverse strategies in this realm. Cataldi *et al.* employed novel fluoroaromatic azobenzene derivatives that allowed the reversible photoswitching of secondary structures in response to amber light, enhancing the applicability of these systems in live-cell imaging and controlled drug delivery (98). This method demonstrates the versatility of tailored synthetic approaches for designing photoresponsive peptides.

Backus *et al.* contributed significantly to the understanding of the biophysical behaviours underpinning the photoswitching phenomenon through the implementation of 2D IR spectroscopy techniques on isotope-labelled peptides. This approach elucidated key insights into the conformational dynamics associated with light-responsive modifications, providing a deeper comprehension of how the structural alterations can yield variations in biological performance (99). Such feedback mechanisms are invaluable for refining the design principles that govern the development photoswitchable peptides for specific biomedical applications.(100)

1.2.5. Applications in biological systems

The application of photoswitchable peptides spans various realms within biological systems, particularly in strategies for antimicrobial action and the precision of drug delivery. The integration of photoswitches into peptide scaffolds has allowed for precise control over secondary and tertiary structures, supramolecular assemblies, and interactions with membranes and proteins (101). However, the use of azobenzene, which is activated by UV light, presents challenges for therapeutic applications due to limited tissue penetration and potential mutagenicity. The development of photoswitches responsive to visible light has further advanced this field. Recent research has increasingly moved away from UV-activated azobenzene photoswitches toward visible-light-responsive probes, which hold greater promise for pharmacological use (102). Activation with visible light presents a structural challenge because the photoactivatable elements originally used are primarily UV-sensitive, and it is extremely difficult to design structural modifications that shift this sensitivity into the visible range.

Photoswitchable therapeutics that operate in the red to near-infrared (NIR) range are highly appealing for biomedical applications. This is due to red light's ability to penetrate tissues more deeply, its reduced side effects, and its widespread acceptance as a non-invasive therapeutic approach—especially in fields such as (onco)dermatology (103–105).

The study by Yeoh *et al.* highlighted how the incorporation of photopharmacological triggers into cyclic antimicrobial peptides allowed for a significant enhancement in antibacterial efficacy against strains like *S. aureus* (106). This illustrates the potential of employing such responsive systems to devise targeted therapies that can effectively respond to specific cellular stimuli.

Recent advances in peptide photoswitching have highlighted the potential of visible-light-responsive systems (81) in regulating protein interactions and cell activity. One key breakthrough involved tetra-*ortho*-chloroazobenzene for cysteine-selective stapling, enabling red-light (660 nm) induced secondary structure changes and enhancing binding affinity of a p53/MDM2-inhibiting peptide by over 240-fold (107).

Another strategy used a perfluorinated azobenzene photoswitch to create a cellpenetrating peptide that shifted from disordered to helical structure under amber light (450 nm). While structurally responsive, it showed no significant cytotoxicity differences across isomer states, suggesting that further functional optimization is needed (98).

Additionally, Vázquez *et al.* developed green-light-responsive backbone photoswitches, including tetra-*ortho*-fluoroazobenzene and cyclic derivatives, to target the WDR5-MLL1 interaction—a key player in leukemia. The *trans* isomer showed 10-fold higher potency, with structural studies explaining this activity difference (75). Building on this, new visible-light-responsive MLL1 inhibitors demonstrated optochemical control of blood development in zebrafish, mimicking genetic knockdown effects (108).

Furthermore, the exploration of self-assembling peptides and hydrogels facilitated by light responsiveness has been exemplified in the work of Chan *et al* (109). Their research demonstrated how minor structural variations can result in substantial outcomes for peptide assembly and nanostructure formation, tuning the system for specific applications within tissue engineering and regenerative medicine. The ability to create a controlled environment for drug delivery vehicles or biosensors using photoswitchable systems holds profound implications for future research in tailored biomedical applications.

1.2.6. Advancements in foldamers

Foldamers are synthetic oligomers designed with the ability to fold into specific three-dimensional structures (110). Unlike natural α peptides, foldamers are resistant to enzymatic degradation and can be precisely engineered without relying on biological folding rules. Incorporating photoswitches like azobenzene enables reversible structural modulation under light, making foldamers promising tools for applications such as ion transport, drug delivery, and biomolecular recognition (111–113).

Notable studies in this area have focused on harmonizing the unique properties of foldamers with azobenzene or other photoswitches to develop stimuli-responsive systems. Zschau and Zacharias documented the intricate folding dynamics of azobenzene-modified foldamers, showcasing their utility in generating responsive materials that can adapt to environmental signals (114). This advancement continues to propel the application landscape of foldamers, particularly concerning their utility in living systems and synthetic biology.

Martins *et al.* investigated the functionality of photoswitchable calixarene activators and their ability to modulate peptide transport across lipid membranes with high efficiency (115). This dynamic capability emphasizes the potential for not only enhanced drug delivery mechanisms but also the broader implications for biological compatibility and molecular recognition in therapeutic contexts. Such efficiencies enable researchers to develop safer and more effective delivery systems for therapeutic agents, ultimately enhancing treatment outcomes in clinical settings.

1.2.7. Biomedical application of photoswitchable foldamers

Bioinspired photoswitchable foldamers have been developed to control chloride ion transport through light-induced structural changes. Chiral aryl-triazole foldamers with azobenzene units can reversibly bind and release chloride ions in nonaqueous environments. UV light induces a *trans*-to-*cis* isomerization, weakening chloride binding by up to 10-fold, while visible light restores binding ability (116). Inspired by halorhodopsin, these foldamers use hydrogen bonding to stabilize a helical, β -sheet-like structure, achieving up to an 84-fold difference in chloride affinity through light-driven conformational changes (Figure 3) (117).

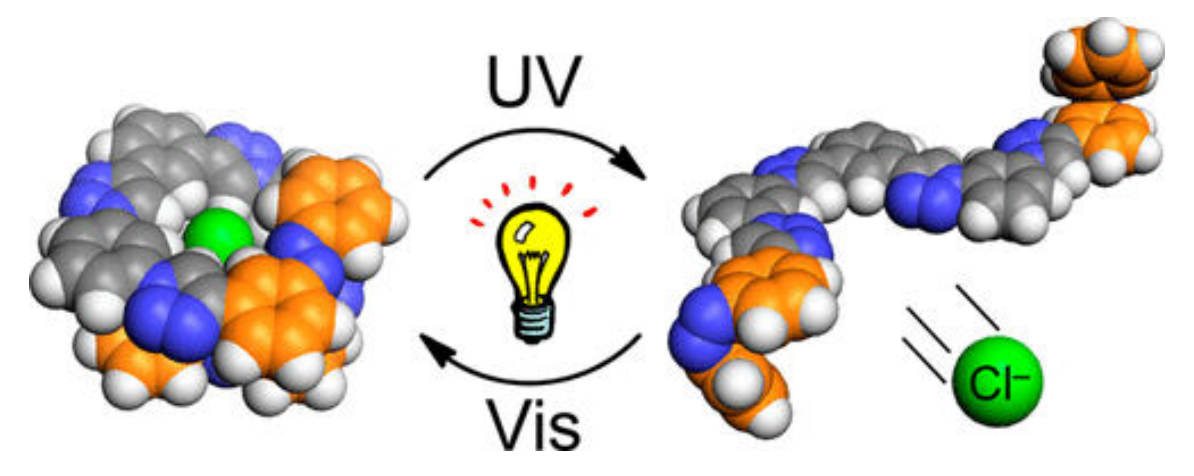


Figure 3. Illustration showing the light-triggered binding and release of chloride ions by a photoresponsive foldameric receptor (117).

Further advancements include C_2 -symmetric foldamers that self-assemble into chloride-templated helices, with their structural equilibrium tuneable by solvent, temperature, and concentration. Sequence modifications influence foldamer stability, highlighting the role of solvophobic π -stacking and anion-stabilizing residues in helix

formation (118). These systems offer significant pharmacological promise, particularly for treating ion imbalance disorders like cystic fibrosis and epilepsy. Their light-responsive behaviour allows for targeted, reversible activation, reducing off-target effects and enabling applications in neuromodulation, optopharmacology, and photoactivated drug delivery (119,120).

Photoswitchable foldamers, capable of light-triggered structural changes, offer exciting potential in drug delivery, targeted therapy, and molecular sensing (8). Systems incorporating hydrogen-bonding units and tetrafluoroazobenzene can fold into spherical structures with tuneable chiroptical properties under visible light, enabling spatiotemporal drug control (121).

Light-responsive vesicles made from α -cyclodextrin and azobenzene foldamers have demonstrated reversible disassembly and enantioselective release of propranolol, favoring the R-isomer-highlighting their utility in precision medicine (122).

These foldamers can also mimic protein unfolding mechanisms, allowing optomechanical drug activation and controlled enzymatic catalysis, relevant for neuromodulation and targeted degradation (123). In tissue engineering, foldamers modulating integrin-RGD interactions enable light-regulated cell adhesion, supporting adaptive biomaterials (124).

Finally, foldamers engineered to simulate prion-like aggregation offer tools for studying neurodegenerative diseases like Parkinson's, where light-induced conformational changes control α-synuclein aggregation (125).

2. Objectives

The main two topics I have been working on were AuNCs and photoswitchable peptides and foldamers

One of my objectives was to create a comprehensive, manually curated, and freely accessible database dedicated to biomedical research involving AuNCs. During its development, we aimed to achieve three primary goals: (*i*) it should be freely accessible; (*ii*) the database should have a user-friendly interface; and (*iii*) it should include a help section containing all the necessary information about the database. We aimed to collect five key pieces of information from the articles: the application, particle size, cell line, and excitation/emission wavelengths. Where TOC (Table of Contents) graphics were available, we included them as well. A database was created, named BioGoldNCDB (Bio = biomedical, NC = nanocluster, DB = database).

Additionally, we wanted to expand our database with information from Chemical Abstracts Service (CAS) database (https://www.cas.org/) by the use of SciFindern (https://scifinder-n.cas.org/).

Currently encompassing 247 articles from 104 peer-reviewed journals, BioGoldNCDB provides a user-friendly web interface that supports multiple device formats, including smartphones, tablets, and personal computers. The database allows users to filter content based on diverse criteria, enhancing accessibility and usability for both newcomers and experienced researchers. As such, BioGoldNCDB serves not only as a practical entry point into the field of AuNCs but also as a valuable tool for data-driven insights and cross-disciplinary collaboration.

My other goal was to gather the latest findings related to photoswitchable foldamers and peptides. In this field, photoswitchable molecules offer a powerful approach to precision medicine by enabling reversible conformational changes between active and inactive states. This light-controlled modulation enhances targeted drug delivery, molecular sensing, and the development of photoresponsive biomaterials and optical devices.

These dynamic systems have significant potential for creating "smart" therapeutics and biomaterials that adapt to environmental effects, revolutionizing biomedical applications. Advances in light-responsive technologies and nanotechnology continue to expand their applications, driving innovation in precision medicine and materials science. As research

progresses, these systems are set to transform drug delivery, diagnostics, and next-generation biomaterials.

3. Methods

3.1. Data collection and processing

BioGoldNCDB comprises manually curated and annotated entries of AuNCs sourced from scientific literature. The initial dataset was compiled using the keyword "gold nanocluster" in the Chemical Abstracts Service (CAS) database (https://www.cas.org/) via SciFinderⁿ (https://scifinder-n.cas.org/).

To refine the search, filters were applied to include English-language journal articles published between 2000 and 2024, specifically focusing on diagnostic and pharmacological applications. Review articles were excluded, narrowing the results to 3,577 publications. A final filter retained only articles whose abstracts contained the term "cluster", resulting in a focused selection of 247 articles.

Six additional manually curated fields were added to each entry: application, cell line, particle size, excitation/emission wavelength, nanobioconjugates, and where it was available table of contents (TOC) graphics. Each article was individually reviewed, and only those directly related to gold nanoclusters were included in the final database. The search was completed on June 27, 2024.

Another search was made for the photoswitchable peptides and foldamers. We used CAS database through SciFinderⁿ too. Two main keywords were added as "photoswitchable" and "peptides".

The query date was August 8, 2024. The first selection was made based on content criteria. Furthermore, we considered it important that the photoactivatable element incorporated into the structure of peptides and foldamers should induce a conformational change. Based on these two criteria, we selected the 30 most relevant articles and summarized it in a mini review.

3.2. Database design and implementation

The BioGoldNCDB web interface was created using Next.js and React for the front end (126), while the back-end processes are handled within a Node.js environment (127). Data is stored in a MySQL relational database, and queries are executed using MySQL commands (128). The spreadsheet-style data visualization on the webpage was developed using the EZGrid React DataGrid component (129). Both the website and the database are hosted on DigitalOcean's cloud infrastructure (130).

4. Results

4.1. Analysis of the manually added columns data in BioGoldNCDB

4.1.1. Application

A report was made for the application of the AuNCs. After data analysis four main group was created: drug delivery, therapy, imaging and other biomedical application. Some studies do not detailed the potential biomedical field, these data were counted in other biomedical application. In several cases, multiple possible applications were given for the AuNCs, for example therapy and imaging. We included all of them separately in the categories. In 3 % of the cases no data was provided (Figure 4.).

Imaging and therapy are the most relevant fields where AuNCs can be promising candidates

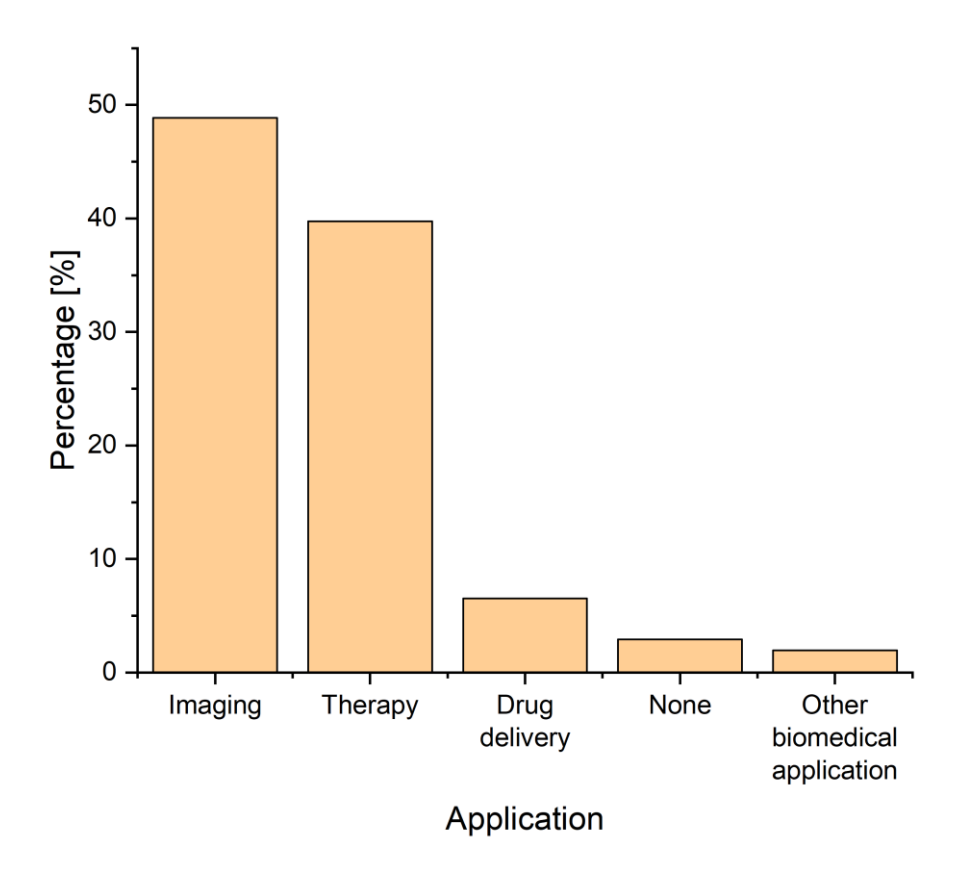


Figure 4. The distribution of the application fields for AuNCs.

Therefore, a more detailed separation was made for therapy (Figure 5.) and imaging (Figure 6.).

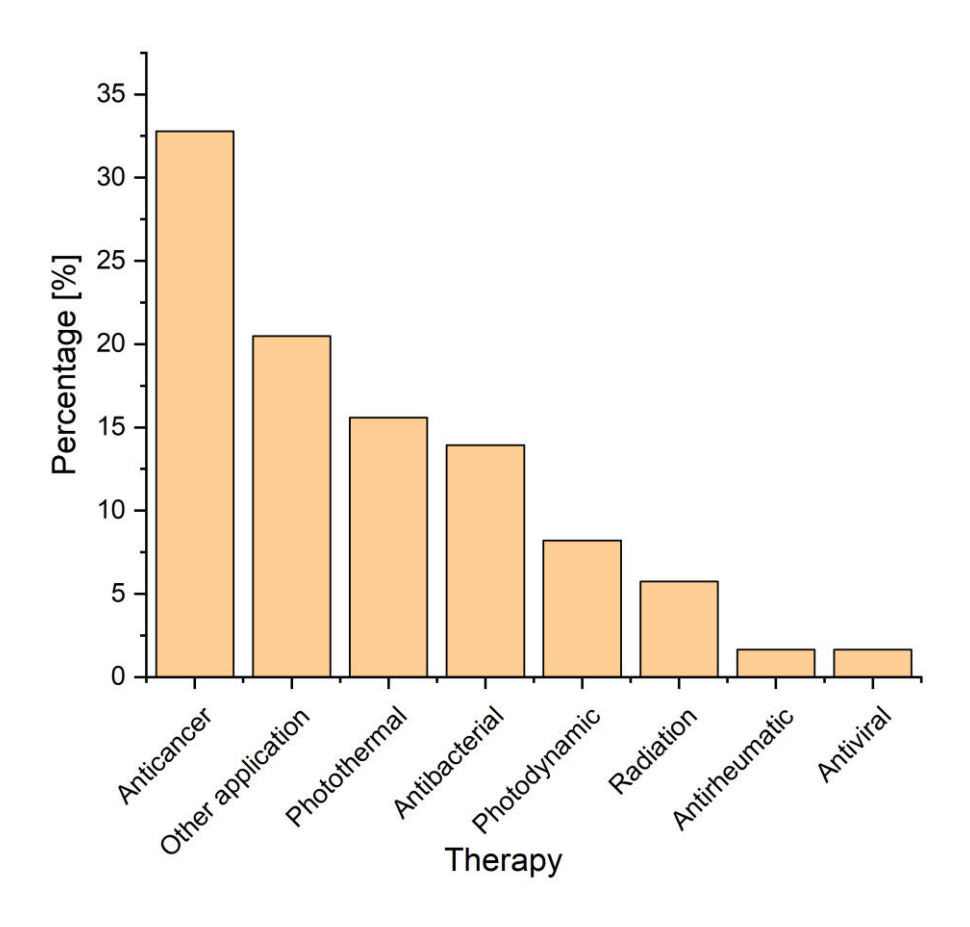


Figure 5. A more detailed classification of AuNCs' therapeutic applications.

In therapy, AuNCs can be effective in anticancer, antibacterial, photothermal and photodynamic fields.

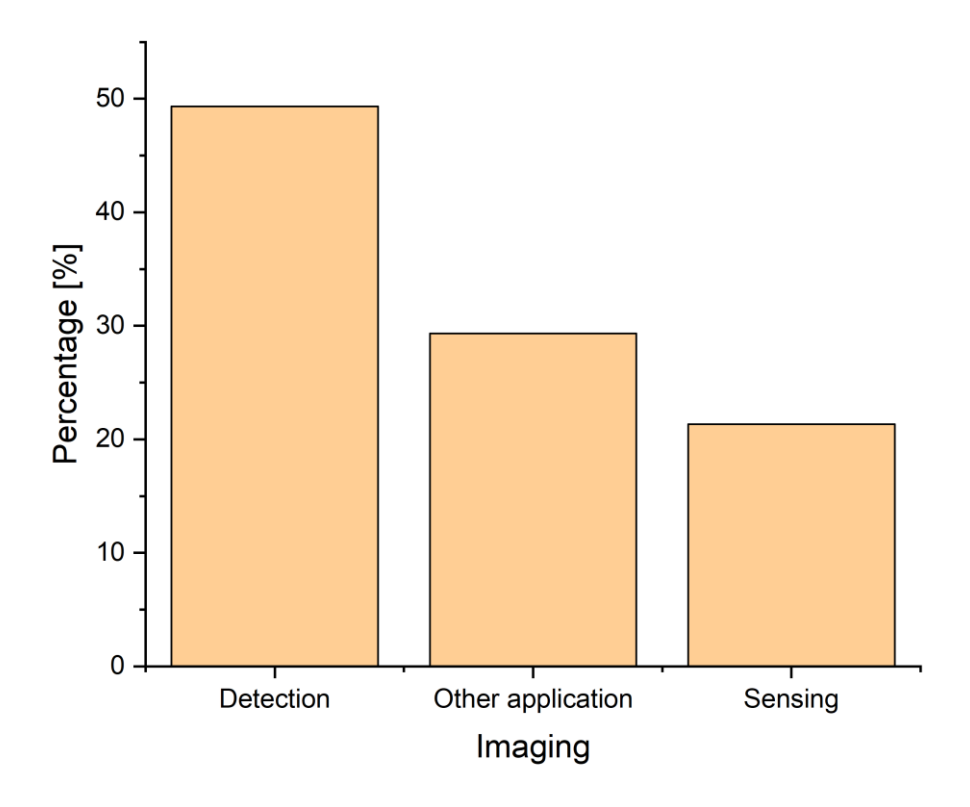


Figure 6. A more specific separation for imaging.

While in imaging ~half of the cases AuNCs were used for detection, which is for imaging in live organs. Third of the cases were used for *in vitro* sensing.

4.1.2. Cell line

A collection was made for the different cell lines where the AuNCs were tested on. The most common ones are shown in Figure 7. There were a lot of promising experiments on MCF-7, HeLa, HepG2 and A549 cell lines.

Also, it must be highlighted that AuNCs were getting positive results in antibacterial therapy, against with *E. coli* and *S. aureus*.

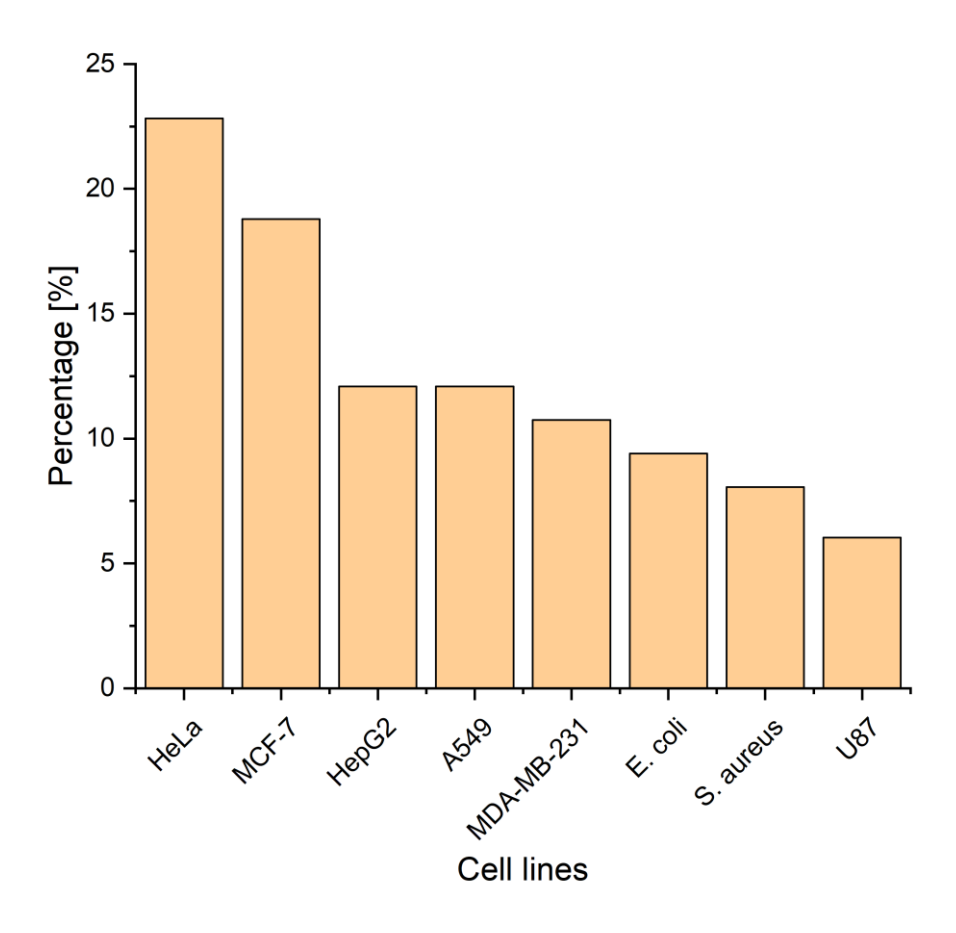


Figure 7. The most common cell line types in BioGoldNCDB.

4.1.3. Particle size

Figure 8 shows the size distribution of AuNCs. The primary aim of data collection was to determine the size of the gold core; however, in many cases only nanobioconjugate sizes were reported, or the core size was not specified. Among AuNCs, 28% are smaller than 2 nm, while related nanoparticles account for nearly half of the entries (30% between 2–10 nm and 18% between 10–50 nm).

In the literature, the size range of gold nanoclusters is not always clearly defined. When gold nanoclusters are defined as being smaller than 2 nanometers, this usually refers to the gold core itself. In many studies the size of the entire nanoparticle, including ligands and cargos, is reported, which may differ from the 2 nm threshold. The core size can be determined by TEM measurements, whereas DLS measurements generally provide the size of the whole molecule.

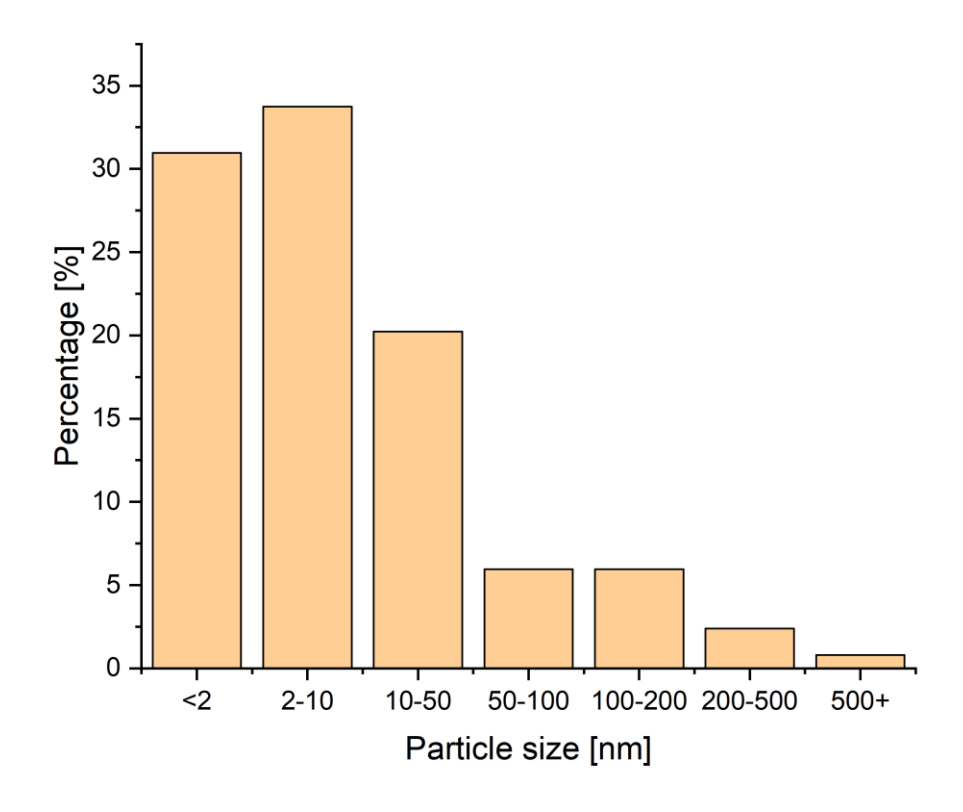


Figure 8. The distribution of the complete particle sizes found for the BioGoldNCDB entries given in nm.

4.1.4. Excitation/emission wavelength

Excitation and emission wavelength data were extracted from the articles and are presented separately in Figures 9 and 10. Most excitation wavelengths fall within 400–500 nm, while emission wavelengths are mainly in the 600–700 nm range.

Notably, excitation data were missing in 33% of cases and emission data in 39%. In some studies, AuNCs were combined with additional metals to form hybrid structures; these were excluded from the analysis, as the conjugated metals alter the properties of gold and would modify the statistical outcomes.

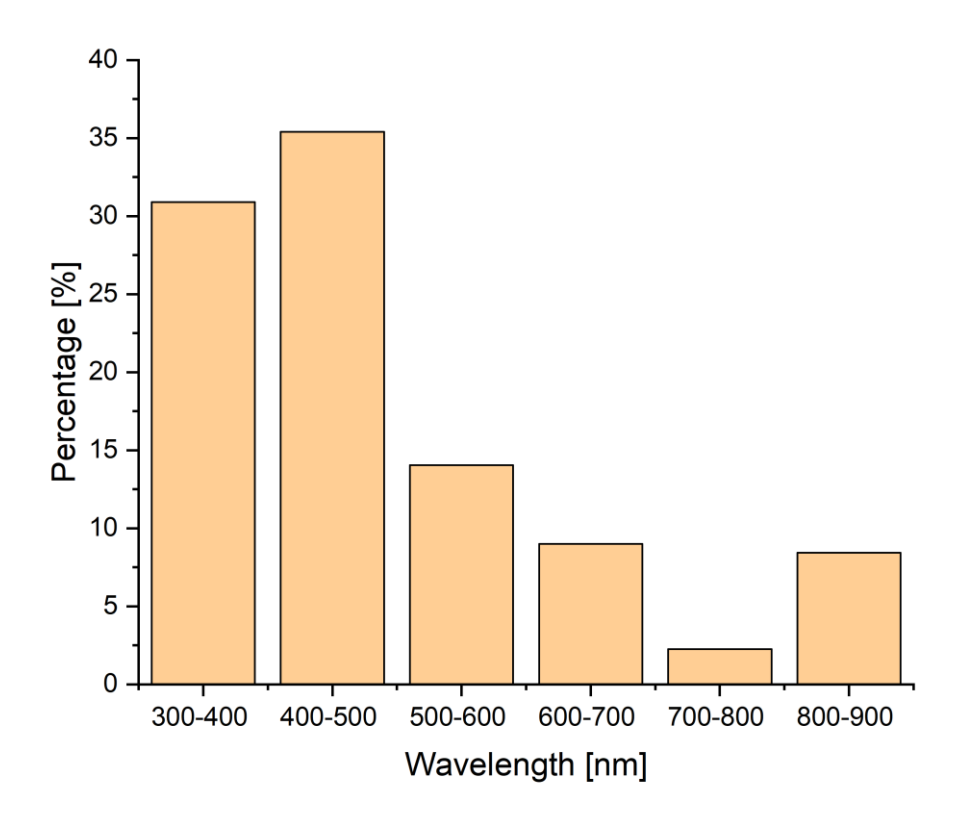


Figure 9. The range of excitation wavelengths reported in the BioGoldNCDB entries.

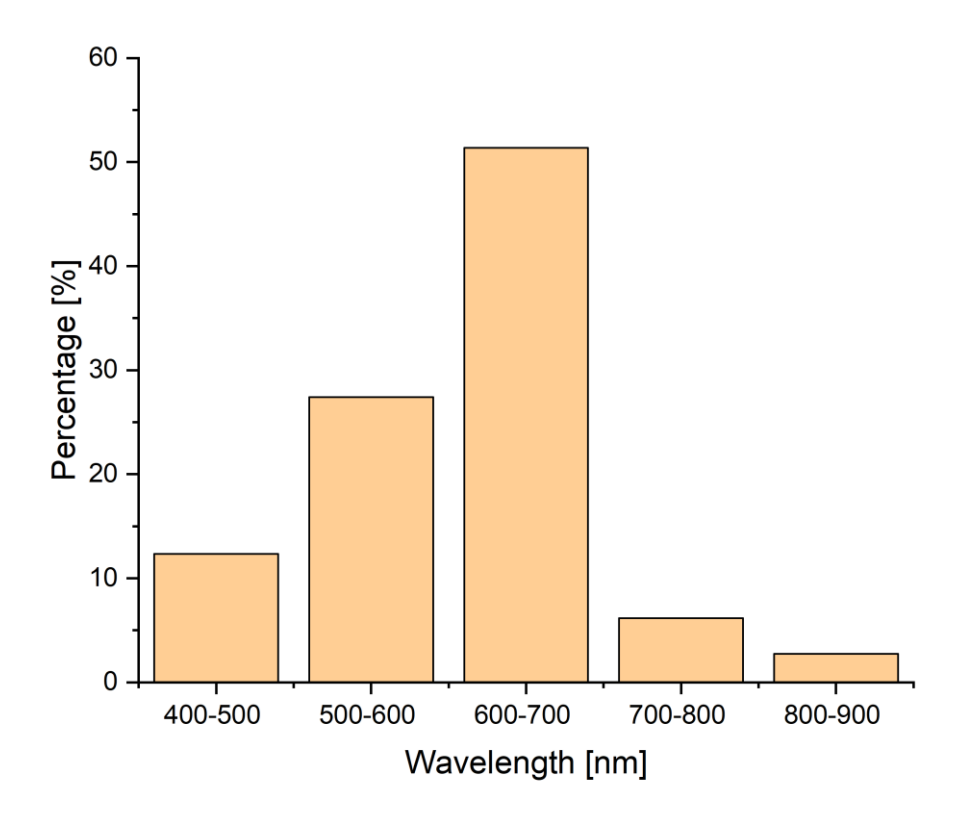


Figure 10. The distribution pattern of emission wavelengths recorded in BioGoldNCDB.

4.1.5. Nanobioconjugates

Nanobioconjugates can be divided in two main parts. One of them is for the stabilization of the AuNCs, while the other, also known as cargos, is take part in the functionalization, therefore responsible for the final properties of the AuNCs.

The surface ligands of AuNCs are crucial for their stability, photophysical properties, and interactions with biomolecules. Thiols and their derivatives are the most commonly used stabilizing agents. However, it is worth to highlight glutathione (GSH) because it can be used both for stabilization and as cargo molecule (Figure 11.).

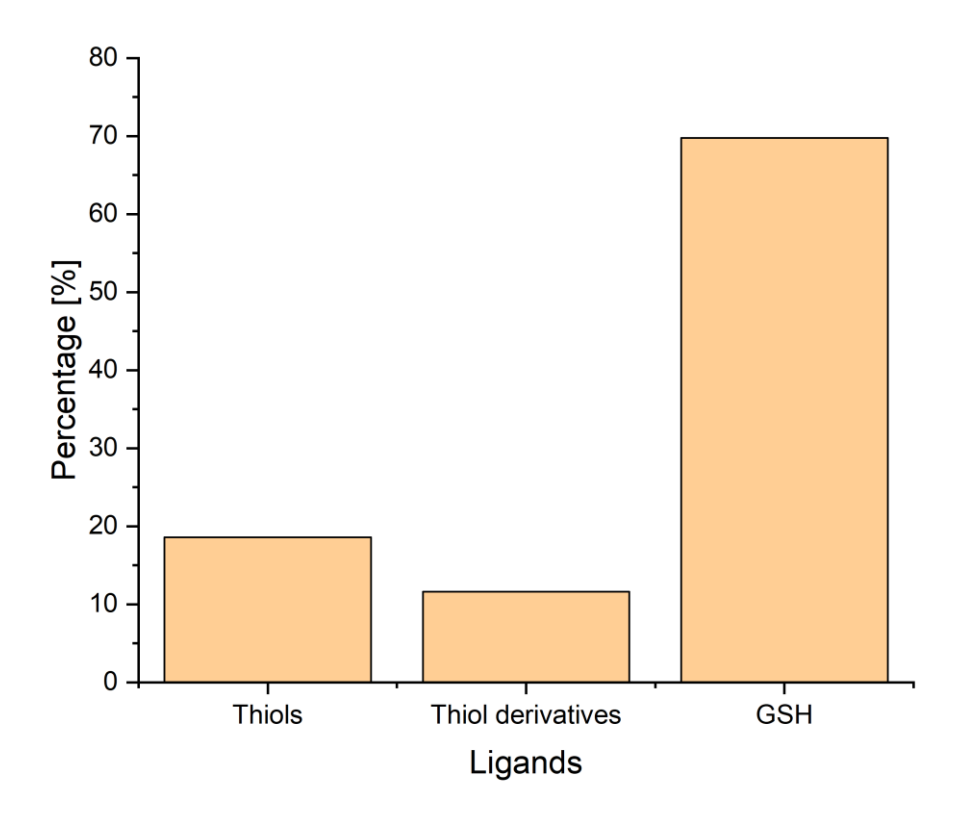


Figure 11. The distribution of ligands in BioGoldNCDB's entries.

Through covalent or noncovalent conjugation, additional biomolecules or cargo molecules can be attached to AuNCs, creating nanobioconjugates with enhanced functionality, targeting ability, and biological activity. Among such cargos, peptides and proteins are most frequently employed, though oligonucleotides and drug molecules are also widely used (Figure 12.).

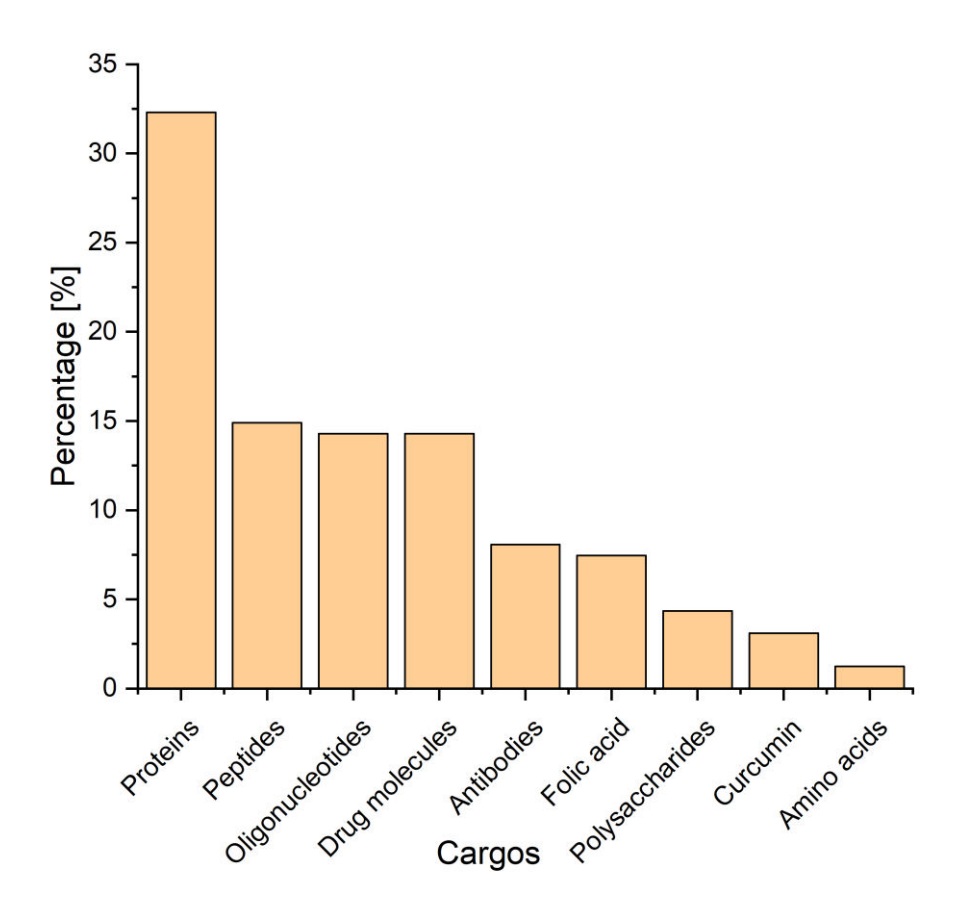


Figure 12. The distribution of cargo molecules in BioGoldNCDB's entries.

4.2. Photoswitchable peptides and foldamers

A summary table was made from the collected articles and reviews. All the sequences were assembled with their structural changes, and the characterization techniques they were verified by. The photostationary state ratio (PSS) in photoswitchable molecules refers to the proportion of isomers (usually *cis* and *trans*) that exist at equilibrium under constant irradiation with light of a specific wavelength. Where PSS ratio was provided, we added them too. Table 1 contains the photoswitchable petides, while Table 2 is for photoswitchable foldamers (131).

Reviews were excluded from the tables.

Table 1. Visible-Light-Photoswitchable peptides. PSS: photostationary state; X: incorporated photoswitch; n.p.: data was not provided.

Entry	References	Peptide sequences	PSS ratio	Structural change between foldamers and peptides	Characterization technique
1	100	CS-VIPs	cis: trans mixture in a ratio ~1:10	peptide macrocycle secondary structure modification	UV/VIS
2	98	Boc-S(tBu)-A-R(Boc) ₂ -A-OH H ₂ N-oF4Azo-V-H(Trt)-l-R(Boc) ₂ - K(Boc)-S(tBu)-CONH ₂ azobenzene containing oligomer	cis/trans 84:16	peptide macrocycle secondary structure modification	HPLC-MS and HRMS (ESI)
3	102	meta-phenylene ethynylene (mPE) azobenzene containing oligomer	E: helical Z: randomized	helix-to- random coil transition	n.p.
4	89	α-helical peptide LK1 X=Decafluoroazobenzene (DFAB)	cis→trans: 86% trans→cis: 89%	amphiphilic helix (α-helix)	UV/VIS, NMR
5	91	T1 and T2 peptide azobenzene containing oligomer	azobenzene Z/E isomerization	random to β- sheet	UV VIS
6	116	c(RGDfK) peptides azobenzene containing peptides	cis/ trans isomerization	secondary structure modification	UV/ VIS, NMR, MS
7	92	Ac-GKKLLACLLAALLAALLC- ALLKKA-NH ₂ X=4,4'-bis(chloroacetamide)- azobenzene	53% cis/47% trans PSS after 365 nm illumination, 4% cis/96% trans PSS after 447 nm illumination	helix to random conversion	FTIR, CD, UV/ VIS
8	88	WHFSYNWRWLPP AMPP, azobenzene containing peptide	n.p.	random to turn	UV/ VIS
9	99	p53/MDM2 inhibitor peptide (PMI; TSFAEYWNNLSP) X=tetra-ortho-chloro azobenzene	Azobenzene Z/E isomerization trans→cis: 82% cis→trans 92%	n.p.	¹ H and ¹⁹ F NMR, UV/ VIS, HPLC

Table 2. Visible-Light-Photoswitchable foldamers. PSS: photostationary state; X: incorporated photoswitch; n.p.: data was not provided.

Entry	References	Peptide sequences	PSS ratio	Structural change between foldamers and peptides	Characterization technique
1	112	Aib foldamers	n.p.	right and left-handed helicity interconversion	¹⁹ F NMR, ¹ H NMR
2	104	aromatic oligoamide sequence X= diazaanthracene-based aromatic β-sheet flanked	n.p.	helix to random geometry covalent bond rearregament	NMR and crystallographic studies
3	108	aryl-triazole foldamer azobenzene containing foldamer	n.p.	trans: helical	UV/ VIS
4	8	oligo(meta-phenylene ethynylene)s (OmPe) foldamers azobenzene containing foldamer	Azobenzene Z/E isomerization	trans → cis: disrupts the helix cis → trans: original helical conformation restored	¹ H NMR spectroscopy, CD, UV/ VIS, electrospray ionization (ESI) MS,and GPC
5	105	H-bonded amide macrocycle based ligjht controlled, host-guest system	spiropirane	n.p.	1D, 2D NMR
6	109	foldamers trapping Cl ⁻ ion azobenzene containing foldamer	cis – trans: ~32%	β-sheet-like H-bonds that interlock the ends of the foldamer to the central helix	NOESY ¹ H NMR, CD, UV/ VIS
7	117	Boc-Ala-DZbAla-Val-DZbAla- Leu-OMe (Z,Z), (E,E) dehidro β-alanine	(Z,Z) → (E,E): 75%	fast β -sheet transition $(Z,Z) \rightarrow (E,E)$	ECD, UV/ VIS
8	103	β-amino acid, (Z)-3-aminoprop-2- enoic acid foldamers X= 3-aminoprop-2-enoic acid	(E) and (Z) are present in a 30%: 70% molar ratio	helix to β-sheet interconversion	¹H NMR
9	87	β -annulus peptide (H-INHVGGTGGAIMAP-Azo- VTRQLVGS-OH) azobenzene containing peptide	cis/trans ratios: trans-rich form: 24/76, cis-richform: 81/19	random coil to β-sheet interconversion	UV/ VIS, ¹ H NMR, CD
10	84	[Pro7,Asn8,Thr10] X= azobenzene containing foldamer	n.p.	random to turn interconversion	¹ H/ ¹³ C/ ¹⁵ N NMR, UV/ VIS
11	113	Peptide based foldamers containing Azobenzene element	cis: ~80 % trans: ~85 %	linear to helical conversion	¹ H/ ¹³ C NMR (NOESY, HSQC), HPLC
12	111	azobenzene containing foldamer X= azobenzene and phenyl-1,2,3- triazole motif	trans→cis: 80% cis→trans 77%	linear to helical conversion	¹H NMR (NOESY)
13	114	M-helical quinoline oligoamide foldamer X= α-cyclodextrine and an azobenzene	azobenzene Z/E isomerization	Vesicle formation is controlled	UV/ VIS
14	115	aromatical oligomer containing azobenzene	cis: ~20-37%	helical to linear interconversion	1H NMR, MALDI-TOF MS, GPC, CD

I was participating in some synthesis of molecules that are not completely identical but essentially similar. Two of them worth to highlight, due to their scructural properties.

Phthalazin-1(2*H*)-one exists as a tautomeric mixture in which the exocyclic double bond can shift onto the benzocondensed heteroring (Scheme 1), accompanied by migration of the nitrogen-bound hydrogen to the oxygen atom. In the lactim tautomer, the heteroring retains its aromaticity, but the resulting hydroxy group is less nucleophilic, leading exclusively to N-alkylation, as observed in all cases.

Scheme 1. The tautomer forms of phthalazin-1(2H)-one.

Comparison of reaction methods (oil bath heating vs. microwave irradiation, MW) and reaction times provides several insights. Due to the higher molecular mass of the substrate, a larger solvent volume was required. Conventional oil heating with Na₂CO₃ and 1 mmol CaCl₂ in 99% propylene carbonate (PC) gave a yield of 28% (Table 3, entry 1, Scheme 2). By contrast, four hours of MW irradiation increased the yield to 50% (Table 3, entry 2), confirming the superior efficiency of MW heating. Further optimization, reducing the reaction time to 2 h and using 99.7% PC, yielded 2-(2-hydroxypropyl)phthalazin-1(2*H*)-one in 55% yield without the need for a drying agent (Table 3, entry 3). This alkylated product is a novel compound, and the results consistently highlight that water exclusion is critical for achieving efficient N-alkylation.

Scheme 2. The N-alkylation reaction of phthalazin-1(2*H*)-one.

Table 3. N-Hydroxyalkylation of phthalazin-1(2*H*)-one.

Entry	Heating	PC (mmol/%)	Na ₂ CO ₃	T (°C)	Time (h)	CaCl ₂	Yield (%) 10
1	oil bath	12/99%	1 mmol	170	4	1 mmol	28
2	MW	12/99%	1 mmol	150	4	1 mmol	50
3	MW	12/99.7%	1 mmol	150	2	none	55

The substrate contains three nitrogen atoms at positions 1, 2, and 3, and occurs in two isomeric forms: 1*H*- and 2*H*-benzotriazole (Scheme 3). The electron-withdrawing nature of the nitrogens makes the adjacent hydrogens readily deprotonatable, generating nucleophiles that can be alkylated with propylene carbonate (PC). The 2-hydroxypropyl side chain introduced during N-alkylation is sterically bulky, making the formation of dialkylated benzotriazole unlikely.

Moreover, because the nucleophile generated at N1 is more stable than that at N2, alkylation is expected to occur preferentially at the N1 position. However, we sought to determine experimentally whether N-alkylation occurs at all.

Scheme 3. Two isomeric forms: 1*H*- and 2*H*-benzotriazoles.

Our experimental results are summarized in Table 4. The data show that N-alkylation can take place at both nitrogen atoms (Scheme 4), with the N1-alkylated product consistently obtained in higher yield than the N2-alkylated product. Using PC with a drying agent and conventional oil-bath heating, we achieved 22% yield of 1-(2H-benzotriazol-2-yl)propan-2-ol and 47% yield of 1-(1H-benzotriazol-1-yl)propan-2-ol. Under identical conditions but with microwave irradiation, the yields of both products increased (entry 2). As anticipated, the best outcome was obtained under MW conditions

with high-purity PC and no drying agent (entry 3). Consistently, N1-alkylation (product 15) gave higher yields (47–55%) compared to N2-alkylation (product 14, 22–35%) (132).

Scheme 4. Results with benzotriazole.

Table 4. N-Alkylation of 1*H*- and 2*H*-benzotriazole.

Entry	Heating	PC (mmol/%)	Na ₂ CO ₃	T (°C)	Time (h)	CaCl ₂	Yield (%) 14,15
1	oil bath	9/99%	1 mmol	170	3	1 mmol	22, 47
2	MW	9/99%	1 mmol	150	3	1 mmol	25, 53
3	MW	9/99.7%	1 mmol	150	4	none	35, 55

5. Discussion

5.1. Database overview

The BioGoldNCDB search function enables efficient navigation of the database through a range of search criteria, covering gold nanoclusters from 247 published studies. Users can search by keywords linked to AuNC properties, particle size, and biomedical applications, while advanced filters allow refinement by size, surface modifications (nanobioconjugates), and other parameters. Integration with SciFinder provides supplementary information, with additional options to narrow results by CAS numbers, journal titles, or identifiers. This flexibility allows researchers to quickly access relevant data to support applications in drug delivery, imaging, and diagnostics. The database serves both newcomers and experienced researchers, with content organized into four main categories: manually curated data, bibliographic information, identifiers, and metadata for straightforward navigation. BioGoldNCDB also offers an intuitive, responsive interface with column sorting, filtering, inline editing, and features such as keyboard navigation, drag-and-drop, and export tools, ensuring seamless exploration and management of large datasets (133).

Link for the database: https://biogoldncdb.ladon.life/

5.1.1. BioGoldNCDB's help desk

The help desk found under the useful information menu contains all the information available in the database, detailing their exact definitions.

Six manually added data:

- Application: Field in which AuNCs may be applied.
- Cell line: Cell culture model used to test AuNC activity.
- Particle size: Reported in nanometers (nm); includes both gold core size and full nanoconjugated dimensions.
- Excitation/Emission wavelength: Excitation refers to the light wavelength absorbed by AuNCs, raising electrons to an excited state; emission refers to the wavelength released when they return to ground state.
- Nanobioconjugates: For surface modification, any molecules connected to the core for stabilizing and funcionalating the AuNCs.

• TOC: table of content graphics.

Bibliographic Information

- ID: Unique identifier assigned by the journal or database.
- Title: Article heading summarizing the content.
- Abstract: Brief overview of aims, methods, results, and conclusions.
- Authors: Researchers who conducted and wrote the study.
- Journal: Scientific journal where the work was published.
- Organization: Author affiliation (e.g., university, institute).
- Database: Online host (e.g., PubMed, ScienceDirect).
- Volume/Issue: Journal volume and issue number.
- Page numbers: Pages where the article appears.
- Publication date: Date of release in the journal.

Identification

- Concepts: Core themes of the article.
- CAS Numbers: Unique identifiers for referenced chemical substances.
- Keywords: Indexing terms improving discoverability.
- Accession number: Database-specific article identifier.
- CAN: Identifier for the Chemical Abstracts Service abstract.
- Section: Journal section (e.g., research, review).
- Section cross-reference: Link to related sections.

Identifiers

- CODEN: Six-character code identifying the journal.
- DOI: Permanent digital identifier for the article.
- Journal code: Abbreviation of the journal title.
- PubMed ID: Identifier assigned in PubMed.
- MeSH terms: Standardized Medical Subject Headings used by MEDLINE/PubMed.

5.1.2. Examples

Below are brief examples of search options available in BioGoldNCDB:

- 1. Free Text Search A keyword-based search that scans multiple database fields, including BioGoldNCDB ID, CAS number, PubMed ID, author, article title, organization, journal name, and year of publication sown on Figure 13a and b.
- 2. Simple Search Enables targeted searches based on specific criteria such as application, cell line type, particle size, nanobioconjugates, and excitation/emission wavelengths.
- 3. Multi-Criteria Search Allows users to combine several parameters simultaneously within BioGoldNCDB, enabling more precise and tailored searches.

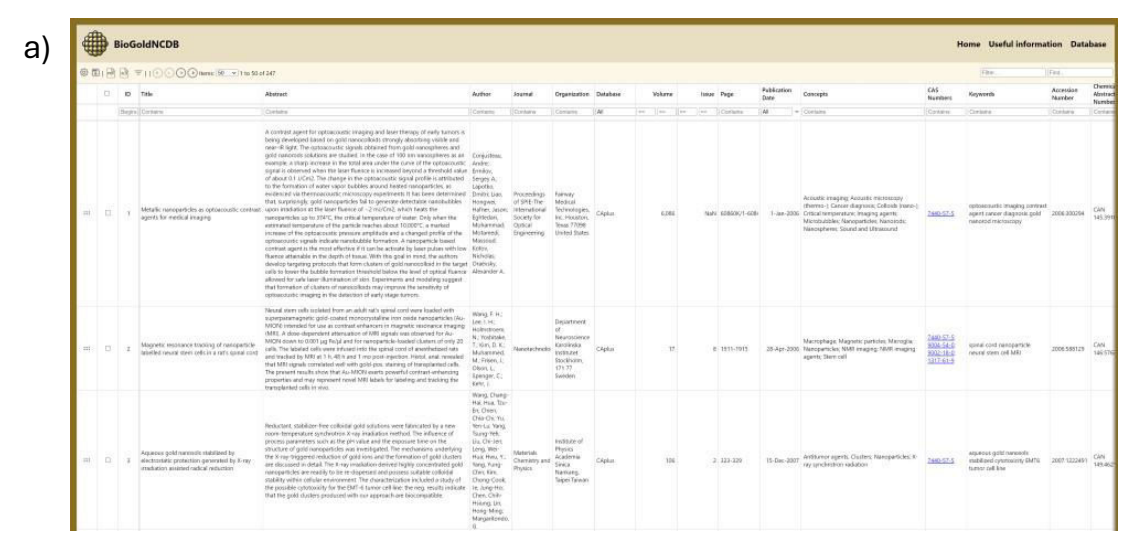




Figure 13. Layout of BioGoldNCDB, showing database entries (a, b) with searchable columns and various filtering options Firstly, the most relevant bibliographic information can be found, then other important identifiers and finally the manually curated data.

The platform offers multiple user-friendly features. Users can filter data within specific columns (e.g., entering anticancerin the "application" column) or perform a comprehensive keyword search across the entire database. Results can be exported in PDF or Excel format, and applied filters can be saved. For instance, searching for anticancer yields 39 entries of AuNCs with anticancer properties (Figure 14).

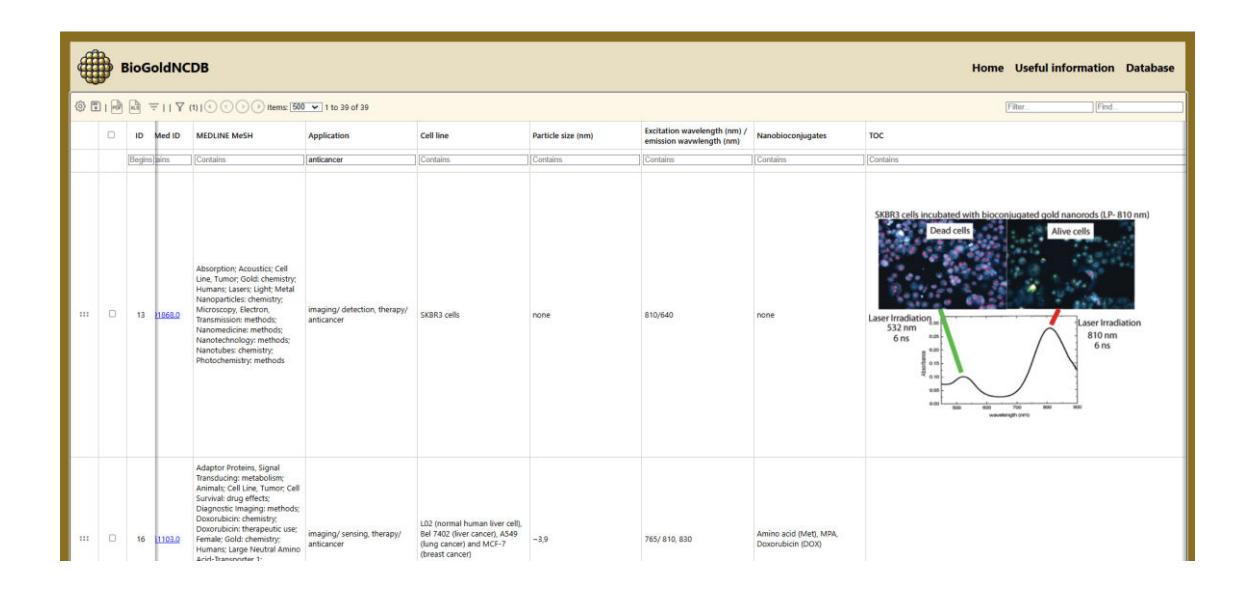


Figure 14. Illustration of the BioGoldNCDB single search opportunity.

BioGoldNCDB also supports multi-criteria searches; for example, combining anticancer with the HeLa cell line narrows the results to just five entries (Figure 15).



Figure 15. Illustration of the BioGoldNCDB multi-criteria search.

With 247 curated entries from 104 journals, BioGoldNCDB stands as the first comprehensive database dedicated to gold nanoclusters, showcasing their promising role in biomedical research.

5.2. Photoswitchable peptides and foldamers

In the mini-review the most recent photoswitchable peptides and foldamers related articles and reviews were collected in. This mini-review wanted to highlight the photoswitchable peptides and foldamers as promising next-generation tools in pharmacology, offering potential in drug delivery, precision medicine, optopharmacology, and responsive biomaterials. Their capacity for reversible, light-induced structural changes allows precise control over molecular and cellular processes, opening new avenues for light-activated therapies with exceptional spatial and temporal accuracy.

Photoswitchable peptides and foldamers leverage chromophores like azobenzene to achieve precise optical control over biological functions. Recent advances in their design—often via SPPS—enable reversible, light-triggered conformational changes that modulate biological interactions, such as enzyme activity and muscle contraction, without degradation over repeated cycles. Spectroscopic tools like 2D IR have deepened our understanding of their dynamic behaviour. Chemical modifications of related building blocks, such as pyridazinone and triazole derivatives, were performed using PC both as a solvent and as a reagent. Importantly, N-alkylation was achieved without the use of genotoxic reagents.

Peptides integrated with photoswitchable units can change their conformation under light, enabling controlled biological activity. Examples include azobenzene-based designs that influence enzyme interactions and muscle contraction. These peptides are robust over multiple light cycles and hold potential for diagnostic and therapeutic use. Recent designs also offer fine-tuned control in live cells, emphasizing their biomedical versatility.

Foldamers—synthetic, foldable oligomers—are resistant to enzymatic degradation and can be engineered with light-responsive elements. Incorporating azobenzene enables precise, reversible control over their structure and function. Foldamers have been used for ion transport, drug delivery, and recognition tasks.

Studies show that foldamers can adapt to environmental changes, form membranecrossing structures, and exhibit advanced molecular recognition. Light-regulated systems have been developed for chloride ion transport, showing efficacy in models of cystic fibrosis and epilepsy (Figure 16). Some foldamers mimic biological processes like protein unfolding and aggregation, offering tools for neuromodulation and neurodegenerative disease research.

These molecules have demonstrated potential in enhancing antimicrobial activity, guiding self-assembly in tissue engineering, and enabling responsive drug delivery systems. The incorporation of photoswitchable elements into foldamers has their field of utilization, particularly in drug transport and molecular recognition, offering fine-tuned responses to environmental stimuli.

Innovative systems, such as photoswitchable calixarene activators, have shown effective control over peptide transport across lipid membranes, improving biological compatibility and therapeutic targeting.

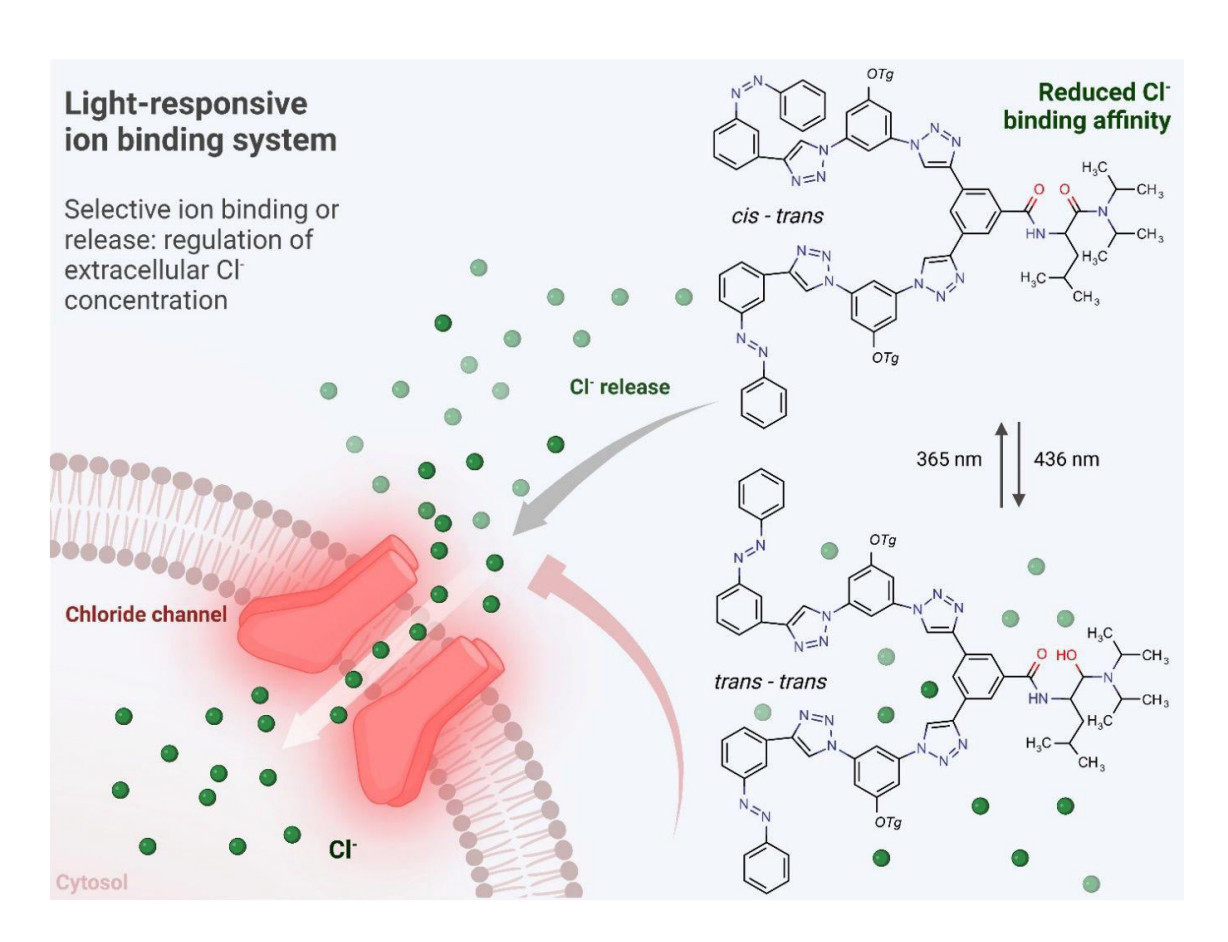


Figure 16. The Z/E isomerization of an azobenzene unit enables a foldameric host system to regulate the binding and release of chloride ions in response to light stimulation (131).

6. Conclusions

Bionanotechnology has rapidly advanced by combining chemistry, physics, biology, and medicine with nanotechnology, leading to significant innovations. Metallic nanoparticles, due to their unique properties and capability to be functionalized, are pivotal in biomedical applications such as diagnostic imaging, biosensing, sample preparation, and therapy.

AuNCs, comprised of a few dozen atoms, have gained significant attention in nanochemistry and nanotechnology. AuNCs are a unique subclass of gold nanoparticles with core sizes of ≤2 nm, exhibiting quantum and molecular-like properties. Their ultrasmall size leads to distinct optical, electronic, and catalytic behaviours due to quantum confinement effects. AuNCs are synthesized with specific ligands that stabilize them and enhance their properties. These properties, along with their biocompatibility and photostability, make AuNCs suitable for a diversity of biomedical applications, like bioimaging, enzyme-mimicking activity, and antimicrobial actions. Recent studies have highlighted their potential in various fields such as in therapy, especially in anticancer and antimicrobial therapy, in imaging, in diagnostics and in immunotherapy.

BioGoldNCDB is a freely available, manually curated database that compiles extensive information on AuNCs, their conjugates, and relevant literature. Each entry provides essential details such as the abstract, CAS number, Chemical Abstracts Number (CAN), DOI, and PubMed ID, along with biomedical applications, particle size, excitation/emission wavelengths, investigated cell lines, and nanobioconjugates used.

The database gives opportunity for complex searches. Firstly, the user can use the free text search which is a keyword-based search. Simple search can be applied on the manually added columns, where the user enters a specific keyword such as anticancer. Multiple search allows to use two or more keyword for searching and gives the result where all the criteria were matched.

The database currently covers 247 articles from 104 journals and features an intuitive, device-compatible web interface (PC, tablet, phone). Multiple filters and a help page assist users in refining their searches. While offering quick insights for newcomers, BioGoldNCDB also provides advanced researchers with a comprehensive resource on the biocompatibility, properties, and biomedical potential of AuNCs, highlighting the importance of this unique class of nanomaterials.

On the other side photoswitchable peptides and foldamers are innovative molecular systems capable of reversible conformational changes when exposed to light, opening up significant applications in drug delivery, biosensing, and therapeutic interventions.

This light-triggered behaviour, enabled by integrating photoactive components like azobenzene and spiropyrans, allows these molecules to alter their physical or chemical properties on demand. This review highlights recent progress in the design, synthesis, and practical use of these light-responsive systems, with a focus on their potential to improve drug performance and support the development of innovative medical treatments.

Photoswitchable peptides are engineered by integrating light-sensitive groups into their structures, allowing for controlled changes in shape when exposed to specific wavelengths of light. Peptides enable precise regulation of biological functions, such as muscle contraction, by controlling molecular interactions with light-offering a highly targeted approach to manipulating cellular processes. Photoswitchable peptides are commonly synthesized using SPPS, a method that enables the precise design of the peptide chains. Recent research has introduced various innovative strategies in this area.

These structures function by incorporating chromophores like azobenzene, enabling precise optical control over biological activity. Key studies have shown their ability to alter conformation and modulate biological interactions, such as enzyme binding or muscle contraction, without degrading over multiple activation cycles. Light-driven control of peptide structure enables high specificity in targeting, making them ideal candidates for responsive drug design. Advanced spectroscopic techniques like 2D IR have provided deeper insights into their structural dynamics. Using PC as both solvent and reagent enabled the modification of pyridazinone and triazole building blocks, allowing N-alkylation to be performed without hazardous genotoxic agents.

Applications in biological systems include enhancing antimicrobial activity and guiding self-assembly into functional nanostructures for tissue engineering. Foldamers have also been enhanced with photoswitchable elements, allowing them to respond dynamically to light stimuli. These adaptations have led to improvements in drug transport across membranes and fine-tuned molecular recognition. Overall, the ability to precisely manipulate peptide behaviour with light enables the development of more sophisticated, controllable platforms for biomedical applications.

Foldamers, synthetic oligomers designed to fold into specific 3D shapes, have been further enhanced by incorporating photoswitchable units, enabling them to respond to external stimulation. Recent studies have demonstrated their potential to create materials that can adapt to environmental effects and expands the applications of foldamers, particularly in synthetic biology and living systems. Other studies investigated photoswitchable calixarene activators, which effectively modulate peptide transport across lipid membranes. This ability to control transport mechanisms not only improves drug delivery but also suggests broader applications in enhancing biological compatibility and molecular recognition, paving the way for safer and more effective therapeutic systems.

In conclusion, photoswitchable peptides and foldamers offer a powerful, modular toolkit for constructing responsive systems that bridge chemistry, biology, and medicine. Their capacity to undergo reversible, light-controlled changes makes them uniquely suited for applications where precision and adaptability are essential. Ongoing advancements in their design and application are likely to play a pivotal role in the future of personalized medicine, dynamic biomaterials, and molecular diagnostics.

7. Summary

AuNCs represent a significant advance in nanotechnology with wide-ranging applications in biomedical fields, showcasing exceptional properties that can be tailored for specific uses. Ongoing research into their synthesis, characterization, and functionalization is crucial for translating these findings into practical applications. Addressing current challenges and exploring new frontiers will drive the future of AuNCs in medicine and beyond.

We have created BioGoldNCDB, a comprehensive and freely accessible database of AuNCs. Each entry in the database was meticulously annotated and manually curated. This database provides essential information, including CAS numbers and PubMed IDs, as well as detailed data on biomedical uses, research cell lines, particle dimensions, and excitation/emission wavelengths.

BioGoldNCDB encompasses 247 publications from 104 journals and features an intuitive web interface accessible via smartphones, tablets, and computers. Users can fine-tune their searches using various filters, and a dedicated help page is available for guidance. Designed to offer quick insights for beginners, BioGoldNCDB is also a valuable tool for researchers across multiple disciplines.

The rapidly evolving research landscape surrounding photoswitchable peptides and foldamers suggests extensive future potential for innovative applications in biomedicine. Their distinct responsiveness to light stimuli presents an opportunity to develop advanced therapeutic agents, enhancer systems for drug delivery, and novel biosensing platforms.

As methodologies in synthetic biology and advanced materials science continue to improve, it is anticipated that these photoswitchable systems will further integrate into precision medicine, providing targeted and effective solutions to complex medical challenges. Pyridazinone and triazole derivatives were modified using PC, enabling N-alkylation without genotoxic reagents.

With ongoing advancements in the chemistry and methodology related to these systems, the prospect of establishing mechanistic pathways for dynamic regulation in therapeutic scenarios becomes increasingly feasible. Continuous innovation in understanding the interactions between photoresponsive materials and biological systems will serve as a cornerstone for developing next-generation medical treatments.

8. References

- Chan WCW. Bionanotechnology Progress and Advances. Biology of Blood and Marrow Transplantation. 2006.;12(1):87–91.
- Salata O. Applications of nanoparticles in biology and medicine. Journal of Nanobiotechnology. 2004;
- 3. Sonia, Komal, Kukreti S, Kaushik M. Gold nanoclusters: An ultrasmall platform for multifaceted applications. Talanta. 2021.;234:122623.
- 4. Kumar D, Saini N, Jain N, Sareen R, Pandit V. Gold nanoparticles: an era in bionanotechnology. Expert Opinion on Drug Delivery. 2013.;10(3):397–409.
- 5. Bai Y, Shu T, Su L, Zhang X. Fluorescent Gold Nanoclusters for Biosensor and Bioimaging Application. Crystals. 2020.;10(5):357.
- 6. Sarma P, Medhi B. Photopharmacology. Indian J Pharmacol. 2017;49(3):221.
- Szymański W, Beierle JM, Kistemaker HAV, Velema WA, Feringa BL. Reversible Photocontrol of Biological Systems by the Incorporation of Molecular Photoswitches. Chem Rev. 2013.;113(8):6114–78.
- 8. Khan A, Hecht S. Towards Photocontrol over the Helix–Coil Transition in Foldamers: Synthesis and Photoresponsive Behavior of Azobenzene-Core Amphiphilic Oligo(*meta* -phenylene ethynylene)s. Chemistry A European J. 2006.;12(18):4764–74.
- 9. Qian H, Zhu M, Wu Z, Jin R. Quantum Sized Gold Nanoclusters with Atomic Precision. Acc Chem Res. 2012. ;45(9):1470–9.
- Chall S, Mati SS, Das I, Kundu A, De G, Chattopadhyay K. Understanding the Effect of Single Cysteine Mutations on Gold Nanoclusters as Studied by Spectroscopy and Density Functional Theory Modeling. Langmuir. 2017.;33(43):12120–9.
- 11. Yang S, Chen S, Xiong L, Liu C, Yu H, Wang S. Total Structure Determination of Au₁₆ (S-Adm)₁₂ and Cd₁ Au₁₄ (S t Bu)₁₂ and Implications for the Structure of Au₁₅ (SR)₁₃. J Am Chem Soc. 2018.;140(35):10988–94.

- 12. Varela-Aramburu S, Wirth R, Lai CH, Orts-Gil G, Seeberger PH. Straightforward and robust synthesis of monodisperse surface-functionalized gold nanoclusters. Beilstein J Nanotechnol. 2016.;7:1278–83.
- 13. Panjaitan BM, Kubiak-Ossowska K, Birch D, Chen Y. Study of Glucose Binding Protein Encapsulated Gold Nanoclusters by Molecular Dynamic Simulation. MSF. 2019.;948:133–9.
- 14. Yao H, Miki K, Nishida N, Sasaki A, Kimura K. Large Optical Activity of Gold Nanocluster Enantiomers Induced by a Pair of Optically Active Penicillamines. J Am Chem Soc. 2005.;127(44):15536–43.
- 15. Yao H, Fukui T, Kimura K. Asymmetric Transformation of Monolayer-Protected Gold Nanoclusters via Chiral Phase Transfer. J Phys Chem C. 2008.;112(42):16281–5.
- 16. Chen D, Li B, Cai S, Wang P, Peng S, Sheng Y. Dual targeting luminescent gold nanoclusters for tumor imaging and deep tissue therapy. Biomaterials. 2016.;100:1–16.
- 17. Tao Y, Li M, Auguste DT. Pattern-based sensing of triple negative breast cancer cells with dual-ligand cofunctionalized gold nanoclusters. Biomaterials. 2017. ;116:21–33.
- 18. Luo D, Wang X, Zeng S, Ramamurthy G, Burda C, Basilion JP. Targeted Gold Nanocluster-Enhanced Radiotherapy of Prostate Cancer. Small. 2019.;15(34):e1900968.
- 19. Zhang Q, Shi D, Guo M, Zhao H, Zhao Y, Yang X. Radiofrequency-Activated Pyroptosis of Bi-Valent Gold Nanocluster for Cancer Immunotherapy. ACS Nano. 2023.;17(1):515–29.
- 20. Jamkhande PG, Ghule NW, Bamer AH, Kalaskar MG. Metal nanoparticles synthesis: An overview on methods of preparation, advantages and disadvantages, and applications. Journal of Drug Delivery Science and Technology. 2019.;53:101174.

- 21. Sengani M, Grumezescu AM, Rajeswari VD. Recent trends and methodologies in gold nanoparticle synthesis A prospective review on drug delivery aspect. OpenNano. 2017; 2:37–46.
- 22. Zhao Y, Zhuang S, Liao L, Wang C, Xia N, Gan Z. A Dual Purpose Strategy to Endow Gold Nanoclusters with Both Catalysis Activity and Water Solubility. J Am Chem Soc. 2020.;142(2):973–7.
- 23. Desplancq D, Groysbeck N, Chiper M, Weiss E, Frisch B, Strub JM. Cytosolic Diffusion and Peptide-Assisted Nuclear Shuttling of Peptide-Substituted Circa 102 Gold Atom Nanoclusters in Living Cells. ACS Appl Nano Mater. 2018.;1(8):4236–46.
- 24. Tam JM, Tam JO, Murthy A, Ingram DR, Ma LL, Travis K. Controlled Assembly of Biodegradable Plasmonic Nanoclusters for Near-Infrared Imaging and Therapeutic Applications. ACS Nano. 2010.;4(4):2178–84.
- 25. Ding H, Chen Z. Nanotheranostic Application of Fluorescent Protein-Gold Nanocluster Hybrid Materials: A Mini-review. Nanotheranostics. 2021;5(4):461–71.
- 26. Liu H, Yang Y, Ma Z, Pei Y. Chiral Inversion of Au₄₀ (SR)₂₄ Nanocluster Driven by Rotation of Gold Tetrahedra in the Kekulé-like Core. J Phys Chem A. 2024.;128(28):5481–9.
- 27. Chen LY, Wang CW, Yuan Z, Chang HT. Fluorescent Gold Nanoclusters: Recent Advances in Sensing and Imaging. Anal Chem. 2015.;87(1):216–29.
- 28. Wang W, Wei QQ, Wang J, Wang BC, Zhang S hui, Yuan Z. Role of thiol-containing polyethylene glycol (thiol-PEG) in the modification process of gold nanoparticles (AuNPs): Stabilizer or coagulant? Journal of Colloid and Interface Science. 2013.;404:223–9.
- 29. Zhao T, Zhang S, Guo Y, Wang Q. TiC 2: a new two-dimensional sheet beyond MXenes. Nanoscale. 2016;8(1):233–42.

- 30. Brach K, Waszkielewicz M, Olesiak-Banska J, Samoc M, Matczyszyn K. Two-Photon Imaging of 3D Organization of Bimetallic AuAg Nanoclusters in DNA Matrix. Langmuir. 2017.;33(36):8993–9.
- 31. Li Q, Zeman CJ, Ma Z, Schatz GC, Gu XW. Bright NIR-II Photoluminescence in Rod-Shaped Icosahedral Gold Nanoclusters. Small. 2021.;17(11):2007992.
- 32. Pniakowska A, Olesiak-Banska J. Plasmonic Enhancement of Two-Photon Excited Luminescence of Gold Nanoclusters. Molecules. 2022.;27(3):807.
- 33. Russell BA, Kubiak-Ossowska K, Mulheran PA, Birch DJS, Chen Y. Locating the nucleation sites for protein encapsulated gold nanoclusters: a molecular dynamics and fluorescence study. Phys Chem Chem Phys. 2015;17(34):21935–41.
- 34. Miyamura H, Matsubara R, Miyazaki Y, Kobayashi S. Aerobic Oxidation of Alcohols at Room Temperature and Atmospheric Conditions Catalyzed by Reusable Gold Nanoclusters Stabilized by the Benzene Rings of Polystyrene Derivatives. Angew Chem Int Ed. 2007.;46(22):4151–4.
- 35. Bonačić-Koutecký V, Le Guével X, Antoine R. Engineering Liganded Gold Nanoclusters as Efficient Theranostic Agents for Cancer Applications. ChemBioChem. 2023;24(4): e202200524.
- 36. Zhang B, Chen C, Chuang W, Chen S, Yang P. Size Transformation of the Au₂₂ (SG)₁₈ Nanocluster and Its Surface-Sensitive Kinetics. J Am Chem Soc. 2020.;142(26):11514–20.
- 37. Santhakumar H, Nair RV, Govindachar DM, Periyasamy G, Jayasree RS. Engineering of Tripeptide-Stabilized Gold Nanoclusters with Inherent Photosensitizing Property for Bioimaging and Photodynamic Therapy. ACS Sustainable Chem Eng. 2023.;11(6):2102–14.
- 38. Poderys V, Matulionytė-Safinė M, Rupšys D, Rotomskis R. Protein stabilized Au nanoclusters: spectral properties and photostability. Lith J Phys. 2016.;56(1).

- 39. Venkatesh V, Shukla A, Sivakumar S, Verma S. Purine-Stabilized Green Fluorescent Gold Nanoclusters for Cell Nuclei Imaging Applications. ACS Appl Mater Interfaces. 2014.;6(3):2185–91.
- 40. Sham TK, Kim PSG, Zhang P. Electronic structure of molecular-capped gold nanoparticles from X-ray spectroscopy studies: Implications for coulomb blockade, luminescence and non-Fermi behavior. Solid State Communications. 2006.;138(10–11):553–7.
- 41. Brzezicka KA, Serna S, Reichardt NC. Fluorescent Neoglycoprotein Gold Nanoclusters: Synthesis and Applications in Plant Lectin Sensing and Cell Imaging. Nanoscale Res Lett. 2018.;13(1):360.
- 42. Shi J, Cooper JK, Lindley S, Williams O, Kliger DS, Xu Y. The excited state dynamics of protein-encapsulated Au nanoclusters. Chemical Physics Letters. 2014.;610–611:125–30.
- 43. Lin Y, Ren J, Qu X. Nano-Gold as Artificial Enzymes: Hidden Talents. Advanced Materials. 2014.;26(25):4200–17.
- 44. An D, Su J, Weber JK, Gao X, Zhou R, Li J. A Peptide-Coated Gold Nanocluster Exhibits Unique Behavior in Protein Activity Inhibition. J Am Chem Soc. 2015.;137(26):8412–8.
- 45. Zheng K, Setyawati MI, Leong DT, Xie J. Antimicrobial Gold Nanoclusters. ACS Nano. 2017.;11(7):6904–10.
- 46. Nirmal GR, Lin ZC, Chiu TS, Alalaiwe A, Liao CC, Fang JY. Chemo-photothermal therapy of chitosan/gold nanorod clusters for antibacterial treatment against the infection of planktonic and biofilm MRSA. International Journal of Biological Macromolecules. 2024.;268:131673.
- 47. Yao LY, Yam VWW. Diphosphine-Stabilized Small Gold Nanoclusters: From Crystal Structure Determination to Ligation-Driven Symmetry Breaking and Anion Exchange Properties. J Am Chem Soc. 2016.;138(48):15736–42.

- 48. Wang X, Wang J, Jiang H, Wang C, Liu C, Amatore C. Design of novel gold nanocluster and its composites for cancer cell imaging and tumor bio-marking. Protocol Exchange. 2014.
- 49. Liu M, Tang F, Yang Z, Xu J, Yang X. Recent Progress on Gold-Nanocluster-Based Fluorescent Probe for Environmental Analysis and Biological Sensing. Journal of Analytical Methods in Chemistry. 2019.;2019:1–10.
- 50. Panjaitan BM, Dwipayana D, Hutnaleontina PN, Nugroho T, Sundari KN, Muliawati NP. Synthesis of Gold Nanoclusters Encapsulated by Human Serum Albumin and its Application as Glucose Detection Based on Fluorescence Technique. In Surakarta, Indonesia; 2024. o. 85–91.
- 51. Zhang J, Yi L, Xu K, Li J, Lai D. New approach for producing fluorescent gold nanoparticles: Poly(ethylene oxide) homopolymers as reductants in the micelles of amphiphilic fluorosilicone-containing block copolymers. J Polym Sci Part A: Polym Chem. 2015.;53(20):2320–5.
- 52. Chen Z, Tu Y, Zhang D, Liu C, Zhou Y, Li X. A thermosensitive nanoplatform for photoacoustic imaging and NIR light triggered chemo-photothermal therapy. Biomater Sci. 2020;8(15):4299–307.
- 53. Li Z, Xiao W, Huang R, Shi Y, Fang C, Chen Z. A Gold Nanoclusters Film Supported on Polydopamine for Fluorescent Sensing of Free Bilirubin. Sensors. 2019.;19(7):1726.
- 54. Mudedla SK, Azhagiya Singam ER, Balamurugan K, Subramanian V. Influence of the size and charge of gold nanoclusters on complexation with siRNA: a molecular dynamics simulation study. Phys Chem Chem Phys. 2015;17(45):30307–17.
- 55. Chen H, Chang Y, Wei R, Zhang P. Gold nanoclusters encapsulated into zinc-glutamate metal organic frameworks for efficient detection of H₂ O₂. Anal Methods. 2022;14(14):1439–44.

- 56. Mudedla SK, Singam ERA, Vijay Sundar J, Pedersen MN, Murugan NA, Kongsted J, Enhancement of Internal Motions of Lysozyme through Interaction with Gold Nanoclusters and its Optical Imaging. J Phys Chem C. 2015.;119(1):653–64.
- 57. Wang M, Wang L, Feng H, Jiang H, Zhou J, Wang X. Precise therapeutic effect of self-assembling gold nanocluster–PTEN complexes on an orthotropic model of liver cancer. J Cancer Res Clin Oncol. 2020.;146(4):875–82.
- 58. Srinivasulu YG, Mozhi A, Goswami N, Yao Q, Xie J. Traceable Nanocluster—Prodrug Conjugate for Chemo-photodynamic Combinatorial Therapy of Non-small Cell Lung Cancer. ACS Appl Bio Mater. 2021.;4(4):3232–45.
- 59. Cerón MR, Izquierdo M, Alegret N, Valdez JA, Rodríguez-Fortea A, Olmstead MM. Reactivity differences of Sc ₃ N@C _{2n} (2n = 68 and 80). Synthesis of the first methanofullerene derivatives of Sc ₃ N@D _{5h} -C ₈₀. Chem Commun. 2016;52(1):64–7.
- 60. Wang X, He H, Wang Y, Wang J, Sun X, Xu H. Active tumor-targeting luminescent gold clusters with efficient urinary excretion. Chem Commun. 2016;52(59):9232–5.
- 61. Shome R, Ghosh SS. Transferrin Coated D -penicillamine—Au-Cu Nanocluster PLGA Nanocomposite Reverses Hypoxia-Induced EMT and MDR of Triple-Negative Breast Cancers. ACS Appl Bio Mater. 2021.;4(6):5033–48.
- 62. Ou YC, Wen X, Johnson CA, Shae D, Ayala OD, Webb JA. Multimodal Multiplexed Immunoimaging with Nanostars to Detect Multiple Immunomarkers and Monitor Response to Immunotherapies. ACS Nano. 2020.;14(1):651–63.
- 63. Matulionyte M, Dapkute D, Budenaite L, Jarockyte G, Rotomskis R. Photoluminescent Gold Nanoclusters in Cancer Cells: Cellular Uptake, Toxicity, and Generation of Reactive Oxygen Species. IJMS. 2017.;18(2):378.
- 64. Van De Looij SM, Hebels ER, Viola M, Hembury M, Oliveira S, Vermonden T. Gold Nanoclusters: Imaging, Therapy, and Theranostic Roles in Biomedical Applications. Bioconjugate Chem. 2022.;33(1):4–23.

- 65. Fan J, Yang Y, Tao C, Li M. Cadmium-Doped and Pincer Ligand-Modified Gold Nanocluster for Catalytic KA² Reaction. Angewandte Chemie. 2023.;135(6):e202215741.
- 66. Pohjolainen E, Malola S, Groenhof G, Häkkinen H. Exploring Strategies for Labeling Viruses with Gold Nanoclusters through Non-equilibrium Molecular Dynamics Simulations. Bioconjugate Chem. 2017.;28(9):2327–39.
- 67. Obstarczyk P, Pniakowska A, Nonappa, Grzelczak MP, Olesiak-Bańska J. Crown Ether-Capped Gold Nanoclusters as a Multimodal Platform for Bioimaging. ACS Omega. 2023.;8(12):11503–11.
- 68. Huang TH, Zhao FZ, Hu QL, Liu Q, Wu TC, Zheng D. Bisphosphine-Stabilized Gold Nanoclusters with the Crown/Birdcage-Shaped Au₁₁ Cores: Structures and Optical Properties. Inorg Chem. 2020.;59(21):16027–34.
- 69. Yin HQ, Bi FL, Gan F. Rapid Synthesis of Cyclic RGD Conjugated Gold Nanoclusters for Targeting and Fluorescence Imaging of Melanoma A375 Cells. Bioconjugate Chem. 2015.;26(2):243–9.
- 70. Yougbare S, Chang TK, Tan SH, Kuo JC, Hsu PH, Su CY. Antimicrobial Gold Nanoclusters: Recent Developments and Future Perspectives. IJMS. 2019.;20(12):2924.
- 71. Chib R, Butler S, Raut S, Shah S, Borejdo J, Gryczynski Z. Effect of quencher, denaturants, temperature and pH on the fluorescent properties of BSA protected gold nanoclusters. Journal of Luminescence. 2015.;168:62–8.
- 72. Gu Y, Tang S, Liu X, Liang X, Zhu Q, Wu H. Stability prediction of gold nanoclusters with different ligands and doped metals: deep learning and experimental tests. J Mater Chem A. 2024;12(8):4460–72.
- 73. Sang D, Luo X, Liu J. Biological Interaction and Imaging of Ultrasmall Gold Nanoparticles. Nano-Micro Lett. 2024.;16(1):44.

- 74. Georgeous J, AlSawaftah N, Abuwatfa WH, Husseini GA. Review of Gold Nanoparticles: Synthesis, Properties, Shapes, Cellular Uptake, Targeting, Release Mechanisms and Applications in Drug Delivery and Therapy. Pharmaceutics. 2024.;16(10):1332.
- 75. Albert L, Vázquez O. Photoswitchable peptides for spatiotemporal control of biological functions. Chem Commun. 2019;55(69):10192–213.
- 76. Velema WA, Szymanski W, Feringa BL. Photopharmacology: Beyond Proof of Principle. J Am Chem Soc. 2014.;136(6):2178–91.
- 77. Xiong H, Xu Y, Kim B, Rha H, Zhang B, Li M. Photo-controllable biochemistry: Exploiting the photocages in phototherapeutic window. Chem. 2023.;9(1):29–64.
- 78. Liu Y, Wang T, Wang W. Photopharmacology and photoresponsive drug delivery. Chem Soc Rev. 2025;54(12):5792–835.
- 79. Schulte AM, Alachouzos G, Szymański W, Feringa BL. Strategy for Engineering High Photolysis Efficiency of Photocleavable Protecting Groups through Cation Stabilization. J Am Chem Soc. 2022.;144(27):12421–30.
- 80. Hammer JA, Ruta A, West JL. Using Tools from Optogenetics to Create Light-Responsive Biomaterials: LOVTRAP-PEG Hydrogels for Dynamic Peptide Immobilization. Ann Biomed Eng. 2020.;48(7):1885–94.
- 81. Albert L, Peñalver A, Djokovic N, Werel L, Hoffarth M, Ruzic D. Modulating Protein–Protein Interactions with Visible-Light-Responsive Peptide Backbone Photoswitches. ChemBioChem. 2019.;20(11):1417–29.
- 82. Szymanski W, Ourailidou ME, Velema WA, Dekker FJ, Feringa BL. Light-Controlled Histone Deacetylase (HDAC) Inhibitors: Towards Photopharmacological Chemotherapy. Chemistry A European J. 2015.;21(46):16517–24.
- 83. Scheiner M, Sink A, Spatz P, Endres E, Decker M. Photopharmacology on Acetylcholinesterase: Novel Photoswitchable Inhibitors with Improved Pharmacological Profiles. ChemPhotoChem. 2021.;5(2):149–59.

- 84. Broichhagen J, Schönberger M, Cork SC, Frank JA, Marchetti P, Bugliani M. Optical control of insulin release using a photoswitchable sulfonylurea. Nat Commun. 2014.;5(1):5116.
- 85. Sarabando SN, Palmeira A, Sousa ME, Faustino MAF, Monteiro CJP. Photomodulation Approaches to Overcome Antimicrobial Resistance. Pharmaceuticals. 2023.;16(5):682.
- 86. Lerch MM, Hansen MJ, van Dam GM, Szymanski W, Feringa BL. Emerging Targets in Photopharmacology. Angew Chem Int Ed. 2016.;55(37):10978–99.
- 87. Mart RJ, Allemann RK. Azobenzene photocontrol of peptides and proteins. Chem Commun. 2016;52(83):12262–77.
- 88. Lawrence RL, Scola B, Li Y, Lim CK, Liu Y, Prasad PN. Remote Optically Controlled Modulation of Catalytic Properties of Nanoparticles through Reconfiguration of the Inorganic/Organic Interface. ACS Nano. 2016.;10(10):9470–7.
- 89. Olagunju MO, Liu Y, Frenkel AI, Knecht MR. Atomically Resolved Characterization of Optically Driven Ligand Reconfiguration on Nanoparticle Catalyst Surfaces. ACS Appl Mater Interfaces. 2021.;13(37):44302–11.
- 90. Erdélyi M, Varedian M, Sköld C, Niklasson IB, Nurbo J, Persson Å. Chemistry and folding of photomodulable peptides stilbene and thioaurone-type candidates for conformational switches. Org Biomol Chem. 2008;6(23):4356.
- 91. Fujimoto K, Maruyama T, Okada Y, Itou T, Inouye M. Development of a new class of photochromic peptides by using diarylethene-based non-natural amino acids. Tetrahedron. 2013.;69(30):6170–5.
- 92. Van Dijken DJ, Kovaříček P, Ihrig SP, Hecht S. Acylhydrazones as Widely Tunable Photoswitches. J Am Chem Soc. 2015.;137(47):14982–91.
- 93. Nuti F, Gellini C, Larregola M, Squillantini L, Chelli R, Salvi PR. A Photochromic Azobenzene Peptidomimetic of a β-Turn Model Peptide Structure as a Conformational Switch. Front Chem. 2019.;7:180.

- 94. Jankovic B, Gulzar A, Zanobini C, Bozovic O, Wolf S, Stock G. Photocontrolling Protein–Peptide Interactions: From Minimal Perturbation to Complete Unbinding. J Am Chem Soc. 2019.;141(27):10702–10.
- 95. Samanta S, Woolley GA. Bis-Azobenzene Crosslinkers for Photocontrol of Peptide Structure. ChemBioChem. 2011.;12(11):1712–23.
- 96. Matsuura K, Fujita S. A Photoresponsive Artificial Viral Capsid Self-Assembled from an Azobenzene-Containing β-Annulus Peptide. IJMS. 2021.;22(8):4028.
- 97. Hayward D, Goddard ZR, Cominetti MMD, Searcey M, Beekman AM. Light-activated azobenzene peptide inhibitor of the PD-1/PD-L1 interaction. Chem Commun. 2024;60(63):8228–31.
- 98. Cataldi E, Raschig M, Gutmann M, Geppert PT, Ruopp M, Schock M. Amber Light Control of Peptide Secondary Structure by a Perfluoroaromatic Azobenzene Photoswitch. ChemBioChem. 2023.;24(5):e202200570.
- 99. Backus EHG, Bloem E, Donaldson PM, Ihalainen JA, Pfister R, Paoli B. 2D-IR Study of a Photoswitchable Isotope-Labeled α-Helix. J Phys Chem B. 2010.;114(10):3735–40.
- 100. Ghosh P, Torner J, Arora PS, Maayan G. Dual Control of Peptide Conformation with Light and Metal Coordination. Chemistry A European J. 2021.;27(35):8956–9.
- 101. Gutiérrez-Salazar M, Santamaría-Aranda E, Schaar L, Salgado J, Sampedro D, Lorenz-Fonfria VA. A photoswitchable helical peptide with light-controllable interface/transmembrane topology in lipidic membranes. iScience. 2021.;24(7):102771.
- 102. Dong M, Babalhavaeji A, Samanta S, Beharry AA, Woolley GA. Red-Shifting Azobenzene Photoswitches for in Vivo Use. Acc Chem Res. 2015.;48(10):2662–70.
- 103. R Hamblin M, 1 Wellman Center for Photomedicine, Massachusetts General Hospital, BAR414, 40 Blossom Street, Boston, MA 02114, USA, 2 Department of Dermatology, Harvard Medical School, Boston, MA 02115, USA, 3 Harvard-MIT

- Division of Health Sciences and Technology, Cambridge, MA 02139, USA. Mechanisms and applications of the anti-inflammatory effects of photobiomodulation. AIMS Biophysics. 2017;4(3):337–61.
- 104. Hüll K, Morstein J, Trauner D. *In Vivo* Photopharmacology. Chem Rev. 2018.;118(21):10710–47.
- 105. Wunsch A, Matuschka K. A Controlled Trial to Determine the Efficacy of Red and Near-Infrared Light Treatment in Patient Satisfaction, Reduction of Fine Lines, Wrinkles, Skin Roughness, and Intradermal Collagen Density Increase. Photomedicine and Laser Surgery. 2014.;32(2):93–100.
- 106. Yeoh YQ, Yu J, Polyak SW, Horsley JR, Abell AD. Photopharmacological Control of Cyclic Antimicrobial Peptides. ChemBioChem. 2018.;19(24):2591–7.
- 107. Kapun M, Pérez-Areales FJ, Ashman N, Rowling PJE, Schober T, Fowler E. Redlight modulated *ortho* -chloro azobenzene photoswitch for peptide stapling *via* aromatic substitution. RSC Chem Biol. 2024;5(1):49–54.
- 108. Albert L, Nagpal J, Steinchen W, Zhang L, Werel L, Djokovic N. Bistable Photoswitch Allows in Vivo Control of Hematopoiesis. ACS Cent Sci. 2022.;8(1):57–66.
- 109. Chan KH, Xue B, Robinson RC, Hauser CAE. Systematic Moiety Variations of Ultrashort Peptides Produce Profound Effects on Self-Assembly, Nanostructure Formation, Hydrogelation, and Phase Transition. Sci Rep. 2017.;7(1):12897.
- 110. Braun S, Böckmann M, Marx D. Unfolding a Photoswitchable Azo-Foldamer Reveals a Non-Covalent Reaction Mechanism. ChemPhysChem. 2012.;13(6):1440–3.
- 111. Marafon G, Crisma M, Moretto A. Intrinsically Photoswitchable α/β Peptides toward Two-State Foldamers. Angew Chem Int Ed. 2018.;57(32):10217–20.
- 112. Gole B, Kauffmann B, Maurizot V, Huc I, Ferrand Y. Light-Controlled Conformational Switch of an Aromatic Oligoamide Foldamer. Angew Chem Int Ed. 2019.;58(24):8063–7.

- 113. Kothapalli SSK, Kannekanti VK, Ye Z, Yang Z, Chen L, Cai Y. Light-controlled switchable complexation by a non-photoresponsive hydrogen-bonded amide macrocycle. Org Chem Front. 2020;7(6):846–55.
- 114. Zschau RL, Zacharias M. Mechanism of β -hairpin formation in AZOCHIGNOLIN and Chignolin. J Comput Chem. 2023.;44(9):988–1001.
- 115. Martins JN, Raimundo B, Rioboo A, Folgar-Cameán Y, Montenegro J, Basílio N. Photoswitchable Calixarene Activators for Controlled Peptide Transport across Lipid Membranes. J Am Chem Soc. 2023.;145(24):13126–33.
- 116. Hua Y, Flood AH. Flipping the Switch on Chloride Concentrations with a Light-Active Foldamer. J Am Chem Soc. 2010.;132(37):12838–40.
- 117. Lee S, Hua Y, Flood AH. β-Sheet-like Hydrogen Bonds Interlock the Helical Turns of a Photoswitchable Foldamer To Enhance the Binding and Release of Chloride. J Org Chem. 2014.;79(17):8383–96.
- 118. Liu Y, Parks FC, Zhao W, Flood AH. Sequence-Controlled Stimuli-Responsive Single–Double Helix Conversion between 1:1 and 2:2 Chloride-Foldamer Complexes. J Am Chem Soc. 2018.;140(45):15477–86.
- 119. Wang Y, Bie F, Jiang H. Controlling Binding Affinities for Anions by a Photoswitchable Foldamer. Org Lett. 2010.;12(16):3630–3.
- 120. De Poli M, Zawodny W, Quinonero O, Lorch M, Webb SJ, Clayden J. Conformational photoswitching of a synthetic peptide foldamer bound within a phospholipid bilayer. Science. 2016.;352(6285):575–80.
- 121. Opie CR, Kumagai N, Shibasaki M. Reversible Stereoselective Folding/Unfolding Fueled by the Interplay of Photoisomerism and Hydrogen Bonding. Angew Chem Int Ed. 2017.;56(12):3349–53.
- 122. Yan T, Li F, Qi S, Tian J, Tian R, Hou J. Light-responsive vesicles for enantioselective release of chiral drugs prepared from a supra-amphiphilic *M* -helix. Chem Commun. 2020;56(1):149–52.

- 123. Yu Z, Hecht S. Control over Unfolding Pathways by Localizing Photoisomerization Events within Heterosequence Oligoazobenzene Foldamers. Angew Chem Int Ed. 2013.;52(51):13740–4.
- 124. Goulet-Hanssens A, Lai Wing Sun K, Kennedy TE, Barrett CJ. Photoreversible Surfaces to Regulate Cell Adhesion. Biomacromolecules. 2012.;13(9):2958–63.
- 125. Marafon G, Crisma M, Masato A, Plotegher N, Bubacco L, Moretto A. Photoresponsive Prion-Mimic Foldamer to Induce Controlled Protein Aggregation. Angewandte Chemie. 2021.;133(10):5233–8.
- 126. Next.js/React Official Documentation: https://react.dev/, https://nextjs.org/docs.
- 127. Node.js Official Documentation: https://nodejs.org/en/docs.
- 128. MySQL Official Documentation: https://dev.mysql.com/doc/.
- 129. EZGrid React DataGrid Component: https://www.ezgrid.com/.
- 130. DigitalOcean Cloud Hosting Official Website: https://www.digitalocean.com/.
- 131. Erdei E, Marcos JT, Varró N, Horváti K, Bacsa B, Mándity IM. Spatiotemporal control in biomedicine: photoswitchable peptides and foldamers. British J Pharmacology. 2025.;bph.70163.
- 132. Czompa A, Bogdán D, Balogh B, Erdei E, Selymes P, Csomos A, Mándity IM. Sustainable and Safe N-alkylation of N-heterocycles by Propylene Carbonate under Neat Reaction Conditions. IJMS. 2024.;25(10):5523.
- 133. Erdei E, Mándoki A, Deák A, Balogh B, Molnár L, Mándity IM. BioGoldNCDB: A Database of Gold Nanoclusters and Related Nanoparticles with Biomedical Activity. Molecules. 2025.; 30, 3310

9. Bibliography of the candidate's publications

Full papers related to the thesis

- Erdei E, Marcos JT, Varró N, Horváti K, Bacsa B, Mándity IM. Spatiotemporal control in biomedicine: photoswitchable peptides and foldamers. British J Pharmacology. 2025.; bph.70163.
- 2. Czompa A, Bogdán D, Balogh B, Erdei E, Selymes P, Csomos A, Mándity IM. Sustainable and Safe N-alkylation of N-heterocycles by Propylene Carbonate under Neat Reaction Conditions. IJMS. 2024.;25(10):5523.
- Erdei E, Mándoki A, Deák A, Balogh B, Molnár L, Mándity IM. BioGoldNCDB: A Database of Gold Nanoclusters and Related Nanoparticles with Biomedical Activity. Molecules. 2025, 30, 3310.

Other full papers

- 1. Varró N, Mándityné Huszka B, Erdei E, Mándoki A, Mándity IM. Upscaled Synthesis of α- and β-Peptides in a Continuous-Flow Reactor Using Propylene Carbonate as an Eco-Friendly Solvent. Chemistry Methods. 2025.;2500010.
- Varró N, Erdei E, Bogdán D, Kalydi E, Deme R, Balogh B, Szigyártó ICS, Beke-Somfai T, Varga Z, Mándity IM. Betaine-conjugated β-peptide foldamers, influence of quaternary change on self-organization and morphology formation. Chemistry Open. 2025.;0, e202500340.

10. Acknowledgements

I am grateful to my supervisor, Dr. István Mándity, Head of the Institute of Organic Chemistry at Semmelweis University, for his guidance of my work, his inspiring ideas, his useful advice and his constructive criticism.

My special thanks are also due to my colleagues and friends, Dr. Beáta Huszka Mándityné, Dr. András Mándoki, Ilona Botos Fülöpné and Nikolett Varró Kormosné, for their continuous support and for their practical advice and inspiring discussions.

I would like to thank Dr. Andrea Deák, Dr. Balázs Balogh, Dr. László Molnár, Dr. Kata Horváthi, Juan Toledo Marcos and Bernadett Bacsa for their contribution and for their help during my writing.

My special thanks go to my family, especially to my Fiancé, to my Parents, and to my Grandparent for their inexhaustible support.

Finally, I owe thanks to my friends, Panka, Móni and Zoli, without them I wouldn't have been able to get this far either.

DOI: 10.1111/bph.70163

MINI-REVIEW



Spatiotemporal control in biomedicine: photoswitchable peptides and foldamers

Eszter Erdei ^{1,2,3} | Juan Toledo Marcos ^{4,5} | Nikolett Varró ^{1,2,3} | Kata Horváti ⁶ | Bernadett Bacsa ^{4,7} | István M. Mándity ^{1,2,3}

Correspondence

István M. Mándity, TTK Lendület Artificial Transporter Research Group, Institute of Materials and Environmental Chemistry, HUN-REN Research Centre for Natural Sciences, Magyar Tudósok krt. 2, Budapest, Hungary. Email: mandity.istvan@semmelweis.hu

Bernadett Bacsa, Division of Medical Physics and Biophysics, Gottfried Schatz Research Center, Medical University of Graz, Neue Stiftingtalstrasse 6, 8010 Graz, Austria. Email: bernadett.bacsa@medunigraz.at

Funding information

National Research, Development and Innovation Fund, Grant/Award Numbers: EFOP-3.6.3-VEKOP-16-2017-00009, RRF-2.3.1-21-2022-00015, TKP2021-EGA-31; Hungarian Science Foundation, Grant/Award Number: OTKA ANN 139484; Austrian Science Fund, Grant/Award Number: 10.55776/I5611; Lendület (Momentum) Program of the Hungarian Academy of Sciences, Grant/Award Number: LP2021-28

Photopharmacology integrates light-based technology with pharmacology to achieve precise control over biological processes, offering non-invasive activation and spatio-temporal regulation of biomolecular activity. Within this field, photoswitchable peptides and foldamers provide a powerful approach in precision medicine, enabling reversible conformational changes that toggle between active and inactive states. This light-driven modulation enhances targeted drug delivery, molecular sensing, and the development of photoresponsive biomaterials and optical devices. These dynamic systems hold immense potential for creating 'smart' therapeutics and biomaterials that adapt to environmental cues, revolutionizing biomedical applications. However, challenges persist in optimizing their stability, specificity and responsiveness in complex biological environments. Advances in light-responsive technologies and nanotechnology continue to push the boundaries of their applications, driving innovation in precision medicine and materials science. As research progresses, these systems are poised to transform drug delivery, diagnostics and next-generation biomaterials.

KEYWORDS

foldamer, light-controlled, peptides, photopharmacology, photoswitchable, precision medicine, spatiotemporal control

Abbreviation: WDR5-MLL1, WD repeat domain 5-mixed lineage leukaemia 1. Eszter Erdei and Juan Toledo Marcos contributed equally to this work.

This is an open access article under the terms of the Creative Commons Attribution License, which permits use, distribution and reproduction in any medium, provided the original work is properly cited.

© 2025 The Author(s). British Journal of Pharmacology published by John Wiley & Sons Ltd on behalf of British Pharmacological Society.

¹TTK Lendület Artificial Transporter Research Group, Institute of Materials and Environmental Chemistry, HUN-REN Research Centre for Natural Sciences, Budapest, Hungary

²Institute of Organic Chemistry, Faculty of Pharmacy, Semmelweis University, Budapest, Hungary

³Center for Pharmacology and Drug Research & Development, Semmelweis University, Budapest, Hungary

⁴Division of Medical Physics and Biophysics, Gottfried Schatz Research Center, Medical University of Graz, Graz, Austria

⁵Laboratory of Computer-Aided Molecular Design, Division of Medicinal Chemistry, Otto Loewi Research Center, Medical University of Graz, Graz, Austria

⁶MTA-HUN-REN TTK Lendület 'Momentum' Peptide-Based Vaccines Research Group, Institute of Materials and Environmental Chemistry, HUN-REN Research Centre for Natural Sciences, Budapest, Hungary

⁷BioTechMed-Graz, Graz, Austria

1 | INTRODUCTION

Photopharmacology merges light-based technologies with pharmacology to precisely regulate biological processes non-invasively. Foldamers, artificial oligomers that mimic protein structures, and photoswitchable peptides enable reversible conformational changes, toggling between active and inactive states. This light-controlled modulation enhances molecular precision for targeted therapies, opening new avenues in precision medicine and biomaterial development.

2 | PHOTOSWITCHABLE PEPTIDES WITH BIOMEDICAL APPLICATION

These systems integrate photoresponsive chromophores, such as azobenzene, into peptides to dynamically control their conformational states, physicochemical properties and biological activity (Albert & Vázquez, 2019). Over the past decade, incorporating photoswitches into peptide scaffolds has enabled precise regulation of secondary and tertiary structures, supramolecular assemblies and affinity to membranes and proteins (Gutiérrez-Salazar et al., 2021). Admittedly, azobenzene response to ultraviolet (UV) light poses a limitation for its therapeutic application due to its poor tissue penetration and mutagenic potential. The emergence of visible-light-responsive switches has further enhanced their biomedical applicability, offering improved tissue penetration and minimal side effects.

2.1 | Dynamic control of peptide secondary structures and self-assemblies with photoswitches

The incorporation of photoswitches into peptides enables precise modulation of their secondary structures, thereby regulating their biological activity. Light-triggered isomerization of azobenzene-modified peptides induces transitions from disordered states to well-defined structures (Albert & Vázquez, 2019), including α -helices, β -turns (Nuti et al., 2019) and β -hairpins (Hayward et al., 2024) (Figure 1). For instance, recent research has demonstrated the incorporation of azobenzene into a peptide inhibitor targeting the programmed cell death protein 1 (PD-1) and programmed cell death ligand 1 (PD-L1) interaction. In this study, light-induced *trans*-to-*cis* isomerization has been shown to stabilize a β -hairpin motif critical for binding. The *cis* isomer exhibited nanomolar inhibitory activity in vitro and showed remarkably selective cellular activity, with no inhibition from the *trans* isomer. This highlights the precision of photoswitchable peptides in targeted cancer immunotherapy (Hayward et al., 2024).

Photoswitches have been shown to regulate peptide tertiary structures, including coiled-coil formations (Ghosh et al., 2021; Torner & Arora, 2021). Briefly, they are defined by a heptad repeat (abcdefg), where hydrophobic residues at positions **a** and **d** stabilize the core through interhelical packing, while long-range electrostatic interactions at other positions govern specificity and affinity. They assemble in parallel or antiparallel orientations with distinct

supercoiling geometries, enabling structural and functional modulation. Torner and Arora (2021) systematically investigated the impact of azobenzene placement within the different positions of a parallel coiled-coil heptad repeat (Figure 1, upper right). The placement of the azobenzene effectively modulated hydrophobic packing, while misplacement caused fraying and impaired switching (Torner & Arora, 2021). Building on this design, the incorporation of 8-hydroxyquinoline groups into the photoswitch-containing coiled-coil peptide introduced metal coordination as an additional modulator. The coordination of zinc(II) ion (Zn²⁺) with these groups facilitated a transition from an α -helical coiled coil to a β -sheet through specific interstrand coordination (Figure 1, lower right), while other metals, such as copper(II) ion (Cu²⁺), primarily stabilized helicity. This dual-control system, combining light-responsive photoswitching and metal coordination, exemplifies the potential of coiled-coil peptides as versatile tools for stimuli-responsive applications (Ghosh et al., 2021).

In an alternative approach, azobenzene was integrated into a β -annulus peptide from the tomato bushy stunt virus (TBSV) to create a photoresponsive viral capsid. The peptide self-assembled into 30- to 50-nm virus-like particles. The light-triggered *trans*-to-*cis* isomerization induced transitions from capsids to aggregates, enabling precise control of guest molecule encapsulation and release (Figure 1, lower left), showcasing the potential of photoswitchable peptides for light-responsive nanocarriers (Matsuura & Fujita, 2021).

These approaches hold significant promises for precision medicine, where light activation can precisely control peptide function by modulating both secondary and tertiary structures, minimizing off-target effects and enabling targeted therapeutic outcomes.

2.2 | Visible-light-activated peptides: innovations in biomedicine

Recent studies have shifted the focus from UV-inducible azobenzene switches to visible-light-responsive probes, which are more relevant for pharmacological applications (Dong et al., 2015). Photoswitchable therapeutics operating in the red/near-infrared (NIR) spectrum are particularly attractive for biomedical use because red light penetrates biological tissues deeply, minimizes adverse effects and is widely accepted as a non-invasive treatment modality, particularly in (onco)dermatology (Hamblin, 2017; Hüll et al., 2018; Wunsch & Matuschka, 2013).

A significant recent development is the use of tetra-ortho-chloro azobenzene for cysteine-selective peptide stapling, enabling a secondary structure shift (82%) via *trans*-to-*cis* isomerization under red light (660 nm) irradiation. This method was applied to staple a model p53/MDM2 interaction-inhibiting peptide. In a fluorescent polarization assay, the *cis* form exhibited over a 240-fold stronger affinity for MDM2 compared to its *trans* counterpart (Kapun et al., 2024), highlighting the efficacy of red light-responsive systems in modulating protein-protein interactions (Table 1; Entry 1).

Another innovative approach utilized a perfluorinated azobenzene switch conjugated to cysteine side chains at the i and i+4

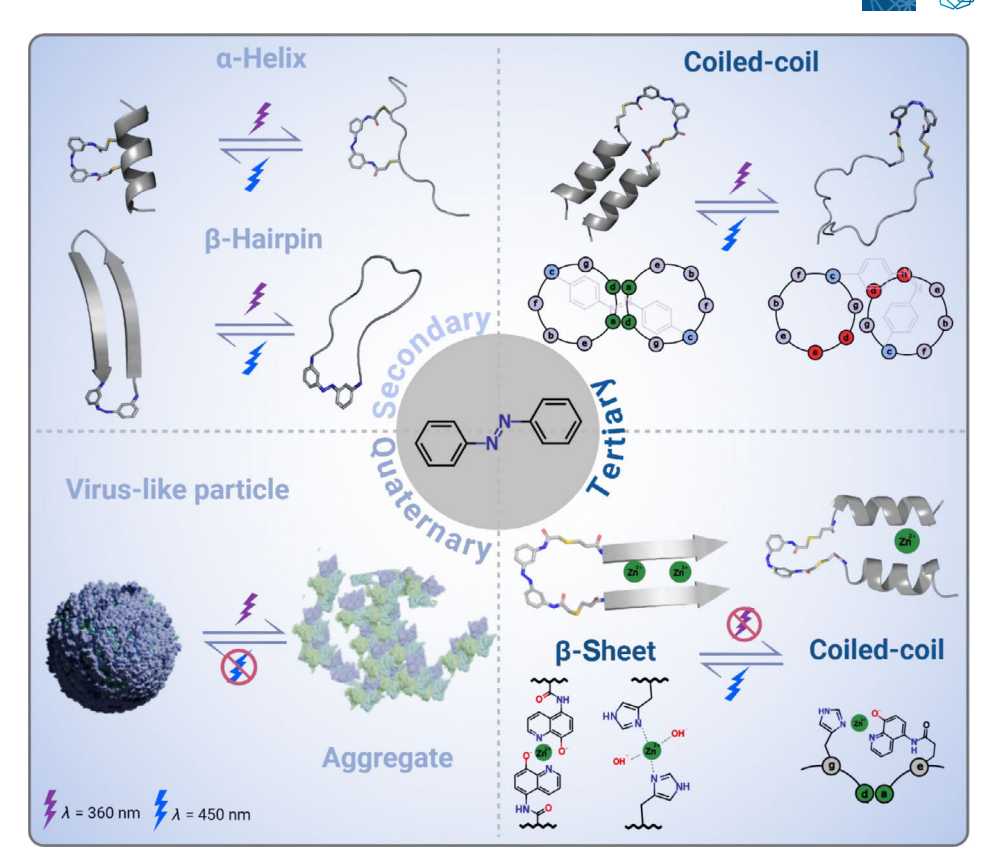


FIGURE 1 Light-induced structural transitions in azobenzene-modified peptides. (Upper left) Photoisomerization of azobenzene disrupts secondary structures, converting α -helices and β -hairpins into unfolded conformations upon *cis*-to-*trans* isomerization, with a reversal to the structured state upon *trans*-to-*cis* isomerization. (Upper right) Light-induced *cis* isomerization of an N-terminally azobenzene-linked c-c' coiled-coil peptide disrupts interhelical packing. Hydrophobic core heptad positions in the canonical right-handed coiled-coil conformation are shown in green, while those failing to support interhelical packing upon *trans*-to-*cis* photoisomerization are shown in red. (Lower right) A coiled-coil peptide modified at the 'e' heptad position with an 8-hydroxyquinoline moiety undergoes a light-controlled transition between coiled-coil and β -sheet structures in the presence of Zn²⁺. When azobenzene is in the *cis* conformation, Zn²⁺ coordination between 8-hydroxyquinoline (position e) and a histidine (position g) stabilizes the coiled-coil structure. Upon *cis*-to-*trans* isomerization, Zn²⁺ is coordinated either by two 8-hydroxyquinoline or two histidine interstrand residues, promoting an irreversible β -sheet transition. (Lower left) Light-induced structural switching between a virus-like particle and an aggregate, regulated via azobenzene-mediated conformational control, with aggregation being irreversible.

positions to generate a stapled cell-penetrating peptide. The photoisomerization of the (LSKT) $_{7-11}$ peptide from the *trans* state to the *cis* state using amber light (450 nm) resulted in a secondary structure transformation from disordered to an amphiphilic helical conformation (Table 1; Entry 2). Despite this structural change, however, cytotoxicity assays performed on human cervical cancer HeLa cells (TKG Cat# TKG 0331, RRID:CVCL_0030) and murine embryonic fibroblast NIH 3T3 cells (CCTCC Cat# GDC0030, RRID:CVCL_0594) showed no significant differences in IC $_{50}$ values between the photostationary states. These findings indicate that while visible-light-responsive peptides hold promise for cell penetration, further optimization may be necessary to enhance their functional activity in this application (Cataldi et al., 2023).

Further advancements in the field include the development of novel visible-light-responsive backbone photoswitches. Albert and Vázquez (2019) introduced tetra-ortho-fluoroazobenzene (Table 1; Entry 3) and a cyclic azobenzene derivative (Table 1; Entry 4), achieving *trans*-to-*cis* photoconversion with high efficiency under green light

(520 nm). The cis-to-trans photostationary state was then reached using blue light (405 nm). These backbone photoswitches were incorporated into peptides to inhibit the WD repeat domain 5-mixed lineage leukaemia 1 (WDR5-MLL1) interaction, a critical target in leukaemogenesis. Notably, the trans isomer demonstrated 10 times higher potency compared to the cis form in vitro. Further investigation into the binding modes of the isomers, as revealed by co-crystal structures and molecular dynamics simulations, has provided a comprehensive explanation for their differential activity (Albert et al., 2019). Building on these results, conformationally strained visible-light photoswitches were developed as a new class of lysine methyltransferase 2A (MLL1) inhibitors. In vivo experiments in zebrafish larvae demonstrated optochemical control of haematopoiesis, with the cis isomer disrupting blood flow and inducing developmental abnormalities, mimicking MLL1 knockdown phenotypes (Albert et al., 2022).

Diarylethene (DAE)-based photoswitchable peptides represent a powerful platform for light-controlled therapeutic and biological

CIETY				
Publication	Kapun et al. (2024)	Cataldi et al. (2023)	Albert et al. (2022)	Albert et al. (2019)
Target	p53-MDM2 interaction	Cell penetration	WDR5-ML1 interaction	WDR5-ML1 interaction
Peptide name/sequence	PMI peptide inhibitor TSFA <u>CYWNGLSC</u> X = oCI-Azo	Stapled cell-penetrating peptide LKKLLKCLKKCLKLAG $X = OFAB$	WDR5-interacting peptides Isobutyryl-c(p-Dab-Arg-Abu-p-Phe-X) X = oF4-Azo	WDR5-interacting peptides SARA-cAzo-VHLRKS
PSS ratio	cis: 82% trans: 92%	cis: 86% trans: 89%	cis: 95% trans: 90%	cis: 100% trans: 16%
Wavelength (nm) cis to trans	415	290	520	520
Wavelength (nm) trans to cis	099	450	405	405
Photoswitch structure	Σ-ν. Σ . Σ . Σ . Σ . Σ . Σ . Σ . Σ . Σ . Σ	x-0 L	O X	ZI Z
Photoswitch name	Tetra-ortho-chloro azobenzene (oCl-Azo)	4,40-(Cys)2octafluoro benzene (2Cys-OFAB)	Tetra-ortho-fluoroazobenzene (oF4-Azo)	5,6-Dihydrodibenzo[<i>c.g</i>][1,2] diazocine (cAzo)
Entry	11	7	м	4

Note: Cysteine crosslinking sites are depicted with a line from residue i to i+n. The underline depicts cyclization between the two cysteines (C). Abbreviations: c(XXX), cyclic peptide; PSS, photostationary state; X, incorporated photoswitch.

14765381, 0, Downloaded from https://bpspubs.onlinelibrary.wiley.com/doi/10.1111/bph.70163 by Semmelweis University, Wiley Online Library on [12/08/2025]. See the Terms and Conditions

on Wiley Online Library for rules of use; OA articles are governed by the applicable Creative Commons

applications. Bicyclic peptides incorporating enzyme-binding and diary-lethene photoswitch units enabled reversible inhibition of serine proteases, allowing light-regulated control over hydrogel degradation and antimicrobial activity (Babii et al., 2021). A gramicidin S-derived peptidomimetic showed potent, oxygen-independent cytotoxicity for photodynamic cancer therapy, with local activation in tumours demonstrated in vivo (Babii et al., 2016). Embryotoxicity studies using Danio rerio larvae established safety windows for 19 diarylethene-modified β -hairpin peptides, validating a rapid *in* vivo toxicity screening model (Afonin et al., 2020). Additionally, diarylethene-stapled analogues of a p53/MDM2 inhibitor revealed light-dependent binding affinities, with the 'open' isomers showing stronger interaction due to entropic advantages (Strizhak et al., 2020). These findings highlight the potential of diarylethene-modified peptides for spatiotemporal control in enzymology, oncology and protein-protein interaction targeting.

3 | PHOTOSWITCHABLE FOLDAMERS WITH BIOMEDICAL APPLICATIONS

Photoswitchable foldamers are synthetic oligomers that mimic protein secondary structures while incorporating light-responsive elements for dynamic control (Braun et al., 2012). Unlike peptides, which rely on natural amino acid sequences and hydrogen bonding for folding, foldamers are designed with non-natural backbones that offer enhanced stability and tunable conformations. The integration of photoswitches,

such as azobenzene, allows foldamers to undergo reversible structural changes upon light exposure (Marafon et al., 2018), modulating their function with high precision (Gole et al., 2019). Compared to peptides, foldamers exhibit greater resistance to enzymatic degradation and can be engineered for specific folding patterns independent of biological constraints. This makes them ideal for applications in ion transport, drug delivery and biomolecular recognition (Kothapalli et al., 2020).

3.1 | Photoswitchable foldamers transporting anions

A bioinspired photoswitchable system has been developed to regulate chloride ion transport through light-controlled structural changes. Chiral aryl-triazole foldamers with azobenzene end groups that bind chloride ions in nonaqueous solutions were created (Hua & Flood, 2010). Upon UV light exposure, the azobenzene undergoes photoisomerization from *trans* to *cis*, reducing the foldamer's stability and chloride binding affinity by 10-fold in acetonitrile (Figure 2). This process is reversible, as visible light restores the *trans* conformation, allowing for chloride reuptake. These properties establish a light-responsive ion transport system, offering potential applications in precision medicine and targeted pharmacological interventions.

Inspired by halorhodopsin, researchers have developed aryltriazole-based foldamers that can selectively bind and release chloride ions in response to light. These foldamers feature an interlocking

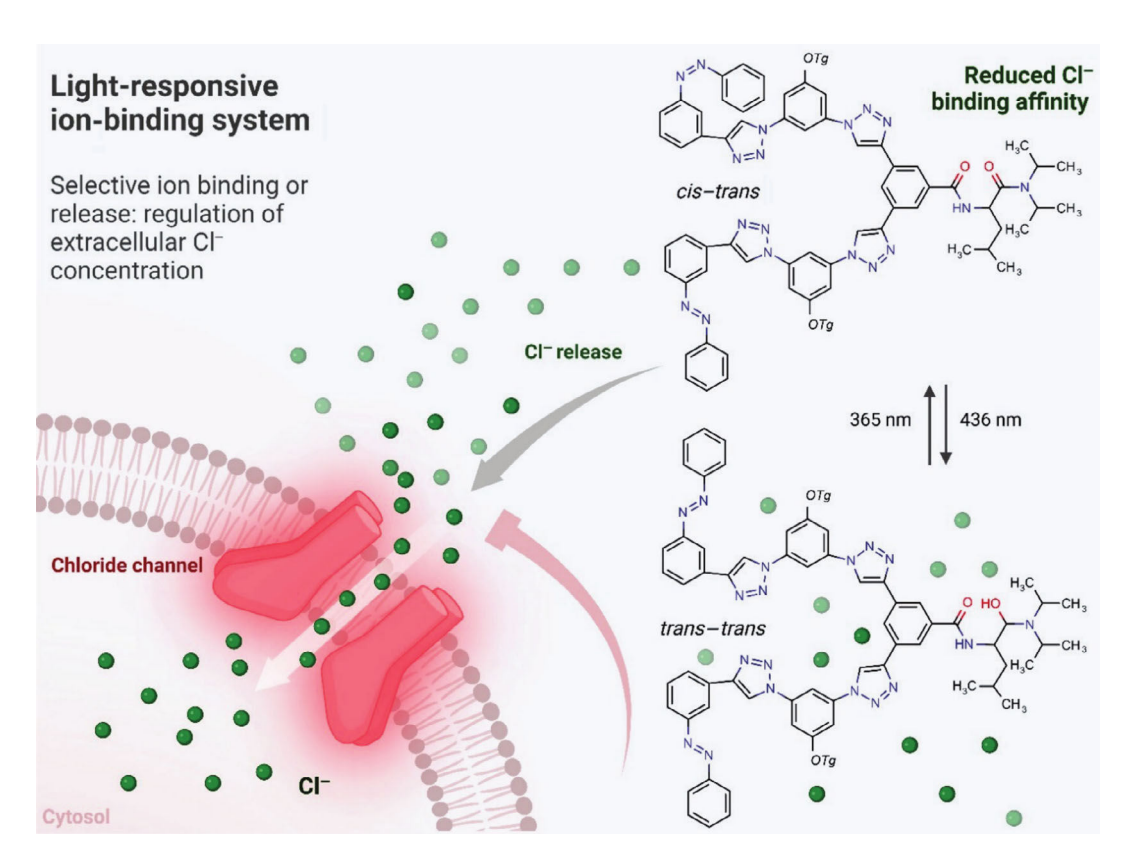


FIGURE 2 Z/E isomerization of an azobenzene element enables light-controlled binding and release of chloride ion by a foldameric host system.

hydrogen-bonding array that stabilizes their helical structure, resembling a β -sheet-like configuration. The study highlights that hydrogen bonding plays a more significant role than π -stacking interactions in stabilizing the helical fold. Light-triggered structural modifications result in up to an 84-fold difference in chloride binding affinity, depending on π - π contacts and hydrogen bond positioning. Such tunable affinity enables precise chloride regulation, making these foldamers highly relevant for pharmacological applications, including anion separation, modulating chloride-dependent enzymatic activity and regulating ion flux in biological systems (Lee et al., 2014).

A related study presents a C_2 -symmetric aryl-triazole foldamer capable of self-assembling into a chloride-templated 2:2 double helix, existing in dynamic equilibrium with a 1:1 single helix. This equilibrium is modulated by solvent composition, temperature and concentration, demonstrating how external factors can regulate foldamer structure. By incorporating $A \leftrightarrow P$ residue substitutions, researchers have shown that a biological sequence design influences structural stability, providing a novel approach for designing therapeutic foldamers with specific ion transport capabilities. The study underscores the importance of solvophobic π -stacking interactions and anion-stabilizing residues in dictating helix formation, offering new strategies for designing biomimetic molecules with tailored ion transport properties (Liu et al., 2018).

The pharmacological potential of these photoswitchable foldamers is vast, as they can serve as next-generation therapeutics for ion imbalance disorders such as cystic fibrosis, epilepsy and neurodegenerative diseases. Their ability to undergo reversible structural changes upon light exposure enables spatiotemporal drug activation, reducing systemic toxicity and off-target effects (Wang et al., 2010). Moreover, these systems hold promise in neuromodulation, optopharmacology and photoactivated drug delivery, positioning photoswitchable foldamers as powerful tools for precision medicine and advanced pharmacological interventions (De Poli et al., 2016).

3.2 | Photoswitchable foldamers in drug delivery and precision medicine

Photoswitchable foldamers, with their ability to undergo light-induced structural transformations, present significant pharmacological potential for drug delivery, targeted therapy and molecular sensing (Khan & Hecht, 2006). A linear molecular system integrating threefold hydrogen-bonding units and a *trans*-tetrafluoroazobenzene segment has been designed to undergo photoisomerization-driven folding, forming a spherical structure with enhanced chiroptical properties. The reversible modification of these structures under visible light offers applications in dynamic drug delivery and responsive molecular systems, allowing for precise spatiotemporal control of therapeutic agents (Opie et al., 2017).

One promising application involves light-responsive vesicles self-assembled from α -cyclodextrin and M-helical azobenzene-containing foldamers. These vesicles reversibly disassemble and reassemble under UV and visible light, enabling the enantioselective release of propranolol, a beta-blocker, with a preference for the R-isomer. This

light-triggered enantioselectivity underscores their potential for precision medicine, allowing targeted drug release and stereoselective pharmacological control, which is critical in chirality-dependent drug efficacy (Yan et al., 2020).

Photoswitchable foldamers also provide a new framework for controlling biomolecular unfolding dynamics. By localizing isomerization events, these molecules enable precise manipulation of protein-like unfolding pathways, mimicking biological helicases and topoisomerases. This capability offers potential applications in dynamic recognition, optomechanical drug activation and controlled enzymatic catalysis, allowing on-demand drug activation via light. Such controlled unfolding pathways are particularly relevant for neuromodulation and targeted protein degradation therapies (Yu & Hecht, 2013).

In the realm of cell adhesion regulation, azobenzene-containing foldamers have been designed to modulate integrin-RGD interactions on biomaterial surfaces. By light-controlled *E/Z* isomerization, researchers have achieved precise regulation of cell adhesion, enhancing or reducing cell binding in response to light stimuli. This innovation offers applications in tissue engineering, regenerative medicine and implantable biomaterials, allowing for adaptive and reversible cellular interactions (Goulet-Hanssens et al., 2012).

Additionally, photoswitchable foldamers have been engineered to mimic prion-like protein aggregation, with applications in neurodegenerative disease research and therapeutic intervention. Light-induced conformational changes in these foldamers promote α -synuclein aggregation, a key event in Parkinson's disease pathology. The ability to control protein misfolding with light provides a tool for studying early-stage aggregation events and developing photo-modulated neurotherapeutics (Marafon et al., 2021).

4 | SUMMARY

These studies position photoswitchable peptides and foldamers as next-generation pharmacological tools, with applications in drug delivery, precision medicine, optopharmacology and dynamic biomaterials. Their ability to undergo reversible, light-driven conformational changes enables unparalleled control over molecular and cellular functions, paving the way for light-activated therapeutics with high spatial and temporal precision.

4.1 | Nomenclature of targets and ligands

Key protein targets and ligands in this article are hyperlinked to corresponding entries in the IUPHAR/BPS Guide to PHARMACOLOGY http://www.guidetopharmacology.org and are permanently archived in the Concise Guide to PHARMACOLOGY 2023/24 (Alexander et al., 2023).

AUTHOR CONTRIBUTIONS

I. M. Mándity: Conceptualization (equal); project administration (equal); supervision (equal); writing—review and editing (equal).

E. Erdei: Data curation (equal); investigation (equal); writing—original draft (equal). J. T. Marcos: Data curation (equal); investigation (equal); writing—original draft (equal). N. Varró: Data curation (equal); investigation (equal). B. Bacsa: Conceptualization (equal); project administration (equal); supervision (equal); writing—review and editing (equal). K. Horváti: Data curation (equal); investigation (equal).

ACKNOWLEDGEMENTS

We gratefully acknowledge the Hungarian Research Foundation (OTKA ANN 139484) and the Austrian Science Fund (FWF) (10.55776/I5611) for their support. Financial support from the National Research, Development and Innovation Office (TKP2021-EGA-31) is also acknowledged. Project No. RRF-2.3.1-21-2022-00015 was implemented with support from the European Union. K.H. acknowledges the support of the Lendület (Momentum) Program of the Hungarian Academy of Sciences (Grant No. LP2021-28). E.E. acknowledges funding from Grant EFOP-3.6.3-VEKOP-16-2017-00009.

CONFLICT OF INTEREST STATEMENT

The authors declare no conflicts of interest.

DATA AVAILABILITY STATEMENT

Data sharing is not applicable to this article because no new data were created or analysed in this study.

REFERENCES

- Afonin, S., Babii, O., Reuter, A., Middel, V., Takamiya, M., Strähle, U., Komarov, I. V., & Ulrich, A. S. (2020). Light-controllable dithienylethene-modified cyclic peptides: Photoswitching the in vivo toxicity in zebrafish embryos. *Beilstein Journal of Organic Chemistry*, 16, 39–49. https://doi.org/10.3762/bjoc.16.6
- Albert, L., Nagpal, J., Steinchen, W., Zhang, L., Werel, L., Djokovic, N., Ruzic, D., Hoffarth, M., Xu, J., Kaspareit, J., Abendroth, F., Royant, A., Bange, G., Nikolic, K., Ryu, S., Dou, Y., Essen, L. O., & Vázquez, O. (2022). Bistable photoswitch allows in vivo control of hematopoiesis. ACS Central Science, 8(1), 57–66. https://doi.org/10.1021/acscentsci.1c00434
- Albert, L., Peñalver, A., Djokovic, N., Werel, L., Hoffarth, M., Ruzic, D., Xu, J., Essen, L.-. O., Nikolic, K., Dou, Y., & Vázquez, O. (2019). Modulating protein-protein interactions with visible-light-responsive peptide backbone photoswitches. *ChemBioChem*, 20(11), 1417–1429. https://doi.org/10.1002/cbic.201800737
- Albert, L., & Vázquez, O. (2019). Photoswitchable peptides for spatiotemporal control of biological functions. *Chemical Communications*, 55(69), 10192–10213. https://doi.org/10.1039/C9CC03346G
- Alexander, S. P. H., Kelly, E., Mathie, A. A., Peters, J. A., Veale, E. L., Armstrong, J. F., Buneman, O. P., Faccenda, E., Harding, S. D., Spedding, M., Cidlowski, J. A., & Zolghadri, Y. (2023). The Concise Guide to PHARMACOLOGY 2023/24: Introduction and other protein targets. *British Journal of Pharmacology*, 180(S2), S1–S22. https://doi. org/10.1111/bph.16176
- Babii, O., Afonin, S., Diel, C., Huhn, M., Dommermuth, J., Schober, T., Koniev, S., Hrebonkin, A., Nesterov-Mueller, A., Komarov, I. V., & Ulrich, A. S. (2021). Diarylethene-based photoswitchable inhibitors of serine proteases. Angewandte Chemie International Edition, 60(40), 21789–21794. https://doi.org/10.1002/anie.202108847
- Babii, O., Afonin, S., Garmanchuk, L. V., Nikulina, V. V., Nikolaienko, T. V., Storozhuk, O. V., Shelest, D. V., Dasyukevich, O. I., Ostapchenko, L. I., lurchenko, V., Zozulya, S., Ulrich, A. S., & Komarov, I. V. (2016). Direct

- photocontrol of peptidomimetics: An alternative to oxygen-dependent photodynamic cancer therapy. *Angewandte Chemie International Edition*, 55(18), 5493–5496. https://doi.org/10.1002/anie.201600506
- Braun, S., Böckmann, M., & Marx, D. (2012). Unfolding a photoswitchable azo-foldamer reveals a non-covalent reaction mechanism. *ChemPhysChem*, 13(6), 1440–1443. https://doi.org/10.1002/cphc.201101001
- Cataldi, E., Raschig, M., Gutmann, M., Geppert, P. T., Ruopp, M., Schock, M., Gerwe, H., Bertermann, R., Meinel, L., Finze, M., Nowak-Król, A., Decker, M., & Lühmann, T. (2023). Amber light control of peptide secondary structure by a perfluoroaromatic azobenzene photoswitch. *ChemBioChem*, 24(5), e202200570. https://doi.org/10. 1002/cbic.202200570
- De Poli, M., Zawodny, W., Quinonero, O., Lorch, M., Webb, S. J., & Clayden, J. (2016). Conformational photoswitching of a synthetic peptide foldamer bound within a phospholipid bilayer. *Science*, 352(6285), 575–580. https://doi.org/10.1126/science.aad8352
- Dong, M., Babalhavaeji, A., Samanta, S., Beharry, A. A., & Woolley, G. A. (2015). Red-shifting azobenzene photoswitches for in vivo use. Accounts of Chemical Research, 48(10), 2662–2670. https://doi.org/10.1021/acs.accounts.5b00270
- Ghosh, P., Torner, J., Arora, P. S., & Maayan, G. (2021). Dual control of peptide conformation with light and metal coordination. *Chemistry—A European Journal*, 27(35), 8956–8959. https://doi.org/10.1002/chem. 202101006
- Gole, B., Kauffmann, B., Maurizot, V., Huc, I., & Ferrand, Y. (2019). Light-controlled conformational switch of an aromatic oligoamide foldamer. Angewandte Chemie International Edition, 58(24), 8063–8067. https://doi.org/10.1002/anie.201902378
- Goulet-Hanssens, A., Lai Wing Sun, K., Kennedy, T. E., & Barrett, C. J. (2012). Photoreversible surfaces to regulate cell adhesion. *Biomacro-molecules*, 13(9), 2958–2963. https://doi.org/10.1021/bm301037k
- Gutiérrez-Salazar, M., Santamaría-Aranda, E., Schaar, L., Salgado, J., Sampedro, D., & Lorenz-Fonfria, V. A. (2021). A photoswitchable helical peptide with light-controllable interface/transmembrane topology in lipidic membranes. *iScience*, 24(7), 102771. https://doi.org/10. 1016/j.isci.2021.102771
- Hamblin, M. R. (2017). Mechanisms and applications of the antiinflammatory effects of photobiomodulation. AIMS Biophysics, 4(3), 337–361. https://doi.org/10.3934/biophy.2017.3.337
- Hayward, D., Goddard, Z. R., Cominetti, M. M. D., Searcey, M., & Beekman, A. M. (2024). Light-activated azobenzene peptide inhibitor of the PD-1/PD-L1 interaction. *Chemical Communications*, 60(63), 8228–8231. https://doi.org/10.1039/D4CC01249F
- Hua, Y., & Flood, A. H. (2010). Flipping the switch on chloride concentrations with a light-active foldamer. *Journal of the American Chemical Society*, 132(37), 12838–12840. https://doi.org/10.1021/ja105793c
- Hüll, K., Morstein, J., & Trauner, D. (2018). In vivo photopharmacology. Chemical Reviews, 118(21), 10710–10747. https://doi.org/10.1021/acs.chemrev.8b00037
- Kapun, M., Pérez-Areales, F. J., Ashman, N., Rowling, P. J. E., Schober, T., Fowler, E., Itzhaki, L. S., & Spring, D. R. (2024). Red-light modulated ortho-chloro azobenzene photoswitch for peptide stapling via aromatic substitution. RSC Chemical Biology, 5(1), 49–54. https://doi.org/ 10.1039/D3CB00176H
- Khan, A., & Hecht, S. (2006). Towards photocontrol over the helix-coil transition in foldamers: Synthesis and photoresponsive behavior of azobenzene-core amphiphilic oligo(meta-phenylene ethynylene)s. Chemistry—A European Journal, 12(18), 4764-4774. https://doi.org/10.1002/chem.200501564
- Kothapalli, S. S. K., Kannekanti, V. K., Ye, Z., Yang, Z., Chen, L., Cai, Y., Zhu, B., Feng, W., & Yuan, L. (2020). Light-controlled switchable complexation by a non-photoresponsive hydrogen-bonded amide macrocycle. *Organic Chemistry Frontiers*, 7(6), 846–855. https://doi.org/10.1039/D0Q000116C

erned by the

applicable Creative Commons

- Lee, S., Hua, Y., & Flood, A. H. (2014). β-Sheet-like hydrogen bonds interlock the helical turns of a photoswitchable foldamer to enhance the binding and release of chloride. The Journal of Organic Chemistry, 79(17), 8383–8396. https://doi.org/10.1021/jo501595k
- Liu, Y., Parks, F. C., Zhao, W., & Flood, A. H. (2018). Sequence-controlled stimuli-responsive single-double helix conversion between 1:1 and 2: 2 chloride-foldamer complexes. *Journal of the American Chemical Society*, 140(45), 15477-15486. https://doi.org/10.1021/jacs.8b09899
- Marafon, G., Crisma, M., Masato, A., Plotegher, N., Bubacco, L., & Moretto, A. (2021). Photoresponsive prion-mimic foldamer to induce controlled protein aggregation. Angewandte Chemie International Edition, 60(10), 5173–5178. https://doi.org/10.1002/anie.202012995
- Marafon, G., Crisma, M., & Moretto, A. (2018). Intrinsically photoswitchable α/β peptides toward two-state foldamers. *Angewandte Chemie International Edition*, *57*(32), 10217–10220. https://doi.org/10.1002/anie.201806035
- Matsuura, K., & Fujita, S. (2021). A photoresponsive artificial viral capsid self-assembled from an azobenzene-containing β-annulus peptide. *International Journal of Molecular Sciences*, 22(8), 4028. https://www.mdpi.com/1422-0067/22/8/4028, https://doi.org/10.3390/iims22084028
- Nuti, F., Gellini, C., Larregola, M., Squillantini, L., Chelli, R., Salvi, P. R., Lequin, O., Pietraperzia, G., & Papini, A. M. (2019). A photochromic azobenzene peptidomimetic of a β-turn model peptide structure as a conformational switch. *Frontiers in Chemistry*, 7, 180. https://doi.org/ 10.3389/fchem.2019.00180
- Opie, C. R., Kumagai, N., & Shibasaki, M. (2017). Reversible stereoselective folding/unfolding fueled by the interplay of photoisomerism and hydrogen bonding. *Angewandte Chemie International Edition*, 56(12), 3349–3353. https://doi.org/10.1002/anie.201610279
- Strizhak, A. V., Babii, O., Afonin, S., Bakanovich, I., Pantelejevs, T., Xu, W., Fowler, E., Eapen, R., Sharma, K., Platonov, M. O., Hurmach, V. V., Itzhaki, L., Hyvönen, M., Ulrich, A. S., Spring, D. R., & Komarov, I. V.

- (2020). Diarylethene moiety as an enthalpy-entropy switch: Photoisomerizable stapled peptides for modulating p53/MDM2 interaction. Organic & Biomolecular Chemistry, 18(28), 5359–5369. https://doi.org/10.1039/D0OB00831A
- Torner, J. M., & Arora, P. S. (2021). Conformational control in a photoswitchable coiled coil. *Chemical Communications*, 57(12), 1442–1445. https://doi.org/10.1039/DOCC08318F
- Wang, Y., Bie, F., & Jiang, H. (2010). Controlling binding affinities for anions by a photoswitchable foldamer. Organic Letters, 12(16), 3630– 3633. https://doi.org/10.1021/ol1014043
- Wunsch, A., & Matuschka, K. (2013). A controlled trial to determine the efficacy of red and near-infrared light treatment in patient satisfaction, reduction of fine lines, wrinkles, skin roughness, and intradermal collagen density increase. *Photomedicine and Laser Surgery*, 32(2), 93–100. https://doi.org/10.1089/pho.2013.3616
- Yan, T., Li, F., Qi, S., Tian, J., Tian, R., Hou, J., Luo, Q., Dong, Z., Xu, J., & Liu, J. (2020). Light-responsive vesicles for enantioselective release of chiral drugs prepared from a supra-amphiphilic M-helix. Chemical Communications, 56(1), 149–152. https://doi.org/10.1039/C9CC08380D
- Yu, Z., & Hecht, S. (2013). Control over unfolding pathways by localizing photoisomerization events within heterosequence oligoazobenzene foldamers. Angewandte Chemie International Edition, 52(51), 13740– 13744. https://doi.org/10.1002/anie.201307378

How to cite this article: Erdei, E., Marcos, J. T., Varró, N., Horváti, K., Bacsa, B., & Mándity, I. M. (2025). Spatiotemporal control in biomedicine: photoswitchable peptides and foldamers. *British Journal of Pharmacology*, 1–8. https://doi.org/10.1111/bph.70163





Article

BioGoldNCDB: A Database of Gold Nanoclusters and Related Nanoparticles with Biomedical Activity

Eszter Erdei ^{1,2,3}, András Mándoki ^{1,2,3}, Andrea Deák ^{2,*}, Balázs Balogh ^{1,3}, László Molnár ^{2,4} and István M. Mándity ^{1,2,3,*}

- ¹ Institute of Organic Chemistry, Semmelweis University, Högyes Endre u. 7, H-1092 Budapest, Hungary; erdei.eszter@ttk.hu (E.E.); mandoki.andras@ttk.hu (A.M.); balogh.balazs@semmelweis.hu (B.B.)
- Artificial Transporter Research Group, Institute of Materials and Environmental Chemistry, HUN-REN Research Centre for Natural Sciences, Magyar Tudósok krt. 2, H-1117 Budapest, Hungary; molnar.laszlo@ttk.hu
- Center for Pharmacology and Drug Research & Development, Semmelweis University, H-1085 Budapest, Hungary
- ⁴ Solid Science Ltd., Podmaniczky utca 57, H-1064 Budapest, Hungary
- * Correspondence: deak.andrea@ttk.hu (A.D.); mandity.istvan@ttk.hu or mandity.istvan@semmelweis.hu (I.M.M.); Tel.: +36-1-3826-514 (A.D.); +36-1-3826-616 (I.M.M.)

Abstract

Interest in gold nanoclusters (AuNCs) has grown significantly in recent decades. AuNCs, with a core size smaller than 2 nm, represent a unique class of functional nanomaterials. Their distinctive properties enable innovative applications across various interdisciplinary fields. Here, we introduce BioGoldNCDB, a freely available, fully annotated, and manually curated database of mainly about AuNCs and related AuNPs. Despite the rapid growth in biomedical applications of gold nanoclusters (AuNCs), the lack of a centralized and structured data resource hinders comparative analysis and rational design. Researchers face challenges in accessing standardized information on AuNCs' structures, properties, and biological activities, which limits data-driven development in this emerging field. The database provides essential information, including CAS numbers and PubMed IDs, as well as specific details such as biomedical applications, cell lines used in research, particle size, and excitation/emission wavelengths. It currently covers 247 articles from 104 journals. Designed with a user-friendly and intuitive web interface, BioGoldNCDB is accessible on multiple devices, including phones, tablets, and PCs. Users can refine searches with multiple filters, and a help page is available for guidance. While offering quick insights for newcomers, BioGoldNCDB also serves as a valuable resource for researchers across various fields.

Keywords: gold; nanocluster; database; application; particle size; therapy



Academic Editor: Jacek Nycz

Received: 16 June 2025 Revised: 1 August 2025 Accepted: 5 August 2025 Published: 7 August 2025

Citation: Erdei, E.; Mándoki, A.; Deák, A.; Balogh, B.; Molnár, L.; Mándity, I.M. BioGoldNCDB: A Database of Gold Nanoclusters and Related Nanoparticles with Biomedical Activity. *Molecules* **2025**, 30, 3310. https://doi.org/10.3390/ molecules30153310

Copyright: © 2025 by the authors. Licensee MDPI, Basel, Switzerland. This article is an open access article distributed under the terms and conditions of the Creative Commons Attribution (CC BY) license (https://creativecommons.org/licenses/by/4.0/).

1. Introduction

Bionanotechnology has been a rapidly advancing field in recent decades, integrating chemistry, physics, biology, and medicine with nanotechnology to drive innovation in modern science [1–3]. Metallic nanoparticles (NPs) play a crucial role in this field due to their unique properties. They can be synthesized and functionalized with various groups, enabling conjugation with peptides, antibodies, ligands, or even drugs [4]. This versatility opens up a wide range of biomedical applications, including diagnostic imaging, biosensing, sample preparation, and therapy [5,6].

Molecules **2025**, 30, 3310 2 of 15

NPs typically range in size from 1 to 150 nm [1,7] and exhibit size-dependent applications and distinctive physical properties, allowing them to interact with cell surface receptors and biomolecules. Additionally, they serve as effective drug delivery agents [8]. Among metallic NPs, a few materials stand out, particularly iron oxide NPs (Fe_3O_4 , Fe_2O_3) [7,9–11], which possess magnetic properties, and silver NPs, which have gained attention due to their antimicrobial and biomedical applications [12–14]. These materials are widely utilized in protein immobilization, MRI imaging, targeted drug delivery, infectious disease treatment, and inflammation control [7,15,16].

AuNPs are among the most widely explored nanomaterials due to their exceptional optical properties, stability, and surface functionalization potential. Their surface can be modified for bioconjugation with peptides, proteins, oligonucleotides, and antibodies [17,18]. AuNPs can function as artificial antibodies, with their binding affinity adjustable by altering the ligand density on their surface [19]. Their multivalency allows them to protect unstable drugs or poorly soluble contrast agents, facilitating effective delivery to otherwise inaccessible tissues. Due to their unique nanoscale properties, AuNPs can modulate cellular processes in ways that small molecules or proteins cannot [20]. Some gold NPs efficiently convert light into heat, enabling precise thermal ablation of diseased tissues. Additionally, their high X-ray absorption enhances cancer radiation therapy and improves imaging contrast in computed tomography (CT) scans. Metallic NPs, in general, exhibit strong absorption and vivid colors due to surface plasmon resonance (SPR) [21], but their fluorescence [22] or luminescence [23] emission is generally weak or negligible. However, gold nanotechnology enables the integration of multiple functionalities into a single construct, allowing for simultaneous targeting, diagnosis, and therapy [24]. These properties make AuNPs an attractive platform for personalized medicine, as they can be chemically tailored for specific diseases or patients [24–31].

Gold nanoclusters (AuNCs) are atomically precise gold nanomaterials typically smaller than 2 nm, exhibiting discrete electronic structures and molecular-like properties. These features fundamentally distinguish them from larger gold nanoparticles (AuNPs), which display bulk-like and plasmonic behavior. Therefore, AuNCs are more accurately regarded as a separate class of nanomaterials, rather than a subclass of AuNPs. Unlike standard AuNPs, AuNCs [32] significantly alter their optical, electronic, and catalytic behaviors. Solid-phase techniques [33] have become more prevalent due to their ease of use and scalability. AuNCs are typically synthesized in the presence of specific ligands, which act as stabilizing agents by forming strong interactions with metal atoms (Scheme 1). Thiolated ligands [34], in particular, directly interact with the Au core via weak coordination bonds, enhancing their sensing and catalytic properties.

Due to their ultrasmall size, AuNCs display molecule-like behavior rather than traditional NP characteristics. This is because their dimensions are comparable to the Fermi wavelength [35] of electrons, leading to the disappearance of conventional metallic properties. Instead, pronounced quantum confinement effects cause the energy bands to transform into discrete electronic states, resulting in distinct optical properties compared to larger NPs [36]. These clusters (Au_{10} , Au_{25} , Au_{38} , Au_{144}) are part of the "magic-number" series of thiolate-protected gold superatoms exhibiting enhanced stability due to closed electronic shells [37–40].

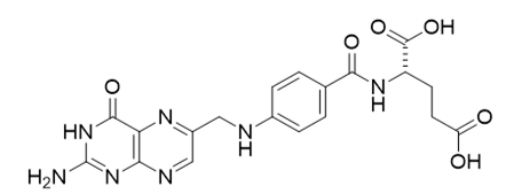
Molecules **2025**, 30, 3310 3 of 15

ne, GSH Polyethylene glycol, PEG

$$H_2N$$
 H_2N
 H_2N
 H_3N
 H_4N
 H_2N
 H_3N
 H_4N
 H_5N
 H_5N

Doxorubicin

RGD (Arginylglycylaspartic acid) peptide



5- fluorouracil

Folic acid

Scheme 1. Structures of the most common nanoconjugates and ligands.

The biocompatibility, photostability, and unique optical properties of AuNCs make them promising candidates for various biomedical applications [28,41,42]: (*i*) fluorescent AuNCs serve as bioimaging and cell imaging agents due to their non-toxic core [43]; (*ii*) functionalized AuNCs exhibit enzyme-mimicking activity, enabling their use in protein activity inhibition and colorimetric detection of analytes [28,44,45]; and (*iii*) ultrasmall AuNCs demonstrate broad-spectrum antimicrobial properties, efficiently targeting both Gram-positive and Gram-negative bacteria by disrupting bacterial metabolism and inducing intracellular reactive oxygen species (ROS) [46] accumulation, ultimately leading to bacterial cell death [47–51].

Over the past few years, a large number of reports have been published to demonstrate applications of AuNCs in oncological cases, ranging from imaging [52] and diagnostic [53] to targeted therapy [54,55], radiotherapy [56,57], and immunotherapy [58]. Their efficacy has been extensively tested in various cancer cell lines, such as HeLa [59], HepG2 [60], A549 lung cancer cells [61], MCF-7 [62], U87 [63] and MDA-MB-231 [64], and even in mice models [65].

A database was created, namely BioGoldNCDB (Bio = biomedical, NC = nanocluster, DB = database), where all the necessary information about gold nanoclusters and related nanoparticles can be found. The database is accessible at https://biogoldncdb.ladon.life/accessed on 15 August 2024.

2. Results

Analysis of Conjugate Applications

The biomedical applications included in BioGoldNCDB and their distribution are shown in Figure 1b. The most common applications are therapy (122 entries) and imaging (150 entries).

Molecules **2025**, 30, 3310 4 of 15

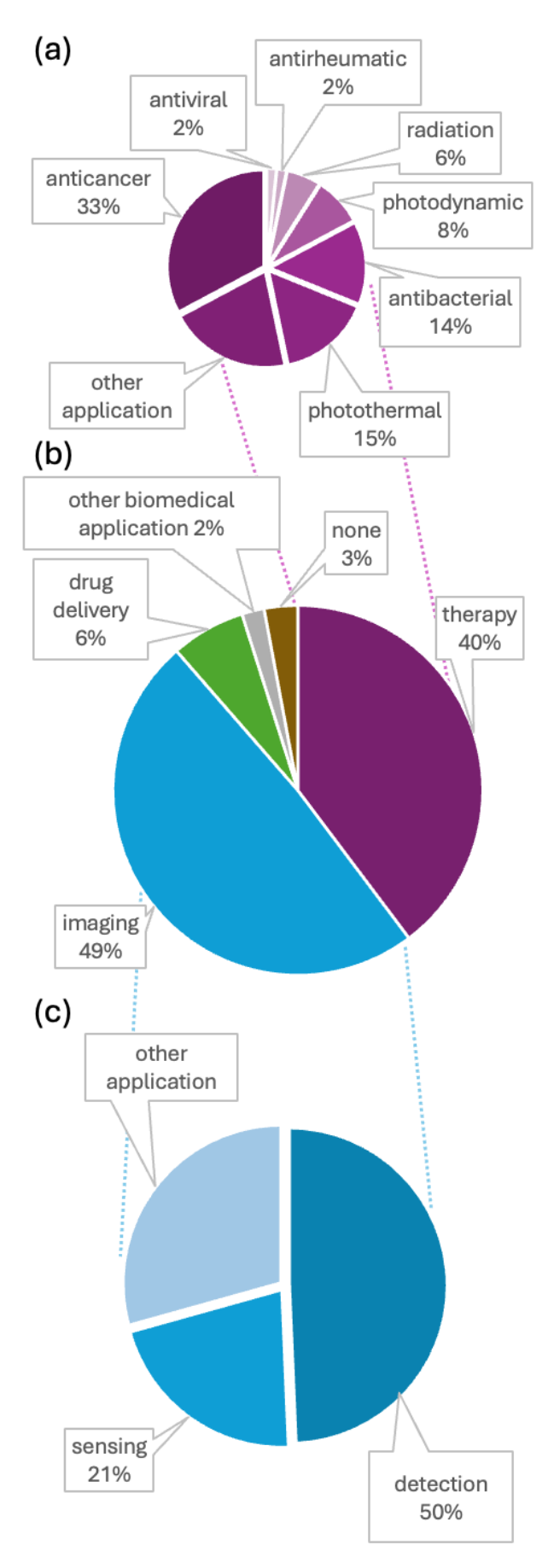


Figure 1. The distribution of applications found for the BioGoldNCDB. (b) A more specific separation was made for therapy (a) and imaging (c).

Molecules **2025**, 30, 3310 5 of 15

The most relevant nanoconjugates and their distribution in BioGoldNCDB are presented in Figure 2. The surface ligands of AuNCs play a critical role in determining their stability, photophysical properties and interactions with additional biomolecules. Thiols and thiol derivatives are the primary functionalization agents for AuNCs (Figure 2a). Glutathione (GSH) is the most commonly used thiolated ligand for the stabilization and functionalization of AuNCs. The covalent or noncovalent conjugation of additional biomolecules or other cargo molecules to AuNCs enables the formation of nanobioconjugates, enhancing their functionality, targeting, and activity in biological environments. Among cargo molecules, peptides and proteins are the most frequently utilized, though oligonucleotides and drug molecules are also common (Figure 2b).

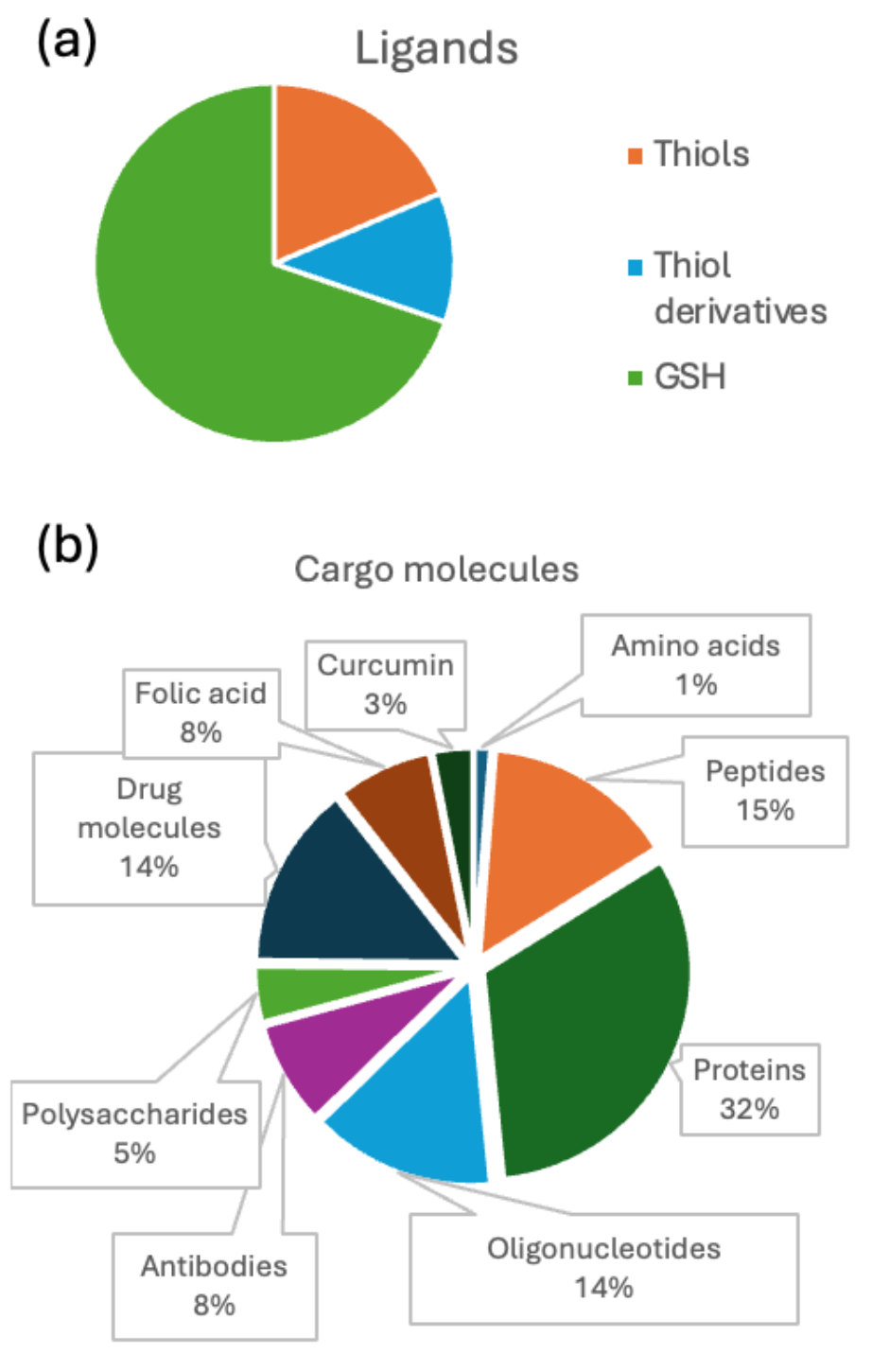


Figure 2. The distribution of ligands (a) and cargos (b) found for the BioGoldNCDB entries.

Molecules **2025**, 30, 3310 6 of 15

The size distribution of AuNCs is shown in Figure 3. During data collection, our primary goal was to obtain the gold core size; however, in many cases, only size data for the nanobioconjugates were available, or the original core size was not determined.

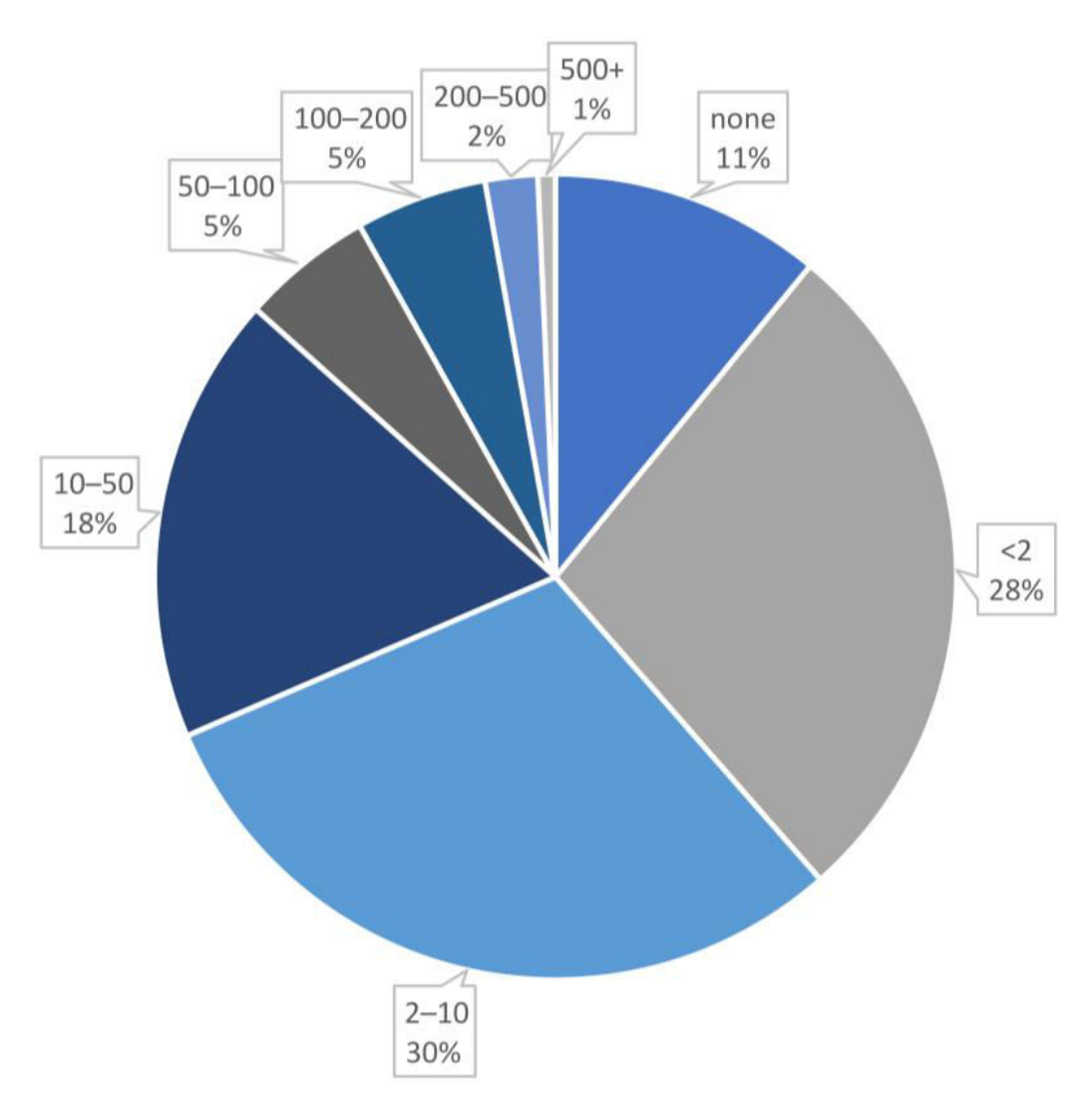


Figure 3. The distribution of the complete particle sizes found for the BioGoldNCDB entries given in nm.

In the case of AuNCs, 28% are smaller than 2 nanometers, while related nanoparticles make up nearly half of the cases (specifically, 30% are between 2 and 10 nm, and 18% are between 10 and 50 nm).

Excitation and emission wavelength data were collected from the articles and are presented separately in Figures 4 and 5. Most excitation wavelengths fall within the 400–500 nm range, while emission wavelengths are primarily in the 600–700 nm range. Notably, excitation wavelength data were missing in 33% of cases, and emission wavelength information was absent in 39% of cases.

In several cases, gold NCs are combined with one or more additional metals, forming hybrid structures. These hybrids were excluded from our analysis, as the conjugated metals alter the properties of gold, thereby affecting the statistical outcomes.

Molecules **2025**, 30, 3310 7 of 15

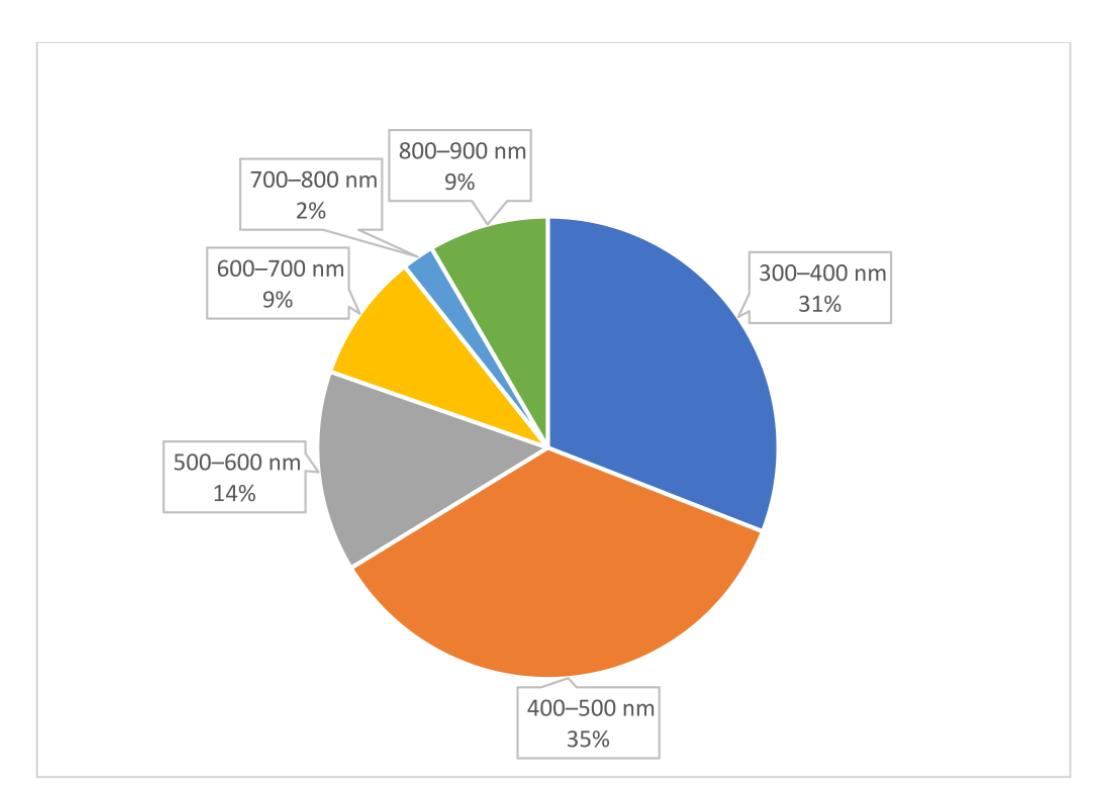


Figure 4. The distribution of excitation wavelengths found for the BioGoldNCDB entries.

The number of AuNCs with reported excitation and emission wavelengths, categorized into 100 nm intervals, is shown in Figure 6. These data clearly demonstrate that most AuNCs are excited at lower wavelengths (300–500 nm), while their emission predominantly occurs at higher wavelengths, typically in the 600–700 nm range.

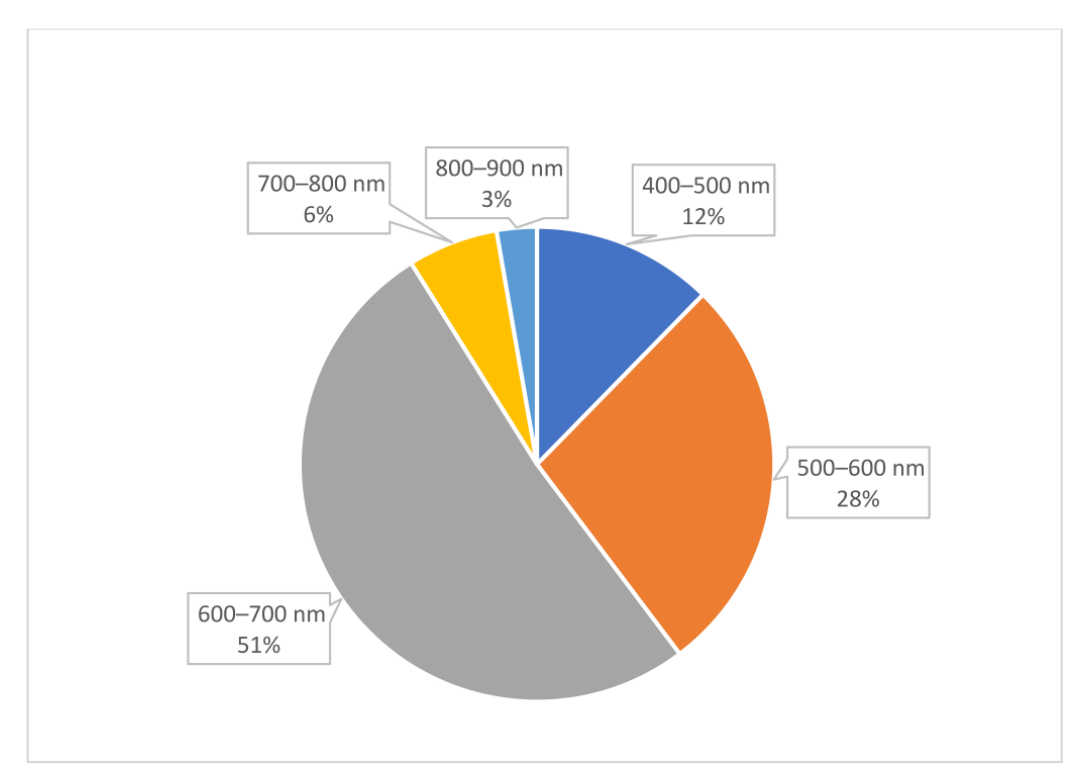


Figure 5. The distribution of emission wavelengths found for the BioGoldNCDB entries.

Molecules **2025**, 30, 3310 8 of 15

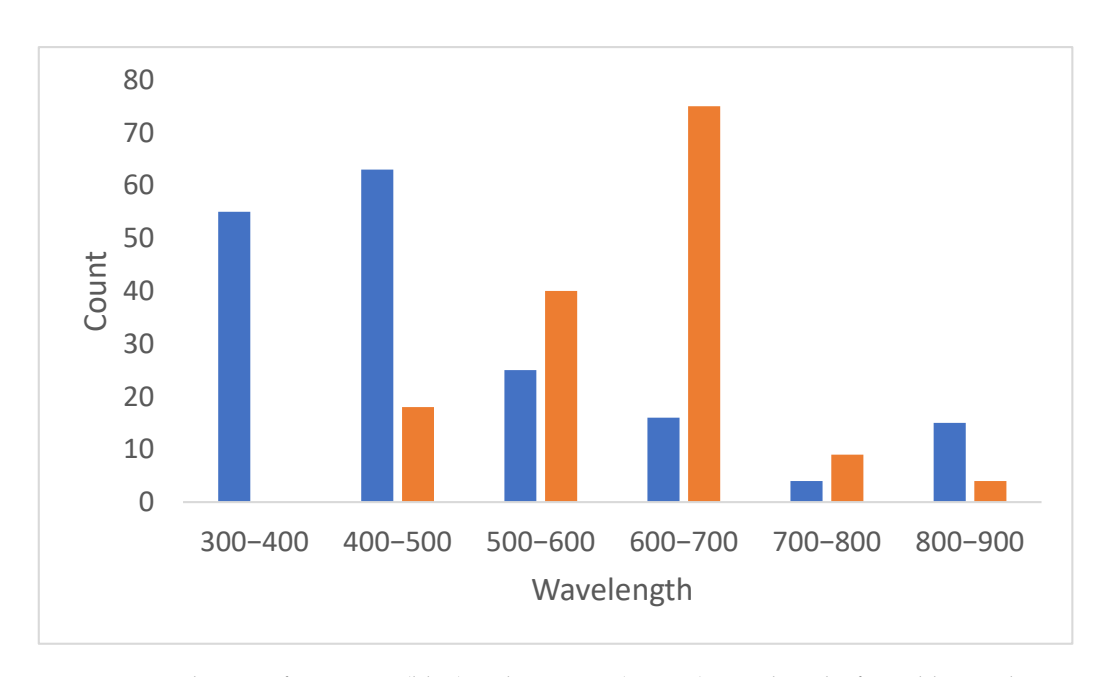


Figure 6. Distribution of excitation (blue) and emission (orange) wavelengths for gold nanoclusters (AuNCs), grouped in 100 nm intervals. The majority of AuNCs exhibit excitation in the lower wavelength range (300–500 nm), while their emission typically occurs at higher wavelengths (600–700 nm), reflecting their characteristic photophysical behavior.

3. Discussion

3.1. Database Overview

3.1.1. Database Content and User Interface Layout

The BioGoldNCDB search function enables users to efficiently explore the database using multiple search criteria. It contains information on gold NCs compiled from 247 published research articles. Users can search by keywords related to NC characteristics, particle size, and biomedical applications. Advanced filters allow for refinement based on particle size, surface modification (nanobioconjugates), and other key parameters. Additionally, BioGoldNCDB integrates SciFinder's data to enhance searches with valuable extra information. Users can further narrow results by specifying CAS numbers, journal names, or other identifiers. By combining these search options, researchers can quickly access specific and relevant data, facilitating the discovery and application of gold NPs in drug delivery, imaging, and diagnostics. The database serves as a valuable resource for both experienced researchers and those new to the field. Its content is categorized into four main groups for easy navigation. BioGoldNCDB features an intuitive and highly responsive user interface, enabling effortless data exploration with column sorting, filtering, and inline editing. With built-in support for keyboard navigation, drag-and-drop functionality, and export options, it enhances usability, allowing users to efficiently manage and interact with large datasets.

3.1.2. Manually Curated Data

- **Application:** The biomedical field in which the AuNCs can be utilized.
- Cell line: The specific cell culture used for testing or biomedical investigation.
- **Particle size:** Includes both the core size (analyzed by TEM technique) and the total size of the nanobioconjugate, measured in nanometers (nm).
- Excitation/emission wavelength: The excitation wavelength refers to the specific wavelength of light that is absorbed by gold AuNCs to promote their electrons to an excited energy state. The emission wavelength is the wavelength of light emitted as the excited electrons return to their ground state.

Molecules 2025, 30, 3310 9 of 15

• **Nanobioconjugates:** Any molecule or material added to gold NCs as part of the functionalization process.

• TOC: Table of Contents figures.

3.1.3. Bibliographic Information

- **ID:** A unique identifier assigned to the article by the database or journal where it is published. (Usually not shown in the article itself).
- **Title:** The main heading of the article that concisely captures its content.
- **Abstract:** A brief summary of the article's purpose, methodology, key findings, and conclusions.
- Author (s): The person (people) who conducted the research and wrote the article.
- Journal: The scientific publication where the article appears.
- **Organization:** The affiliation of the author (s), typically their university or research institution.
- **Database:** The online platform where the article can be accessed (e.g., PubMed Central, ScienceDirect).
- **Volume:** The volume number of the journal issue where the article is published.
- **Issue:** The specific issue number within the volume.
- Paper: (uncommon) Sometimes used interchangeably with article.
- **Page numbers:** The page range where the article appears within the journal issue.
- **Publication date:** The date the article was published in the journal.

3.1.4. Identification

- **Concepts:** The main topics or ideas explored in the article.
- **CAS Numbers:** Unique identifiers assigned by the Chemical Abstracts Service to chemical substances mentioned in the article.
- Keywords: A list of terms relevant to the article's subject matter used for indexing and searchability.
- Accession Number: An identification number assigned to the article by a specific database.
- Chemical Abstracts Number (CAN): Unique identifier for the abstract text of the publication assigned by Chemical Abstracts Service.
- **Section:** The specific section of the journal where the article is published (e.g., research articles, reviews).
- **Section Cross-Reference:** A reference to a related section within the journal where additional relevant information might be found.

3.1.5. Identifiers

- **CODEN:** A unique six-character code assigned to a specific journal title.
- **DOI (Digital Object Identifier):** A unique identifier for an article that remains constant even if the location of the article changes online.
- **Journal Code:** An abbreviation used to identify a specific journal.
- **PubMed ID:** A unique identifier assigned to an article by the PubMed database.
- **MEDLINE MeSH (Medical Subject Headings):** A controlled vocabulary used by MEDLINE/PubMed to index articles in the life sciences.

3.2. Examples

Below are brief examples of some search options available in BioGoldNCDB (Figure 7):

1. **Free Text Search:** A keyword-based free text search enables users to explore various database fields, including BioGoldNCDB ID, CAS number, PubMed ID, author name,

- article title, organization, journal name, and year of publication. More details are available at https://biogoldncdb.ladon.life/.
- 2. **Simple Search:** Users can also search for specific entries in BioGoldNCDB based on application, cell line type, particle size, nanoconjugates, and excitation/emission wavelengths, etc.
- 3. **Multi-criteria search:** Users can also search using multiple criteria in BioGoldNCDB.

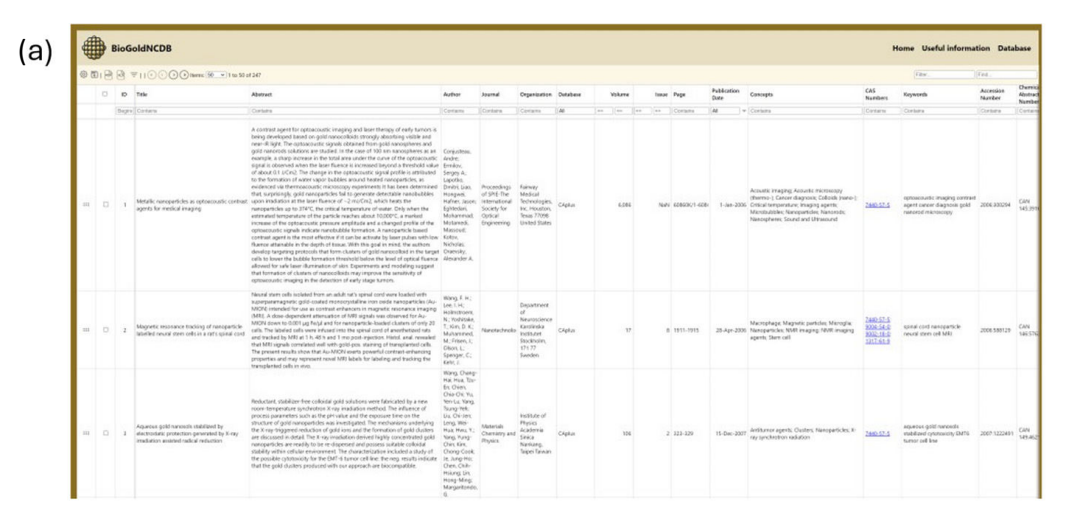




Figure 7. The layout of BioGoldNCDB, displaying database entries melyek (a) and amelyek (b), with columns accompanied by various search options.

The platform offers several user-friendly features. Users can filter data by specific columns (e.g., searching for the keyword 'anticancer' within the application column) or perform a comprehensive keyword search across the entire database. Additionally, results can be exported in PDF and Excel formats using dedicated buttons, and applied filters can be saved within the database. As an example of a single search, searching for 'anticancer' returns 39 results for gold NCs with anticancer properties (Figure 8).

The database allows for multi-criteria searches using two or more keywords. For example, instead of searching only for anticancer applications, we can also filter for entries tested on the HeLa cell line. Using these criteria, only five results were found (Figure 9).



Figure 8. An illustration of a BioGoldNCDB for single search example.



Figure 9. An illustration of a BioGoldNCDB for multi-criteria search example.

4. Materials and Methods

4.1. Data Collection and Processing

Each entry in BioGoldNCDB is a manually curated and annotated record of gold NCs collected from the literature. The initial search was performed using the keyword 'gold nanocluster' in the Chemical Abstracts Service (CAS) database (https://www.cas.org/) via SciFinder (https://scifinder-n.cas.org/). Search filters were applied to include publications from 2000 to 2024, journal articles (as document type) in English, and substances with roles in diagnostic use and pharmacological activity were included only. Review articles were excluded, resulting in 3577 articles. A final filter retained only those whose abstracts contained the keyword 'cluster', refining the selection further. Six additional manually curated data fields were incorporated, covering application, cell line, particle size, excitation/emission wavelength, nanobioconjugates, and table of content (TOC) graphics. The search was conducted on 27 June 2024. Each literature entry was manually reviewed, and only those specifically related to gold NCs and related nanoparticles were included in the final database. The total number of selected articles was 247.

4.2. Database Design and Implementation

The BioGoldNCDB web interface was developed using Next.js and React for the front end [66], while back-end processes are managed within a Node.js environment [67]. Data

storage relies on a MySQL relational database, with queries executed through MySQL commands [68]. The spreadsheet-style data visualization on the webpage was built using the EZGrid React DataGrid component [69]. Both the website and database are hosted on DigitalOcean's cloud infrastructure [70].

5. Conclusions

In conclusion, we have developed BioGoldNCDB, a publicly available database that compiles extensive information on AuNCs and related AuNPs, their conjugates, and relevant literature. The database features an intuitive, user-friendly interface, making it accessible not only to experienced researchers but also to newcomers in the field. All data were manually collected and processed to present relevant insights into the biocompatibility, usability, and key properties of gold NCs in this rapidly evolving field. Each entry includes basic details such as the abstract, CAS Number (CAS RN), Chemical Abstracts Number (CAN), DOI, and PubMed ID. Additionally, the database provides information on applications, particle size, excitation and emission wavelengths, investigated cell lines, and nanoconjugates used.

BioGoldNCDB currently contains 247 entries sourced from 104 different journals. To our knowledge, this is the first freely available comprehensive database dedicated to gold NCs. We believe that BioGoldNCDB highlights the significance of this unique class of nanomaterials and showcases their promising biomedical potential.

While the database serves as a valuable resource for newcomers, we are confident that advanced researchers will also find substantial information relevant to this important field.

Future developments for BioGoldNCDB include periodic incorporation of newly published experimental data, potential integration with related nanomaterial databases to enhance interoperability, and the implementation of advanced features such as customizable filtering options, interactive data visualizations, and improved user navigation to support diverse research needs. While our primary focus remains on gold nanoclusters (AuNCs), we have also included related gold nanoparticles (AuNPs) when they were reported in the same original studies, in order to preserve the context and completeness of the biomedical findings.

Author Contributions: E.E. drafted the original manuscript, collected and curated data, and contributed to methodology. A.M. and B.B. assisted with data collection and curation. L.M. was responsible for visualization and software development. A.D. contributed to conceptualization and final manuscript proofreading. I.M.M. contributed to conceptualization, data handling, and final manuscript proofreading, as well as providing financial support. All authors have read and agreed to the published version of the manuscript.

Funding: We are grateful to the Hungarian Research Foundation (OTKA ANN 139484). The financial support of the National Research, Development and Innovation Office TKP2021-EGA-31 is acknowledged. Project no. RRF-2.3.1-21-2022-00015 has been implemented with support provided by the European Union. E.E. and A.M. acknowledge the grant of EFOP-3.6.3-VEKOP-16-2017-00009.

Institutional Review Board Statement: Not applicable.

Informed Consent Statement: Not applicable.

Data Availability Statement: All database entries are freely available at https://biogoldncdb.ladon. life/. Accessed on 15 August 2024.

Conflicts of Interest: Author László Molnár was employed by the company Solid Science Ltd. The remaining authors declare that the research was conducted in the absence of any commercial or financial relationships that could be construed as a potential conflict of interest.

Abbreviations

The following abbreviations are used in this manuscript:

AuNCsI Gold nanoclusters
AuNPsJ Gold nanoparticles
CT Computed tomography

GSH Glutathione

SPR Surface plasmon resonance

References

1. Kumar, D.; Saini, N.; Jain, N.; Sareen, R.; Pandit, V. Gold nanoparticles: An era in bionanotechnology. *Expert Opin. Drug Deliv.* **2013**, *10*, 397–409. [CrossRef]

- 2. Chan, W.C.W. Bionanotechnology Progress and Advances. Biol. Blood Marrow Transplant. 2006, 12, 87–91. [CrossRef]
- 3. Lee, Y.-C.; Moon, J.-Y. Introduction to Bionanotechnology; Springer: Singapore, 2020; ISBN 9789811512926.
- 4. Jamkhande, P.G.; Ghule, N.W.; Bamer, A.H.; Kalaskar, M.G. Metal nanoparticles synthesis: An overview on methods of preparation, advantages and disadvantages, and applications. *J. Drug Deliv. Sci. Technol.* **2019**, *53*, 101174. [CrossRef]
- 5. Materón, E.M.; Miyazaki, C.M.; Carr, O.; Joshi, N.; Picciani, P.H.S.; Dalmaschio, C.J.; Davis, F.; Shimizu, F.M. Magnetic nanoparticles in biomedical applications: A review. *Appl. Surf. Sci. Adv.* **2021**, *6*, 100163. [CrossRef]
- 6. Moghimi, S.M.; Hunter, A.C.; Murray, J.C. Nanomedicine: Current status and future prospects. *FASEB J.* **2005**, *19*, 311–330. [CrossRef] [PubMed]
- 7. Mody, V.; Siwale, R.; Singh, A.; Mody, H. Introduction to metallic nanoparticles. J. Pharm. Bioallied Sci. 2010, 2, 282–289. [CrossRef]
- 8. Shnoudeh, A.J.; Hamad, I.; Abdo, R.W.; Qadumii, L.; Jaber, A.Y.; Surchi, H.S.; Alkelany, S.Z. Synthesis, Characterization, and Applications of Metal Nanoparticles. In *Biomaterials and Bionanotechnology*; Elsevier: Amsterdam, The Netherlands, 2019; pp. 527–612. ISBN 978-0-12-814427-5.
- 9. Chertok, B.; Moffat, B.A.; David, A.E.; Yu, F.; Bergemann, C.; Ross, B.D.; Yang, V.C. Iron oxide nanoparticles as a drug delivery vehicle for MRI monitored magnetic targeting of brain tumors. *Biomaterials* **2008**, 29, 487–496. [CrossRef]
- 10. Peng, X.-H.; Qian, X.; Mao, H.; Wang, A.Y.; Chen, Z.G.; Nie, S.; Shin, D.M. Targeted magnetic iron oxide nanoparticles for tumor imaging and therapy. *Int. J. Nanomed.* **2008**, *3*, 311–321. [CrossRef]
- 11. Ali, A.; Zafar, H.; Zia, M.; Ul Haq, I.; Phull, A.R.; Ali, J.S.; Hussain, A. Synthesis, characterization, applications, and challenges of iron oxide nanoparticles. *Nanotechnol. Sci. Appl.* **2016**, *9*, 49–67. [CrossRef]
- 12. Atiyeh, B.S.; Costagliola, M.; Hayek, S.N.; Dibo, S.A. Effect of silver on burn wound infection control and healing: Review of the literature. *Burns* **2007**, *33*, 139–148. [CrossRef]
- 13. Lansdown, A.B.G. Silver in Health Care: Antimicrobial Effects and Safety in Use. In *Current Problems in Dermatology*; Hipler, U.-C., Elsner, P., Eds.; KARGER: Basel, Switzerland, 2006; Volume 33, pp. 17–34. ISBN 978-3-8055-8121-9.
- 14. Ravindran, A.; Chandran, P.; Khan, S.S. Biofunctionalized silver nanoparticles: Advances and prospects. *Colloids Surf. B Biointer-faces* **2013**, 105, 342–352. [CrossRef]
- 15. Salata, O. Applications of nanoparticles in biology and medicine. J. Nanobiotechnol. 2004, 2, 3. [CrossRef] [PubMed]
- 16. Morrone, E.; Sancey, L.; Dalonneau, F.; Ricciardi, L.; La Deda, M. Conjugated Human Serum Albumin/Gold-Silica Nanoparticles as Multifunctional Carrier of a Chemotherapeutic Drug. *Int. J. Mol. Sci.* **2024**, 25, 13701. [CrossRef] [PubMed]
- 17. Yeh, Y.-C.; Creran, B.; Rotello, V.M. Gold nanoparticles: Preparation, properties, and applications in bionanotechnology. *Nanoscale* **2012**, *4*, 1871–1880. [CrossRef]
- 18. Mout, R.; Moyano, D.F.; Rana, S.; Rotello, V.M. Surface functionalization of nanoparticles for nanomedicine. *Chem. Soc. Rev.* **2012**, 41, 2539–2544. [CrossRef]
- 19. Zhang, L.; Mazouzi, Y.; Salmain, M.; Liedberg, B.; Boujday, S. Antibody-Gold Nanoparticle Bioconjugates for Biosensors: Synthesis, Characterization and Selected Applications. *Biosens. Bioelectron.* **2020**, *165*, 112370. [CrossRef]
- 20. Liu, J.; Peng, Q. Protein-gold nanoparticle interactions and their possible impact on biomedical applications. *Acta Biomater.* **2017**, 55, 13–27. [CrossRef]
- 21. Liang, A.; Liu, Q.; Wen, G.; Jiang, Z. The surface-plasmon-resonance effect of nanogold/silver and its analytical applications. *TrAC Trends Anal. Chem.* **2012**, 37, 32–47. [CrossRef]
- 22. Halawa, M.I.; Lai, J.; Xu, G. Gold nanoclusters: Synthetic strategies and recent advances in fluorescent sensing. *Mater. Today Nano* **2018**, *3*, 9–27. [CrossRef]
- 23. Díaz, S.A.; Hastman, D.A.; Medintz, I.L.; Oh, E. Understanding energy transfer with luminescent gold nanoclusters: A promising new transduction modality for biorelated applications. *J. Mater. Chem. B* **2017**, *5*, 7907–7926. [CrossRef]
- 24. Rai, M.; Ingle, A.P.; Birla, S.; Yadav, A.; Santos, C.A. Strategic role of selected noble metal nanoparticles in medicine. *Crit. Rev. Microbiol.* 2015, 19, 1–24. [CrossRef]

Molecules **2025**, 30, 3310 14 of 15

25. Wilson, R. The use of gold nanoparticles in diagnostics and detection. Chem. Soc. Rev. 2008, 37, 2028–2045. [CrossRef] [PubMed]

- 26. Sztandera, K.; Gorzkiewicz, M.; Klajnert-Maculewicz, B. Gold Nanoparticles in Cancer Treatment. *Mol. Pharm.* **2019**, *16*, 1–23. [CrossRef]
- 27. Dreaden, E.C.; Alkilany, A.M.; Huang, X.; Murphy, C.J.; El-Sayed, M.A. The golden age: Gold nanoparticles for biomedicine. *Chem. Soc. Rev.* **2012**, *41*, 2740–2779. [CrossRef] [PubMed]
- 28. Sonia; Komal; Kukreti, S.; Kaushik, M. Gold nanoclusters: An ultrasmall platform for multifaceted applications. *Talanta* **2021**, 234, 122623. [CrossRef]
- 29. Yañez-Aulestia, A.; Gupta, N.K.; Hernández, M.; Osorio-Toribio, G.; Sánchez-González, E.; Guzmán-Vargas, A.; Rivera, J.L.; Ibarra, I.A.; Lima, E. Gold nanoparticles: Current and upcoming biomedical applications in sensing, drug, and gene delivery. *Chem. Commun.* 2022, 58, 10886–10895. [CrossRef]
- 30. Sardar, R.; Funston, A.M.; Mulvaney, P.; Murray, R.W. Gold Nanoparticles: Past, Present, and Future. *Langmuir* **2009**, 25, 13840–13851. [CrossRef]
- 31. Sancey, L.; Motto-Ros, V.; Busser, B. Preclinical Evaluation of Nanoparticle Behavior in Biological Tissues by LIBS. In *Laser-Induced Breakdown Spectroscopy in Biological, Forensic and Materials Sciences*; Galbács, G., Ed.; Springer Nature: Cham, Switzerland, 2025; pp. 191–198. ISBN 978-3-031-85974-8.
- 32. Qian, H.; Zhu, M.; Wu, Z.; Jin, R. Quantum Sized Gold Nanoclusters with Atomic Precision. *Acc. Chem. Res.* **2012**, *45*, 1470–1479. [CrossRef]
- 33. Sengani, M.; Grumezescu, A.M.; Rajeswari, V.D. Recent trends and methodologies in gold nanoparticle synthesis—A prospective review on drug delivery aspect. *OpenNano* **2017**, *2*, 37–46. [CrossRef]
- 34. Wang, W.; Wei, Q.-Q.; Wang, J.; Wang, B.-C.; Zhang, S.; Yuan, Z. Role of thiol-containing polyethylene glycol (thiol-PEG) in the modification process of gold nanoparticles (AuNPs): Stabilizer or coagulant? J. Colloid Interface Sci. 2013, 404, 223–229. [CrossRef]
- 35. Sham, T.K.; Kim, P.-S.G.; Zhang, P. Electronic structure of molecular-capped gold nanoparticles from X-ray spectroscopy studies: Implications for coulomb blockade, luminescence and non-Fermi behavior. *Solid State Commun.* **2006**, *138*, 553–557. [CrossRef]
- Abbaszadeh, Z.; Mousavi, M.-M.; Mahmoudpour, M. Surface functionalized gold nanoclusters based on optical biosensors for detecting pesticide residues in agricultural foods: A critical review. *Microchem. J.* 2024, 207, 111988. [CrossRef]
- 37. Juarez-Mosqueda, R.; Malola, S.; Häkkinen, H. Ab initio molecular dynamics studies of Au₃₈(SR)₂₄ isomers under heating. *Eur. Phys. J. D* **2019**, 73, 62. [CrossRef]
- 38. Zhang, W.; Kong, J.; Li, Y.; Kuang, Z.; Wang, H.; Zhou, M. Coherent vibrational dynamics of Au₁₄₄(SR)₆₀ nanoclusters. *Chem. Sci.* **2022**, *13*, 8124–8130. [CrossRef]
- 39. Juarez-Mosqueda, R.; Mpourmpakis, G. Elucidating the optical spectra of [Au₂₅(SR)₁₈]^q nanoclusters. *Phys. Chem. Chem. Phys.* **2019**, *21*, 22272–22282. [CrossRef]
- Maysinger, D.; Maršić, Ž.S.; Gran, E.R.; Shobo, A.; Macairan, J.-R.; Zhang, I.; Bakulić, M.P.; Antoine, R.; Multhaup, G.; Bonačić-Kouteckỳ, V. Insights into the Impact of Gold Nanoclusters Au₁₀ SG₁₀ on Human Microglia. ACS Chem. Neurosci. 2022, 13, 464–476. [CrossRef] [PubMed]
- 41. Bai, Y.; Shu, T.; Su, L.; Zhang, X. Fluorescent Gold Nanoclusters for Biosensor and Bioimaging Application. *Crystals* **2020**, 10, 357. [CrossRef]
- 42. Maysinger, D.; Gran, E.R.; Bertorelle, F.; Fakhouri, H.; Antoine, R.; Kaul, E.S.; Samhadaneh, D.M.; Stochaj, U. Gold nanoclusters elicit homeostatic perturbations in glioblastoma cells and adaptive changes of lysosomes. *Theranostics* **2020**, *10*, 1633–1648. [CrossRef]
- 43. Chen, L.-Y.; Wang, C.-W.; Yuan, Z.; Chang, H.-T. Fluorescent Gold Nanoclusters: Recent Advances in Sensing and Imaging. *Anal. Chem.* **2015**, *87*, 216–229. [CrossRef]
- 44. Lin, Y.; Ren, J.; Qu, X. Nano-Gold as Artificial Enzymes: Hidden Talents. Adv. Mater. 2014, 26, 4200–4217. [CrossRef] [PubMed]
- 45. An, D.; Su, J.; Weber, J.K.; Gao, X.; Zhou, R.; Li, J. A Peptide-Coated Gold Nanocluster Exhibits Unique Behavior in Protein Activity Inhibition. *J. Am. Chem. Soc.* **2015**, *137*, 8412–8418. [CrossRef] [PubMed]
- 46. Zhang, I.; Maysinger, D.; Beus, M.; Mravak, A.; Yu, Z.; Bakulić, M.P.; Dion, P.A.; Rouleau, G.A.; Bonačić-Koutecký, V.; Antoine, R.; et al. Gold nanoclusters Au₂₅ AcCys₁₈ normalize intracellular ROS without increasing cytoplasmic alarmin acHMGB1 abundance in human microglia and neurons. *Nanoscale* 2025, 17, 1092–1104. [CrossRef]
- 47. Zheng, K.; Setyawati, M.I.; Leong, D.T.; Xie, J. Antimicrobial Gold Nanoclusters. ACS Nano 2017, 11, 6904–6910. [CrossRef]
- 48. Nirmal, G.R.; Lin, Z.-C.; Chiu, T.-S.; Alalaiwe, A.; Liao, C.-C.; Fang, J.-Y. Chemo-photothermal therapy of chitosan/gold nanorod clusters for antibacterial treatment against the infection of planktonic and biofilm MRSA. *Int. J. Biol. Macromol.* **2024**, 268, 131673. [CrossRef]
- 49. Zhou, T.; Cheng, Y.; Zhang, H.; Wang, G. Sunlight-Mediated Antibacterial Activity Enhancement of Gold Nanoclusters and Graphene Co-decorated Titanium Dioxide Nanocomposites. *J. Clust. Sci.* **2019**, *30*, 985–994. [CrossRef]
- 50. Ding, H.; Yang, D.; Zhao, C.; Song, Z.; Liu, P.; Wang, Y.; Chen, Z.; Shen, J. Protein–Gold Hybrid Nanocubes for Cell Imaging and Drug Delivery. ACS Appl. Mater. Interfaces 2015, 7, 4713–4719. [CrossRef]

Molecules **2025**, 30, 3310 15 of 15

51. Fakhouri, H.; Bakulić, M.P.; Zhang, I.; Yuan, H.; Bain, D.; Rondepierre, F.; Brevet, P.-F.; Maršić, Ž.S.; Antoine, R.; Bonačić-Koutecký, V.; et al. Ligand impact on reactive oxygen species generation of Au₁₀ and Au₂₅ nanoclusters upon one- and two-photon excitation. *Commun. Chem.* **2023**, *6*, 97. [CrossRef] [PubMed]

- 52. Chen, D.; Li, B.; Cai, S.; Wang, P.; Peng, S.; Sheng, Y.; He, Y.; Gu, Y.; Chen, H. Dual targeting luminescent gold nanoclusters for tumor imaging and deep tissue therapy. *Biomaterials* **2016**, *100*, 1–16. [CrossRef]
- 53. Tao, Y.; Li, M.; Auguste, D.T. Pattern-based sensing of triple negative breast cancer cells with dual-ligand cofunctionalized gold nanoclusters. *Biomaterials* **2017**, *116*, 21–33. [CrossRef]
- 54. Samani, R.K.; Tavakoli, M.B.; Maghsoudinia, F.; Motaghi, H.; Hejazi, S.H.; Mehrgardi, M.A. Trastuzumab and folic acid functionalized gold nanoclusters as a dual-targeted radiosensitizer for megavoltage radiation therapy of human breast cancer. *Eur. J. Pharm. Sci.* **2020**, *153*, 105487. [CrossRef] [PubMed]
- 55. Sharma, P.; Yuan, H.; Verma, R.; Mehla, N.; Hemant, H.; Sagar, P.; Comby-Zerbino, C.; Russier-Antoine, I.; Moulin, C.; Brevet, P.; et al. Intrinsically Pro-Apoptotic Gold Nanoclusters for Optical Tracing and Inhibition of Solid Tumors. *Adv. Healthc. Mater.* 2025, 14, 2405005. [CrossRef]
- 56. Luo, D.; Wang, X.; Zeng, S.; Ramamurthy, G.; Burda, C.; Basilion, J.P. Targeted Gold Nanocluster-Enhanced Radiotherapy of Prostate Cancer. *Small* **2019**, *15*, 1900968. [CrossRef]
- Gutierrez, N.M.C.; Clainche, T.L.; Bulin, A.; Leo, S.; Kadri, M.; Abdelhamid, A.G.A.; Pujol-Solé, N.; Obaid, G.; Hograindleur, M.; Gardette, V.; et al. Engineering Radiocatalytic Nanoliposomes with Hydrophobic Gold Nanoclusters for Radiotherapy Enhancement. Adv. Mater. 2024, 36, 2404605. [CrossRef]
- 58. Zhang, Q.; Shi, D.; Guo, M.; Zhao, H.; Zhao, Y.; Yang, X. Radiofrequency-Activated Pyroptosis of Bi-Valent Gold Nanocluster for Cancer Immunotherapy. *ACS Nano* **2023**, *17*, 515–529. [CrossRef]
- 59. Zhao, T.; Zhang, S.; Guo, Y.; Wang, Q. TiC₂: A new two-dimensional sheet beyond MXenes. *Nanoscale* **2016**, *8*, 233–242. [CrossRef] [PubMed]
- 60. Wang, M.; Wang, L.; Feng, H.; Jiang, H.; Zhou, J.; Wang, X. Precise therapeutic effect of self-assembling gold nanocluster–PTEN complexes on an orthotropic model of liver cancer. *J. Cancer Res. Clin. Oncol.* **2020**, *146*, 875–882. [CrossRef]
- 61. Srinivasulu, Y.G.; Mozhi, A.; Goswami, N.; Yao, Q.; Xie, J. Traceable Nanocluster–Prodrug Conjugate for Chemo-photodynamic Combinatorial Therapy of Non-small Cell Lung Cancer. *ACS Appl. Bio Mater.* **2021**, *4*, 3232–3245. [CrossRef] [PubMed]
- 62. Cerón, M.R.; Izquierdo, M.; Alegret, N.; Valdez, J.A.; Rodríguez-Fortea, A.; Olmstead, M.M.; Balch, A.L.; Poblet, J.M.; Echegoyen, L. Reactivity differences of $Sc_3N@C_{2n}$ (2n = 68 and 80). Synthesis of the first methanofullerene derivatives of $Sc_3N@D_{5h}-C_{80}$. Chem. Commun. 2016, 52, 64–67. [CrossRef] [PubMed]
- 63. Wang, X.; He, H.; Wang, Y.; Wang, J.; Sun, X.; Xu, H.; Nau, W.M.; Zhang, X.; Huang, F. Active tumor-targeting luminescent gold clusters with efficient urinary excretion. *Chem. Commun.* **2016**, *52*, 9232–9235. [CrossRef]
- 64. Shome, R.; Ghosh, S.S. Transferrin Coated D-penicillamine–Au-Cu Nanocluster PLGA Nanocomposite Reverses Hypoxia-Induced EMT and MDR of Triple-Negative Breast Cancers. *ACS Appl. Bio Mater.* **2021**, *4*, 5033–5048. [CrossRef]
- 65. Ou, Y.-C.; Wen, X.; Johnson, C.A.; Shae, D.; Ayala, O.D.; Webb, J.A.; Lin, E.C.; DeLapp, R.C.; Boyd, K.L.; Richmond, A.; et al. Multimodal Multiplexed Immunoimaging with Nanostars to Detect Multiple Immunomarkers and Monitor Response to Immunotherapies. ACS Nano 2020, 14, 651–663. [CrossRef] [PubMed]
- 66. Next.js/React. Official Documentation. Available online: https://react.dev/ (accessed on 5 August 2024).
- 67. Node.js. Official Documentation. Available online: https://nodejs.org/en/docs (accessed on 5 August 2024).
- 68. MySQL. Official Documentation. Available online: https://dev.mysql.com/doc/ (accessed on 5 August 2024).
- 69. EZGrid React DataGrid Component. Available online: https://reactdatagrid.com/ (accessed on 5 August 2024).
- 70. DigitalOcean Cloud Hosting. Official Website. Available online: https://www.digitalocean.com/ (accessed on 5 August 2024).

Disclaimer/Publisher's Note: The statements, opinions and data contained in all publications are solely those of the individual author(s) and contributor(s) and not of MDPI and/or the editor(s). MDPI and/or the editor(s) disclaim responsibility for any injury to people or property resulting from any ideas, methods, instructions or products referred to in the content.





Article

Sustainable and Safe *N*-alkylation of *N*-heterocycles by Propylene Carbonate under Neat Reaction Conditions

Andrea Czompa ¹, Dóra Bogdán ^{1,2}, Balázs Balogh ¹, Eszter Erdei ^{1,2}, Patrik Selymes ¹, Attila Csomos ^{3,4} and István M. Mándity ^{1,2},*

- Institute of Organic Chemistry, Semmelweis University, Högyes Endre utca 7, H-1092 Budapest, Hungary; czompa.andrea@semmelweis.hu (A.C.); bogdan.dora@semmelweis.hu (D.B.); balogh.balazs@semmelweis.hu (B.B.); erdei.eszter@stud.semmelweis.hu (E.E.); patrik.selymes@gmail.com (P.S.)
- HUN-REN Artificial Transporters Research Group, Institute of Materials and Environmental Chemistry, Research Centre for Natural Sciences Magyar Tudósok körútja 2, H-1117 Budapest, Hungary
- ³ Femtonics Ltd., Tüzoltó utca 59, H-1094 Budapest, Hungary; attila.csomos@femtonics.eu
- ⁴ Hevesy György PhD School of Chemistry, Eötvös Loránd University, Pázmány Péter sétány 1/A, H-1117 Budapest, Hungary
- * Correspondence: mandity.istvan@ttk.hu; Tel.: +36-205-230-081

Abstract: A new, eco-friendly process utilising the green solvent propylene carbonate (PC) has been developed to perform N-alkylation of N-, O- and/or S-containing heterocyclic compounds. PC in these reactions served as both the reagent and solvent. Importantly, no genotoxic alkyl halides were required. No auxiliary was necessary when using anhydrous PC. Product formation includes nucleophilic substitution with the concomitant loss of water and carbon dioxide. Substrates prepared, including the newly invented PROTAC drugs, are widely used.

Keywords: propylene carbonate; N-alkylation; heterocycles; neat conditions; green chemistry



Citation: Czompa, A.; Bogdán, D.; Balogh, B.; Erdei, E.; Selymes, P.; Csomos, A.; Mándity, I.M. Sustainable and Safe *N*-alkylation of *N*-heterocycles by Propylene Carbonate under Neat Reaction Conditions. *Int. J. Mol. Sci.* **2024**, *25*, 5523. https://doi.org/10.3390/ ijms25105523

Academic Editors: José Justicia and Rachid Chahboun

Received: 19 April 2024 Revised: 15 May 2024 Accepted: 16 May 2024 Published: 18 May 2024



Copyright: © 2024 by the authors. Licensee MDPI, Basel, Switzerland. This article is an open access article distributed under the terms and conditions of the Creative Commons Attribution (CC BY) license (https://creativecommons.org/licenses/by/4.0/).

1. Introduction

Propylene carbonate (PC) has been ranked as one of the greenest solvents according to the GlaxoSmithKline sustainability guide [1]. PC is a carbon-neutral, polar aprotic solvent with a boiling point of 242 °C, serving as an excellent solvent to perform chemical reactions at higher temperatures [2]. All three carbon atoms of the ring are electrophilic sites [3]. PC has been shown to be an efficient solvent for several transformations under various conditions. Various Suzuki-Miyaura reactions were carried out in PC [4]. Interestingly, aside from C-C bond formation, in a few cases, N-alkylation occurred and products with a 2-hydroxypropyl side chain were observed, as PC served not only as a reagent, but also as a solvent. Several remarkable examples are reported for alkylation reactions on heteroatoms with PC, including 2-hydroxypropylation of adenine with PC and NaOH in DMF [5]. The O-alkylation of phenol was performed in the presence of NaOCH₃ and with glycerol carbonate as the reagent and solvent [3,6]. The synthesis of N-(2,3-dihydroxy) propylanilines and the mechanism of the reaction were also investigated in a reaction of glycerol carbonate with primary amines catalysed by faujasites [7]. Aminolysis as a side reaction was also reported in the transformation of glycerol carbonate with butylamine [8]. The alkylation of resorcinol with ethylene carbonate was carried out using a triorgano-substituted phosphane catalyst [9]. In another study, a similar reaction was executed using alkali-loaded largepore zeolites as catalysts [10]. Inspired by these results, we have decided to explore the possibilities of applying PC both as a solvent and reagent in order to perform alkylation of certain N-, O- and S-containing substrates in one step. Usually, the alkylation of a nitrogen heteroatom can be achieved with alkyl halides or epoxides [11]; however, these reagents are generally considered as genotoxic agents [12]. To overcome these considerable restrictions, several reactions were carried out where less reactive reagents, like carboxylic acids, were

used for *N*-alkylation [13]. However, these reactions needed a special catalyst or special experimental set-up, like the safe handling of hydrogen gas. In a similar way, nitroarenes were utilised for *N*-alkylation under reductive conditions [14]. Alcohols were also used for *N*-alkylation, but this reaction required catalytic conditions as well [15,16]. In 2010, M. Selva and co-workers published the selective synthesis of bis-*N*-(2-hydroxy)alkylanilines with ethylene and propylene carbonate [17], respectively, starting with primary aniline and in the presence of a catalytic amount of phosphonium-based ionic liquids. They conclude that the reactions with PC take place at higher temperatures than those for ethylene carbonate (EC), but only in the presence of phosphonium ionic liquid. By studying the kinetic properties of the reaction of aniline with EC, they found that in the first two hours, the concentration of *N*-2-hydroxyethylaniline increased as the concentration of starting aniline decreased, but in the following hours, the concentration of bis-*N*-(2-hydroxyethyl)aniline increased with a parallel decrease of concentration of the monoalkylated product.

The aim of this work is to study the catalyst-free alkylating nature of PC under alkaline conditions with the aid of a microwave (Scheme 1).

Scheme 1. General outline of the performed reactions.

Substrates used in the study are phthalimide (1), isatin (2), phthalazin-1(2H)-one (3), pyrimidin-4(3H)-one (4), 6-methylpyrimidine-2,4(1H,3H)-dione (5), 1H-benzotriazole (6) and 2-thiouracil (7) (Figure 1). These compounds have been selected since they are substructures of drug molecules discovered previously. Phthalimide (1) is a subunit of anticancer pomalidomide [1B] and PROTACs [1B], which promote protein degradation [2B]. The other investigated heterocycles are structural elements in CNS drugs or antimicrobial agents [2B] (isatin), antihistamine azelastine [2B] (phthalazinone), antipsychotic risperidone [2B] (pyrimidinone), 5-HT2 and B1 receptor antagonist ketanserin [2B2] (6-methyluracil). 1B1-benzotriazole derivatives were found to influence metabotropic glutamate receptors [2B3], while 2-thiouracil is a subunit of the PI3KB3 inhibitor dezapelisib [2B3].

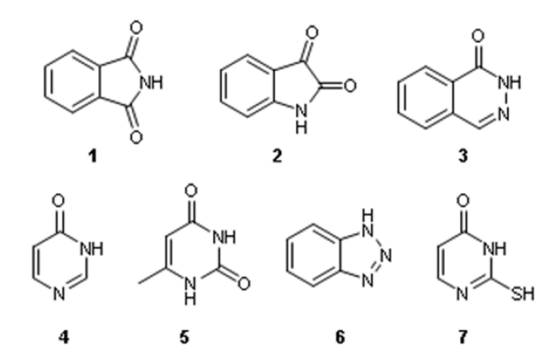


Figure 1. The structures of substrates studied.

2. Results

Due to our experiences with Suzuki–Miyaura reactions [4a] and green chemical transformation [4b, c, d], we returned to the 1M solution of Na_2CO_3 used as a base in the N-alkylation reaction of N-heterocyclic compounds mentioned before.

All seven substrates contain a nitrogen atom with an acidic hydrogen attached. Our aim was to demonstrate that the corresponding nitrogen nucleophile, formed via proton

loss in the presence of a base, can attack the most electrophilic and less sterically hindered side of PC that is the CH₂ group. In order to achieve our goal, we tried to optimise the quantity of PC. Note, however, that it needs to be used in excess, because it is the reagent and solvent as well.

2.1. Phthalimide (1)

Our prototype molecule was phthalimide [27–31] with a nitrogen atom in between two electron-withdrawing carbonyl groups. It is a symmetric molecule existing in a tautomeric equilibrium of **1a** and **1b** (Scheme 2).

Scheme 2. Tautomer of phthalimide.

The reaction mixture was heated either by an oil bath or microwave (MW) irradiation. In order to optimise the amount of substances and reaction conditions, we started using 1 mmol each of the substrates, $1M \, \text{Na}_2 \, \text{CO}_3$ and varied amounts of PC (6, 9, 12 and 18 mmol). The reaction temperature was $130 \, ^{\circ} \text{C}$ under MW conditions, which corresponds to $150 \, ^{\circ} \text{C}$ in the oil bath (Table 1). PC in excess amounts was found to be detrimental. In the beginning, we used a temperature of $130 \, ^{\circ} \text{C}$ in the MW. Unfortunately, our attempt failed with the use of aq. $1M \, \text{Na}_2 \, \text{CO}_3$ (Table 1, entry 1). Similar results were found with $1M \, \text{of} \, \text{K}_2 \, \text{CO}_3$, KOH and NaOAc. Our attempts to add para-toluenesulfonic acid to protonate the hydroxy function and form a better leaving group, as well as raising the temperature to $170 \, ^{\circ} \text{C}$ (oil bath) and $150 \, ^{\circ} \text{C}$ (MW), were also unsuccessful.

Table 1. *N*-Hydroxyalkylation of phthalimide (1).

Entry	Heating	PC (mmol/%)	Base	T (°C)	Time (h)	Drying Agent	Yield (%) 8
1	MW	6/99%	1 mmol 1M Na ₂ CO ₃	130	2	none	-
2	MW	9/99%	1 mmol 1M Na ₂ CO ₃	130	2	100 mg MS (3 Å)	49
3	MW	9/99%	1 mmol Na ₂ CO ₃ a	150	1	1 mmol CaCl ₂	63
4	MW	9/99.7%	1 mmol Na ₂ CO ₃ a	150	1	none	70
5	oil bath	9/99%	1 mmol Na ₂ CO ₃ a	170	4	1 mmol CaCl ₂	66

^a Aqueous or powder.

It has been suspected that the 99% purity of PC used in excess was a problem. Consequently, a small amount (100 mg) of molecular sieve as a drying agent (Table 1, entry 2) was added. The reaction under these modified conditions resulted in successful N-alkylation of phthalimide with a yield of 49% (Scheme 3). Then, the molecular sieve was swapped with anhydrous CaCl $_2$ (entry 3) that raised the yield to 63% at 150 °C using the MW, and to 66% at 170 °C in the oil bath, although the reaction time had to be increased from 1 to 4 h (entry 5). Finally, the alkylation with similar ratios of reagents and high-purity (99.7%) PC without a drying agent was carried out; the highest yield of 70% was achieved (150 °C, 1 h, MW; entry 4).

Scheme 3. *N*-Hydroxyalkylation of phthalimide (1).

2.2. Isatin (2)

For this substance (Scheme 4), both conventional heating and microwave irradiation were tested using both 99% and high-purity (99.7%) PC. Unfortunately, at the beginning, the reaction was unsuccessful (see, for example, Table 2, entry 1). In the single successful attempt performed with 99.7% PC, the desired substance [32,33], 1-(2-hydroxypropyl)-1*H*-indole-2,3-dione (9), was isolated in a 77% yield (Table 2, entry 2) without a drying agent. We have tried to interpret these experimental results. In a study, isatine was shown to be water sensitive [34,35]; we surmise that a possible ring opening of isatine may contribute to the results found.

Scheme 4. N-Alkylation of isatine (2).

Table 2. *N*-Hydroxyalkylation of isatine (2).

Entry	Heating	PC (mmol/%)	Na ₂ CO ₃	T (°C)	Time (h)	CaCl ₂	Yield (%) 9
1	MW	9/99%	1 mmol	160	1	1 mmol	-
2	MW	9/99.7%	1 mmol	150	1	none	77

2.3. Phthalazin-1(2H)-One (3)

Phthalazin-1(2*H*)-one also exists as a tautomeric mixture in which the *exo*-cyclic double bond shifts to the benzocondensed heteroring (Scheme 5) and the hydrogen attached to the nitrogen atom moves to the oxygen atom. In the lactim tautomer we have an aromatic heteroring system, but the hydroxy group formed has lower nucleophilicity; thus, only *N*-alkylation will occur, as in all other cases.

Scheme 5. Tautomers of phthalazin-1(2*H*)-one.

In the case of phthalazinone, some conclusions can be drawn by comparing reaction methods (oil heating and microwave irradiation) and reaction time. More solvent was used than for the previous cases, because of the increased molecular mass of the substrate. A yield of 28% was found using traditional oil heating in the presence of Na_2CO_3 and 1 mmol $CaCl_2$ with 99% PC (Table 3, entry 1, Scheme 6). The 4 h MW irradiation improved the yield to 50% (Table 3, entry 2), demonstrating that MW heating is more efficient than oil heating. In a further test, reducing the reaction time to 2 h and utilising 99.7% PC has created the product 2-(2-hydroxypropyl)phthalazin-1(2H)-one (10) with the highest yield of 55%, even without using the drying agent (Table 3, entry 3). This latter alkylated product is a new compound (Scheme 6). Furthermore, we can start to see a pattern, implying that the absence of water is critical in these N-alkylation reactions.

Table 3. *N*-Hydroxyalkylation of phthalazin-1(2*H*)-one (3).

Entry	Heating	PC (mmol/%)	Na ₂ CO ₃	T (°C)	Time (h)	CaCl ₂	Yield (%) 10
1	oil bath	12/99%	1 mmol	170	4	1 mmol	28
2	MW	12/99%	1 mmol	150	4	1 mmol	50
3	MW	12/99.7%	1 mmol	150	2	none	55

Int. J. Mol. Sci. 2024, 25, 5523 5 of 14

Scheme 6. *N*-Alkylation of phthalazin-1(2*H*)-one (3).

2.4. Pyrimidin-4(3H)-One (4)

In pyrimidin-4(3H)-one (4), one N-atom is in the near proximity of the oxo functional group and the other is further from it, and because of this, it produces two different derivatives, namely a 1N- and 3N-alkylated products molecule. In addition, the 1N-alkylated product (12) was the major product (Schemes 7 and 8).

Scheme 7. The structure of pyrimidin-4(3*H*)-one anions.

Scheme 8. *N*-Alkylation of pyrimidin-4(3*H*)-one (4).

Oil bath treatment has provided a decent yield of 28% of the 3N-alkylated (11) product and 54% of the 1N-alkylated derivative (12) (Table 4, entry 1). Under MW irradiation, 99% purity PC provided a lower amount of product 11 (17%), but 12 was isolated with a similar yield of 58% (data not shown). Testing 99.7% PC resulted in the highest yields of 42% and 57%, respectively, proving the great reactivity of this substance (Table 4, entry 2) towards the alkylating agent. An explanation for this phenomenon could be the higher acidity of the hydrogen attached to the 3N due to the proximity of the strong electron-withdrawing carbonyl group. Consequently, the base will abstract this proton and the formed negative charge will be in conjugation with the adjacent double bond, generating a partial negative charge on the 1N (Scheme 7). Consequently, it has a higher stability than the other one, because of the resulting quinoidal structure. This accounts for the observed selectivity pattern. Both synthesised products, 11 and 12, are new compounds.

Table 4. *N*-Hydroxyalkylation of pyrimidin-4(3*H*)-one (4).

Entry	Heating	PC (mmol/%)	Na ₂ CO ₃	T (°C)	Time (h)	CaCl ₂	Yield (%) 11,12
1	oil bath	9/99%	1 mmol	170	3	1 mmol	28, 54 42, 57
2	MW	9/99.7%	1 mmol	150	1	non	

2.5. 6-Methylpyrimidine-2,4(1H,3H)-Dione (5)

While using solvent in high excess, oil bath conditions required a long time to detect any product at all. Products were barely detected with 99% PC, which made the use of 1 mmol CaCl₂ necessary (a yield of 6%, Table 5, entry 4). Nevertheless, under MW conditions with less PC, we could synthesise the dialkylated product 1,3-bis(2-hydroxypropyl)-6-methylpyrimidine-2,4(1*H*,3*H*)-dione (13) (Scheme 9) with a yield twice as high (Table 5, entry 1).

Entry	Heating	PC (mmol/%)	Na ₂ CO ₃	T (°C)	Time (h)	CaCl ₂	Yield (%) 13
1	MW	9/99%	1 mmol	150	6	1 mmol	12
2	MW	9/99.7%	1 mmol	150	2	none	22
3	MW	9/99.7%	1 mmol	150	6	none	49
4	oil bath	12/99%	1 mmol	170	9	1 mmol	6

Table 5. Results with 6-methylpyrimidine-2,4(1*H*,3*H*)-dione (5).

Scheme 9. *N*-Alkylation of 6-methylpyrimidine-2,4(1*H*,3*H*)-dione (5).

With higher-quality PC, adding the drying agent was no longer required and we attained a yield of 22% in 2 h (Table 5, entry 2). The highest productivity (49% yield) was achieved by using the MW for 6 h without the drying agent (Table 5, entry 3). The synthesis of 1,3-bis(2-hydroxypropyl)-6-methylpyrimidine-2,4(1*H*,3*H*)-dione (13) appeared in a Polish patent synthetised by carcinogenic reagents [36]. In our method, using the green PC as a reagent and solvent allowed us to obtain the dialkylated product (13) in a similar yield (49%), with a decreased reaction time of 6 h (Table 5, entry 3). Interestingly, in the transformation of 6-methylpyrimidine-2,4(1*H*,3*H*)-dione (5) we could not detect any monoalkylated molecule; only dialkylated compound 13 was formed (Scheme 9). Presumably, the nitrogen atom between the carbonyl groups is alkylated first, leading to a product with a single 2-hydroxypropyl side chain. The latter then undergoes a second reaction, resulting in product 13 (Scheme 10).

Scheme 10. Possible transformation routes in the alkylation of 6-methylpyrimidine-2,4(1H,3H)-dione.

It seems that PC is a good alkylating agent, and the proximal electron-donating methyl group does not influence the alkylation of both nitrogen atoms. In order to confirm the alkylating power of the present system, we decided to probe its reactivity with a substrate which does not contain such a strong electron-withdrawing group as the carbonyl group.

2.6. 1H-Benzotriazole (6)

This substrate has three nitrogen atoms in positions 1, 2 and 3 and it has the following two isomers: 1*H*- and 2*H*-benzotriazole (Scheme 11). The nitrogen atoms have an electron-withdrawing effect and, consequently, the attached hydrogen atoms can be removed by a base, while the nucleophiles obtained can be alkylated by PC. The 2-hydroxypropyl side chain obtained after *N*-alkylation has a steric demand. As a result, it is not expected to deliver a dialkylated product at the benzotriazole ring. Furthermore, if one considers that

the nucleophile obtained by deprotonation of the 1N atom is more stable than the 2N atom, alkylation is expected to take place on the 1N atom [37,38]. Nevertheless, we were curious to know if N-alkylation occurs at all.

Scheme 11. Isomeric 1H- and 2H-benzotriazoles.

The results of our experiments with benzotriazole are summarised in Table 6. These data show that N-alkylation can take place on both nitrogen atoms (Scheme 12). In each case, the quantity of the 1N-alkylated product (15) was higher than that of the 2N-alkylated product (14). Using PC in the presence of the drying agent and oil bath heating, we measured 22% of 1-(2H-benzotriazol-2-yl)propan-2-ol (14) and 47% of 1-(1H-benzotriazol-1-yl)propan-2-ol (15). Under identical reaction conditions, using microwave irradiation, the amounts of both 14 and 15 increased (entry 2). As usual, the best results were achieved without the drying agent ($CaCl_2$) and by utilising high-purity PC under MW conditions (entry 3). As expected, in all cases, the 1N-alkylation reaction (product 15) occurs at a higher percentage (47–55%) than the 2N-alkylation process (product 14, 22–35%).

Table 6. *N*-Alkylation of 1*H*-benzotriazole (6).

Entry	Heating	PC (mmol/%)	Na ₂ CO ₃	T (°C)	Time (h)	CaCl ₂	Yield (%) 14, 15
1	oil bath	9/99%	1 mmol	170	3	1 mmol	22, 47
2	MW	9/99%	1 mmol	150	3	1 mmol	25, 53
3	MW	9/99.7%	1 mmol	150	4	none	35, 55

Scheme 12. Results with benzotriazole (6).

2.7. 2-Thiouracil (7)

The last substrate in our N-alkylation experiments was 2-thiouracil. It is already known that 2-thiouracil and its 5- and 6-methyl derivatives are oxidisable with hypervalent iodine [39], for example, using iodosylbenzene or employing ozone. In each case, the thiocarbonyl moiety is attacked and desulfurisation occurs, creating uracil and carbonyl compounds [40]. According to the literature, 2-thioxo-1,2,3,4-tehtrahydropyrimidin-4-one reacted with propylene oxide in a similar manner [41]. However, propylene oxide is not an environmentally benign reagent. In this report, NaOMe/MeOH, KOH/MeOH and NaOH/H₂O as base–solvent systems were applied, and in each case, the desired derivatives were isolated in an almost quantitative yield. It seems that, in the presence of a base, the thiol functional group between the two nitrogen atoms of the starting 2-thiouracil is replaced by a hydroxy group, as depicted in Scheme 13.

Based on these findings, we were not surprised to obtain two products; both monoalky-lated 1-(2-hydroxypropyl) pyrimidine-2,4(1*H*,3*H*)-dione (**16**) and dialkylated-uracil (**17**) were detected (Scheme **14**). 1,3-Bis(2-hydroxypropyl)pyrimidine-2,4(1*H*,3*H*)-dione (**16**) is mentioned in a patent [42], but it has not yet been characterised. We observed both monoalkylation (11%) and dialkylation (5%) in oil bath heating (Table 7, entry 1). The yields are not satisfactory, and the reaction under MW irradiation provided similar results with a more balanced product ratio. By increasing the reaction time to 7 h, the two compounds were produced in an equal amount of 13%.

Scheme 13. Hydrolysis of 2-thiouracil and its tautomer.

Scheme 14. N-Alkylation of 2-thiouracil (7) with 99% PC and CaCl₂.

Table 7. *N*-Alkylation of 2-thiouracil (7).

Entry	Heating	PC (mmol/%)	Na ₂ CO ₃	T (°C)	Time (h)	CaCl ₂	Yield (%) 16, 17, 18, 19
1	oil bath	9/99%	1 mmol	170	3	1 mmol	11, 5, n.i., n.i.
2	MW	9/99.7%	1 mmol	150	2	none	n.i., 7, 34, 17
3	MW	9/99.7%	1 mmol	150	4	none	n.i., 30, 20, 14

Next, 99% PC was replaced by 99.7% PC and reactions were performed without CaCl₂. Under these modified conditions, three products (17, 18 and 19; Scheme 15) were detected with 1,3-bis(2-hydroxypropyl)pyrimidine-2,4(1*H*,3*H*)dione (17) in a significantly decreased yield of 7%. As already discussed, (Scheme 13) both 2-thiouracil and uracil are present in the alkaline solution. The high-quality PC increases the cyclisation rate (Table 7, entry 2) of the mono-*N*-alkylated product (16) to serve the following two new products: one with an oxazole ring (18, 34%) [43,44] and the other with a thiazole ring (19, 17%). By increasing the reaction time (Table 7, entry 3), the amount of both products 18 and 19 decreases somewhat (20% and 14%), while more dialkylated product can be obtained (17, 30%).

Scheme 15. *N*-Alkylation of 2-thiouracil (7) with 99.7% PC without CaCl₂.

We have demonstrated that the sensible equilibrium, observed in previous studies performing alkylation of 2-thiouracil, exists under our conditions as well, serving different products. We assume that the cyclised compounds (18, 19) can be obtained after monoalkylation has taken place on the 1N atom, followed by elimination of a water molecule from the alkylated side chain and the hydrogen of the hydroxy or thiol group attached to the C-2 atom (Scheme 16). Dialkylated product 17 and thiazole-condensed product 19 have not yet been published.

Scheme 16. Cyclisation products of uracil and 2-thiouracil.

2.8. Theoretical Calculations

For the elucidation of the results obtained, theoretical calculations were carried out [44–47] and pKa values were determined for compounds 1–7. In the case of 1–3, there is only a single protic hydrogen in the molecules, attached to the nitrogen atom with calculated pKa values of 8.63, 9.70 and 11.89, respectively. These data indicate that under alkaline conditions, protons can be removed and the formed anions as nucleophiles are capable of opening PC, providing the *N*-alkylated product.

Considering compound 4, there is only a single C–H in the molecule with a protic nature, but the two nitrogen atoms can also carry protic hydrogens. As a consequence, two products are expected. The pKa values calculated are 7.91 and 8.40 for 1*N* and 3*N*, respectively, indicating that the 1*N* position is more acidic. This corroborates our experimental results, since the 1*N*-alkylated product was formed with a larger amount. Importantly, no doubly alkylated product was observed.

Regarding compound 5, both nitrogen atoms bear a hydrogen of protic nature; thus, double alkylation might be expected. The pKa values calculated are 9.44 and 9.34 for 1N and 3N, respectively. According to these data, the first alkylation may happen in position 3. The pKa value calculated for the 3N-alkylated derivative of 5 is 8.81. Accordingly, the alkylation of 5 in position 3 enhanced the acidity of position 1, and this explains why the doubly alkylated product was isolated as the sole derivative.

Concerning compound **6**, there is only a single hydrogen of protic character in the molecule. However, the anion formed after deprotonation has two mesomeric forms, with the negative charge located at either position 1 or position 2. Theoretical calculations suggest that the latter mesomeric form is slightly more stable (~1 kcal/mol); thus, charge transition is possible.

Finally, for compound 7, results may be expected to be like those of 5. The pKa values calculated are 6.54 and 7.15 for 1N and 3N, respectively. Both protons have a significant acidic nature, and the observed double alkylation is in harmony with theoretical calculations.

The results of the reactions are summarised in Table 8.

The cyclised compounds (18, 19) can be obtained only after monoalkylation has taken place on the 1N atom, followed by elimination of a water molecule.

Table 8. Product yields under optimised reaction conditions.

Reactant	Product(s) Yield (%)
1	N—————————————————————————————————————

Table 8. Cont.

Reactant	Product(s) Yield (%)
2	OH OH
3 [a]	9: 77% O N OH 10: 55%
4	OH OH
5 [b]	11: 42% 12: 57% OH OH OH 13: 49%
6 [c]	HO TOO
7 [c]	14: 35% 15: 55% OH OH 17: 30% 18: 20% 19: 14%

[a]: reaction time 2 h, [b]: reaction time 6 h, [c]: reaction time 4 h.

3. Materials and Methods

Experimental

Phthalimide (99%) and propylene carbonate (99%) were purchased from Alfa Aesar. 1(2*H*)-Phthalazinone (99%), 4(3*H*)-pyrimidone (98%), 2,4-dihydroxy-6-methylpyrimidine (97%) and propylene carbonate (99.7%) were purchased from Sigma-Aldrich. Isatin (98%) was purchased from Reanal, 1*H*-benzotriazole (99%) was purchased from Merck, 2-thiouracil (98%) was purchased from Fluka, sodium carbonate (99.5%) was purchased from Acidum and calcium chloride (98.1%) was purchased from Molar.

Thin-layer chromatography (TLC) was performed on aluminium sheets precoated with Merck 5735 Kieselgel 60F254 (Merck, Darmastadt). Column chromatography was carried out with Merck 5735 Kieselgel 60F (0.040–0.063 nm mesh). All other chemicals and

solvents were purchased from different commercial sources and used as received without further purification.

Freeze-drying was performed one night in a LYPH-Lock 1L lyophiliser LabConco (Kansas City, MI, USA) with a high vacuum pump at 10 mmHg and $-50\,^{\circ}$ C. Melting points were measured on a Büchi M-550 apparatus (Büchi Labortechnik AG, Flawil, Switzerland) and are not corrected.

Procedures

Method A: Reaction under oil bath (with 99% PC and drying agent)

The substrate (4 mmol of 1, 2, 4, 5, 6 or 7, except for 3: 3 mmol), the solid Na₂CO₃ (4 mmol in the case of 1, 2, 4, 5, 6 or 7, except for 3: 3 mmol), the drying agent CaCl₂ (4 mmol in the case of 1, 2, 4, 5, 6 or 7, except for 3: 3 mmol) and 99% propylene carbonate (36 mmol, 3 mL, d = 1.204 g/mL in the case of 1, 2, 3, 4, 6 or 7, except for 5: 48 mmol, 4 mL,d = 1.204 g/mL) were measured into a round-bottom flask with a Liebig-condenser and gas-outlet adapter and the suspension was treated at reflux temperature at a max. oil bath temperature of 170 °C. After the different reaction time (Tables S2-S8), the suspension was cooled down and the unreacted solid filtered off. After washing with water, the mother liquid was neutralised with 10% HCl solution and the aqueous layer was extracted with CHCl₃ (3 \times 25 mL, in the case of 2, 5) and EtOAc (3 \times 25 mL, in the case of 1, 3, 4, 6, 7), respectively. Usually, the organic phase contained the product (10, 11, 12, 16 and 17), but in some cases, the extraction was satisfactory only to separate the unreacted propylene carbonate and propylene glycol from the raw product, which remained in the neutralised aqueous phase (product 8, 9, 13, 14, 15, 18 and 19). The collected organic phase was washed with 10% CuSO₄ solution (2 \times 15 mL) and evaporated after drying over Na₂SO₄ and filtration. In each case, the crude product was lyophilised overnight at 10 mmHg and -50 °C and weighted before the product was purified by column chromatography (silica gel, 0.040-0.063 mesh size, except product 10, obtained after treatment with hexane). The unsuccessful reactions are not described in detail, but some are mentioned in Tables S2 and S3. All pure products—8, 9, 10, 11, 12, 13, 14, 15, 16, 17, 18 and 19—were characterised by ¹H-, ¹³C-NMR spectroscopy and HPLC-MS.

Method B: Reactions under MW conditions (with and without drying agent)

MW-assisted experiments were carried out in a monomode CEM-Discover MW reactor using the standard configuration as delivered, including proprietary software. The experiments were executed in 80 mL MW process vials, a dynamic method with control of the temperature by infrared detection. Conditions: 5 min. ramp time, 150 °C temperature, different hold time, max. 200 Psi pressure and 300 W power. The amount of reagents was identical to that used in Method A; however, in spite of that, the use of drying agent was not necessary when 99.7% PC was the reagent and solvent too. After the corresponding reaction time (Tables S2–S8), the vial was cooled to 50 °C by air jet cooling, followed by the usual work-up, described in Method A.

Structure characterisation data:

72 mg (11%) yellowish oil **1-(2-hydroxypropyl)pyrimidine-2,4(1***H***,3***H***)-dione (16), C_7H_{10}N_2O_3: 170.17, CAS Reg. No: 1479918-99-4, Rf = 0.40 (CHCl₃/MeOH 5/1), rt = 0.23′ (94%), m/z = 171.**

¹H NMR (400 MHz, DMSO- d_6): δ = 1.04 (d, J = 6.2 Hz, 3H, CH₃), 3.38 (dd, J = 13.6, 8.4 Hz, 1H, CH₂), 3.71 (dd, J = 13.6, 3.6 Hz, 1H, CH₂), 3.82 (m, 1H, C<u>H</u>OH), 5.49 (d, J = 7.8 Hz, 1H, O=CCH), 7.52 (d, J = 7.8 Hz, 1H, NCH).

¹³C NMR (100 MHz, DMSO- d_6): $\delta = 20.7, 54.5, 64.0, 100.0, 146.9, 151.3, 164.1.$

42 mg (5%) white oily solid **1,3-bis(2-hydroxypropyl)pyrimidine-2,4(1***H***,3***H***)-dione (17), C_{10}H_{16}N_2O_4: 228.25, Rf = 0.55 (CHCl₃/MeOH 5/1), rt = 0.22′ (100%), m/z = 229.**

¹H NMR (400 MHz, DMSO- d_6): δ = 1.00 (d, J = 6.0 Hz, 3H, N³CH₂CHC \underline{H}_3), 1.05 (d, J = 6.2 Hz, 3H, N¹CH₂CHC \underline{H}_3), 3.44 (m, 1H, N¹CH₂), 3.66 (m, 1H, N³CH₂), 3.77 (m, 1H, N¹CH₂), 3.84 (m, 1H, N³CH₂), 3.83 (m, 1H, N¹CH₂C \underline{H}), 3.89 (m, 1H, N³CH₂C \underline{H}), 4.67 (d, J = 5.2 Hz, 1H, N³CH₂CHO \underline{H}), 4.93 (d, J = 4.8 Hz, 1H, N¹CH₂CHO \underline{H}) 5.63 (d, J = 7.8 Hz, 1H, O=CCH), 7.54 (d, J = 7.8 Hz, 1H, NCH).

¹³C NMR (100 MHz, DMSO- d_6): δ = 20.7, 21.1, 47.1, 55.7, 63.3, 64.0, 99.4, 145.3, 151.5, 162.9.

4. Conclusions

We have studied the *N*-alkylation power of PC functioning as both an alkylating agent and solvent, under alkaline conditions (solid Na₂CO₃), either without the use (anhydrous PC (99.7%)) or in the presence of a drying agent (CaCl₂, 99% PC) in one-pot reactions. In each case, *N*-alkylation took place, and we were able to prepare new monoalkylated compounds **12** and **14**. In the case of 6-methyluracil (5) and 2-thiouracil (7), dialkylation occurs under our reaction conditions, suggesting that the electron-donating methyl and thiol groups activate the heterocyclic system towards the electrophilic carbon atom of PC. In the case of 2-thiouracil (7), both dialkylation and monoalkylation were observed, delivering new compounds **9** and **19**, in addition to the monoalkylated product **8** and the oxazole-condensed ring system **18**. It is suggested that the most productive *N*-alkylation is achieved with the use of anhydrous PC under MW conditions. We were also able to transform compound **7** into two cyclised compounds (**18**, **19**) by dehydration. *N*-Alkylation was also successful in the case of benzotriazole (**6**), synthesizing two monoalkylated products. This is despite the lack of the electron-withdrawing carbonyl group. Finally, the observed experimental data were supported by theoretical calculations.

Supplementary Materials: The following supporting information can be downloaded at: https://www.mdpi.com/article/10.3390/ijms25105523/s1.

Author Contributions: Conceptualisation, A.C. (Andrea Czompa) and I.M.M.; methodology, I.M.M.; validation, A.C. (Andrea Czompa) and I.M.M.; formal analysis, I.M.M.; investigation, A.C. (Andrea Czompa), D.B., B.B., P.S., E.E. (Eszter Erdei) and A.C. (Attila Csomos); resources, I.M.M.; data curation, B.B.; writing—original draft preparation, A.C. and E.E.; writing—review and editing, I.M.M.; visualisation, B.B.; supervision, I.M.M.; funding acquisition, I.M.M. All authors have read and agreed to the published version of the manuscript.

Funding: This research was funded by the Hungarian Research Foundation (OTKA ANN 139484). The financial support of the National Research, Development and Innovation Office (TKP2021-EGA-31) is acknowledged. Project no. RRF-2.3.1-21-2022-00015 has been implemented with support provided by the European Union. E.E. acknowledges the grant of EFOP-3.6.3-VEKOP-16-2017-00009. This work was supported by the KDP-2021 program of the Ministry of Innovation and Technology from the Source of the National Research, Development, and Innovation Fund (NKFIH).

Data Availability Statement: Data are contained within the article or Supplementary Materials.

Acknowledgments: We are grateful to the Hungarian Research Foundation (OTKA ANN 139484). The financial support of the National Research, Development and Innovation Office (TKP2021-EGA-31) is acknowledged. Project no. RRF-2.3.1-21-2022-00015 has been implemented with support provided by the European Union. E.E. acknowledges the grant of EFOP-3.6.3-VEKOP-16-2017-00009.

Conflicts of Interest: Mr. Attila Csomos was employed at Femtonics Ltd. The authors declare that this research was conducted in the absence of any commercial or financial relationships that could be construed as a potential conflict of interest. The funders had no role in the design of the study; in the collection, analyses, or interpretation of data; in the writing of the manuscript or in the decision to publish the results. The authors declare no conflicts of interest.

References

- 1. Alder, C.M.; Hayler, J.D.; Henderson, R.K.; Redman, A.M.; Shukla, L.; Shuster, L.E.; Sneddon, H.F. Updating and further expanding GSK's solvent sustainability guide. *Green Chem.* **2016**, *18*, 3879–3890. [CrossRef]
- 2. Agatemor, C.; Quintana, A.A.; Sztapka, L.M.; Ebinuma, V.C.S. Enabling sustainable chemistry with ionic liquids and deep eutectic solvents: A fad or the future? *Chem. Int. Ed.* **2022**, *37*, e202205609.
- 3. Tabanelli, T.; Giliberti, C.; Mazzoni, R.; Cucciniello, R.; Cavani, F. An innovative synthesis pathway to benzodioxanes: The peculiar reactivity of glycerol carbonate and catechol. *Green Chem.* **2019**, *21*, 329–338. [CrossRef]
- 4. Czompa, A.; Pasztor, B.L.; Sahar, J.A.; Mucsi, Z.; Bogdan, D.; Ludanyi, K.; Varga, Z.; Mandity, I.M. Scope and limitation of propylene carbonate as a sustainable solvent in the Suzuki-Miyaura reaction. *RSC Adv.* **2019**, *9*, 37818–37824. [CrossRef]

5. Chavakula, R.; Mutyala, N.; Chennupati, S. Synthesis of (*E*)-9-(Propen-1-yl)-9*H*-adenine, a Mutagenic Impurity in Tenofovir Disoproxil Fumarate. *Org. Prep. Proced. Int.* **2013**, 45, 336–340. [CrossRef]

- Du, X.X.; Zi, Q.X.; Wu, Y.M.; Jin, Y.; Lin, J.; Yan, S.J. An environmentally benign multi-component reaction: Regioselective synthesis of fluorinated 2-aminopyridines using diverse properties of the nitro group. Green Chem. 2019, 21, 1505–1516. [CrossRef]
- 7. Selva, M.; Fabris, M. The reaction of glycerol carbonate with primary aromatic amines in the presence of Y-and X-faujastites: The synthesis of *N*-(2,3-dihydroxy)propyl anilines and the reaction mechanism. *Green Chem.* **2009**, *11*, 1161–1172. [CrossRef]
- 8. Nohra, B.; Candy, L.; Blanco, J.-F.; Raoul, Y.; Mouloungui, Z. Aza-Michael versus aminolysis reaction of glycerol carbonate acrylate. *Green Chem.* **2013**, *15*, 1900–1909.
- Dressler, H. CA 2043455C.
- 10. Kinage, A.K.; Gupte, S.P.; Chaturvedi, R.K.; Chaudhari, R.V. Highly selective synthesis of mono-ethylene glycol phenyl ethers via hydroxyalkoxylation of phenols by cyclic carbonates using large pore zeolites. *Catal. Commun.* **2008**, *9*, 1649–1655. [CrossRef]
- 11. Osterman-Golkar, S.; Bailey, E.; Farmer, P.B.; Gorf, S.M.; Lamb, J.H. Scand, Monitoring exposure to propylene oxide through the determination of hemoglobin alkylation. *J. Work Environ. Health* **1984**, *10*, 99–102. [CrossRef]
- 12. Sobol, Z.; Engel, M.E.; Rubitski, E.; Ku, W.W.; Aubrecht, J.; Schiestl, R.H. Genotoxicity profiles of common alkyl halides ad esters with alkylating activity. *Mutat. Res.* **2007**, *633*, 80–94. [CrossRef] [PubMed]
- 13. Sorribes, I.; Cabrero-Antonino, J.R.; Vicent, C.; Junge, K.; Beller, M. Catalytic *N*-alkylation of amines using carboxylic acids and molecular hydrogen. *J. Am. Chem. Soc.* **2015**, *137*, 13580–13587. [CrossRef] [PubMed]
- 14. Wahba, A.E.; Hamann, M.T. Reductive *N*-alkylation of nitroarenes: A green approach for the *N*-alkylation of Natural Products. *J. Org. Chem.* **2012**, *77*, 4578–4585. [CrossRef] [PubMed]
- 15. Wie, D.; Yang, P.; Yu, C.; Zhao, F.; Wang, Y.; Peng, Z. *N*-alkylation of amines with alcohols catalyzed by manganese(II) chloride or bromopentacarbonylmanganese(I). *J. Org. Chem.* **2021**, *86*, 2254–2263.
- 16. Elangovan, S.; Neumann, J.; Sortais, J.B.; Junge, K.; Darcel, C.; Beller, M. Efficient and selective *N*-alkylation of amines with alcohols catalysed by manganese pincer complexes. *Nat. Commun.* **2016**, *7*, 12641. [CrossRef] [PubMed]
- 17. Selva, M.; Fabris, M.; Lucchini, V.; Perosa, A.; Noé, M. The raction of primary aromatic amines with alkylene carbonates fort he selective synthesis of bis-*N*-(2-hydroxy)alkylanilines: The catalytic effect of phosphonium-based ionic liquids. *Org. Biomol. Chem.* **2010**, *8*, 5187–5198. [CrossRef]
- 18. Lacy, M.Q.; Hayman, S.R.; Gertz, M.A.; Dispenzieri, A.; Buadi, F.; Kumar, S.; Greipp, P.R.; Lust, J.A.; Russell, S.J.; Dingli, D.; et al. Pomalidomide (CC4047) plus low-dose dexamethasone as therapy for relapsed multiple myeloma. *J. Clin. Oncol.* **2009**, 27, 5008–5014. [CrossRef]
- 19. Lu, J.; Qian, Y.; Altieri, M.; Dong, H.; Wang, J.; Raina, K.; Hines, J.; Winkler, J.D.; Crew, A.P.; Coleman, K.; et al. Hijacking the E3 ubiquitin ligase cereblon to efficiently target BRD4. *Chem. Biol.* **2015**, 22, 755–763. [CrossRef]
- 20. Neklesa, T.K.; Winkler, J.D.; Crews, C.M. Targeted protein degeneration by PROTACs. *Pharmacol. Ther.* **2017**, 174, 138–144. [CrossRef]
- Varun, C.; Sonam; Kakkar, R. Isatin and its derivatives: A survey of recent syntheses, reactions, and application. Med. Chem. Commun. 2019, 10, 351–368. [CrossRef]
- 22. Kemp, J.P.; Meltter, E.O.; Orgel, H.A.; Welch, M.J.; Bucholtz, G.A.; Middleton, E., Jr.; Spector, S.L.; Newton, J.J.; Perhach, J.L., Jr. A dose-response study of the bronchodilator action of azelastine in asthma. *J. Allergy Clin. Immunol.* 1987, 79, 893–899. [CrossRef] [PubMed]
- 23. Grant, S.; Fitton, A. Risperidone: A review of its pharmacology and therapeutic potential in the treatment of schizophrenia. *Drugs* 1994, 48, 253–273. [CrossRef] [PubMed]
- 24. Brogden, R.N.; Sorkin, E.M. Ketanserin: A review of its pharmacodynamic and pharmacokinetic properties, and therapeutic potential in hypertension and peripheral vascular disease. *Drugs* **1990**, *40*, 903–949. [CrossRef] [PubMed]
- 25. Beshore, D.C.; Dudkin, V.; Garbaccio, R.M.; Johnson, A.W.; Kuduk, S.D.; Skudlarek, J.W.; Wang, C.; Fraley, M.E. US 2012/0135977A1.
- 26. Sun, J.; Feng, Y.; Huang, Y.; Zhang, S.-Q.; Xin, M. Research advances on selective phosphatidylinositol 3 kinase δ (PI3Kδ) inhibitors. *Bioorg. Med. Chem. Lett.* **2020**, *30*, 127457. [CrossRef] [PubMed]
- 27. Ranise, A.; Spallarossa, A.; Cesarini, S.; Bondavalli, F.; Schenone, S.; Bruno, O.; Menozzi, G.; Fossa, P.; Mosti, L.; La Colla, M.; et al. Structure-based design, parallel synthesis, structure—activity relationship, and molecular modeling studies of thiocarbamates, new potent non-nucleoside HIV-1 reverse transcriptase inhibitor isosteres of phenethylthiazolylthiourea derivatives. *Med. Chem.* 2005, 48, 3858–3873. [CrossRef] [PubMed]
- 28. Fry, F.S., Jr.; Maienthal, M.; Benson, W.R. Synthesis of isopromethazine hydrochloride. *J. Pharm. Sci.* **1983**, 72, 568–569. [CrossRef] [PubMed]
- 29. Sikoraiová, J.; Marchalın, S.; Daıch, A.; Decroix, B. Acid-mediated intramolecular cationic cyclization using an oxygen atom as internal nucleophile: Synthesis of substituted oxazolo-, oxazino-and oxazepinoisoindolinones. *Tetrahedron Lett.* **2002**, 43, 4747–4751. [CrossRef]
- 30. Thibadeau, S.; Martin-Mingot, A.; Jouannetaud, M.-P.; Karam, O.; Zunino, F. A novel, facile route to β-fluoroamines by hydrofluorination using superacid HF–SbF5. *Chem. Comm.* **2007**, *30*, 3198–3200. [CrossRef]
- 31. Gupta, P.; Rouf, A.; Shah, B.A.; Mukherjee, D.; Taneja, S.C. Efficient Preparation of Biologically Important 1, 2-Amino Alcohols. *Synth. Commun.* **2013**, *43*, 505–519. [CrossRef]
- 32. Faldi, A.; Saunier, J.P.; Metais, E. FR 2915887A1.
- 33. Moeller, H.; Oberkobusch, D.; Hoeffkes, H. EP 1300132A2.

34. Shmidt, M.S.; Reverdito, A.M.; Kremenchuzky, L.; Perillo, I.A.; Blanco, M.M. Simple and efficient microwave assisted *N*-alkylation of isatin. *Blanco Mol.* **2008**, *13*, 831–840. [CrossRef]

- 35. Casey, L.A.; Galt, R.; Page, M.I. The mechanism of hydrolysis of the γ-lactam isatin and its derivatives. *J. Chem. Soc. Perkin Trans.* **1993**, 2, 23–28. [CrossRef]
- 36. Chmiel-Szukiewicz, E. PL 228504B1.
- 37. Molnar, I. In 1-und in 2-Stellung dialkylaminoalkylierte Benztriazole. Helv. Chimica Acta 1963, 46, 1473–1479. [CrossRef]
- 38. Pchelka, B.K.; Loupy, A.; Petit, A. Preparation of various enantiomerically pure (benzotriazol-1-yl)-and (benzotriazol-2-yl)-alkan-2-ols. *Tetrahedron Asymmetry* **2006**, *17*, 2516–2530. [CrossRef]
- 39. Moriarty, R.M.; Prakash, I.; Clarisse, D.E.; Penmasta, R.; Awasthi, A.K. Conversion of Thiocarbonyl into Carbonyl in Uracil, Uridine, and *Escherichia coli* Transfer RNA using Hypervalent iodine oxidation. *J. Chem. Soc. Chem. Commun.* 1987, 16, 1209–1210. [CrossRef]
- 40. Matsui, M.; Kamiya, K.; Kawamura, S. Ozonization of thio-and azauracils. Bull. Chem. Soc. Jpn. 1989, 62, 2939–2941. [CrossRef]
- 41. Novakov, I.A.; Orlinson, B.S.; Navrotskii, M.B. Desulfurization of 2-thioxo-1,2,3,4-tetrahydropyrimidin-4-ones with oxiranes and 2-haloacetonitriles. *Russ. J. Org. Chem.* **2005**, *41*, 607–609. [CrossRef]
- 42. Atanu, R.; Conlee, C.R.; Defougerolles, A.; Fraley, A.W. WO 2015/089511A2.
- 43. Agami, C.; Dechoux, L.; Melaimi, M. An Efficient Synthesis of Pyrimidines from β-Amino Alcohols. *Org. Lett.* **2000**, *2*, 633–634. [CrossRef] [PubMed]
- 44. Agami, C.; Dechoux, L.; Hamon, L.; Melaimi, M.J. An efficient synthesis of a new series of acyclonucleosides starting from β-amino alcohols. *Org. Chem.* **2000**, *65*, 6666–6669. [CrossRef]
- 45. Bochevarov, A.D.; Watson, M.A.; Greenwood, J.R.; Philipp, D.M. Multiconformation, density functional theory-based pK_a prediction in application to large, flexible organic molecules with diverse functional groups. *J. Chem. Theory Comput.* **2016**, 12, 6001–6019. [CrossRef]
- 46. Yu, H.S.; Watson, M.A.; Bochevarov, A.D. Weighted averaging scheme and local atomic descriptor for pK_a prediction based on density functional theory. *J. Chem. Inf. Mod.* **2018**, *58*, 271–286. [CrossRef]
- 47. Klicić, J.J.; Friesner, R.A.; Liu, S.Y.; Guida, W.C. Accurate prediction of acidity constans in aqueous solution via density functional theory and self-consistent reaction field methods. *J. Phys. Chem. A* **2002**, *106*, 1327–1335. [CrossRef]

Disclaimer/Publisher's Note: The statements, opinions and data contained in all publications are solely those of the individual author(s) and contributor(s) and not of MDPI and/or the editor(s). MDPI and/or the editor(s) disclaim responsibility for any injury to people or property resulting from any ideas, methods, instructions or products referred to in the content.